Investigation of Structural, Optical and Electrical Properties of Zinc Selenide Thin Films Prepared by Chemical Bath Deposition Technique

by

Tanvir Ahmmed

M.Sc. in Physics

Roll No. 1014142514F

Session: October, 2014

A dissertation submitted to the Department of Physics, Bangladesh University of Engineering and Technology (BUET) in partial fulfillment of the requirement for the degree of MASTER OF SCIENCE (M.Sc.) in Physics

BUET

Department of Physics

BANGLADESH UNIVERSITY OF ENGINEERING AND TECHNOLOGY (BUET)

DHAKA-1000

BANGLADESH UNIVERSITY OF ENGINEERING & TECHNOLOGY (BUET)
DHAKA
DEPARTMENT OF PHYSICS

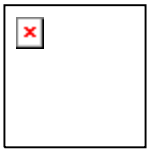

CERTIFICATION OF THESIS

The thesis titled "**Investigation of Structural, Optical and Electrical Properties of Zinc Selenide Thin Films Deposited by Chemical Bath Deposition Technique**" submitted by **Tanvir Ahmmed**, Roll No: 1014142514F, Session: **October/2014**, has been accepted as satisfactory in partial fulfillment of the requirement for the degree of **Master of Science (M.Sc.) in Physics** on 17 January 2017.

BOARD OF EXAMINERS

1. _____
Dr. Mohammad Jellur Rahman — **Chairman (Supervisor)**
Assistant Professor,
Department of Physics, BUET, Dhaka

2. _____
Mrs. Fahima Khanam — **Member (Ex-Officio)**
Professor & Head
Department of Physics, BUET, Dhaka

3. _____
Dr. Md. Abu Hashan Bhuiyan — **Member**
Professor
Department of Physics, BUET, Dhaka

4. _____
Dr. Mohammed Abdul Basith — **Member**
Associate Professor
Department of Physics, BUET, Dhaka

5. _____
Dr. A. B. M. Obaidul Islam — **Member (External)**
Professor
Department of Physics, University of Dhaka

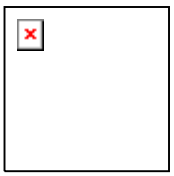

BUET

CANDIDATE'S DECLARATION

It is hereby declared that this thesis or any part of it has not been submitted elsewhere for the award of any degree or diploma.

_____

(**Tanvir Ahmmed**)

Roll No. 1014142514

Session: October/2014

Dedicated to
My beloved Parents and honorable Teachers
Who inspired and influenced me in higher study

C O N T E N T S

List of Figures

List of Tables

A c k n o w l e d g e m e n t s

The fulfillment of any work requires the support of many people. At the very first, I express my satisfaction to praise the almighty Allah who has given me strength and opportunity to complete my thesis work.

Regarding the outcomes and completion of this thesis work, I express my deepest sense of gratitude and profound respect to my supervisor Dr. Mohammad Jellur Rahman, Department of Physics, BUET, for his invaluable time dedication, close supervision, inspiration and helpful attitude provided during the work as well as for acquainting me with the arena of advanced research.

I am grateful to my respected teacher Prof. Fahima Khanam, Head, Department of Physics, BUET for providing necessary facilities to carry out this research work. I am thankful to my respectable teacher Prof. Dr. Md. Abu Hashan Bhuiyan, for his valuable suggestions regarding my thesis. I am obliged to, Prof. Dr. Jiban Podder, Prof. Dr. Md. Feroz Alam Khan, Prof. Dr. A. K. M. Akther Hossain, Prof. Dr. Md. Mostak Hossain, Prof. Dr. Afia Begum, Prof. Dr. Md. Forhad Mina, Prof. Md. Rafi Uddin, Dr. Nasreen Akter, Dr. M. A. Basith, Dr. A. Sayem Karal, Dr. Muhammad Rakibul Islam, Mr. A. T. M. Shafiul Azam, Dr. Parvin Sultana, Mrs. Mehnaz Sharmin and Mr. Mehdi Masud, Department of Physics, BUET for their inspiration, affection and constructive suggestions for advanced research. I am thankful to the authority of BUET for giving me necessary permission and providing with the financial support for this research work.

I am grateful to Nano Technology Research Lab, BUET for providing me the facility of measuring mass of the chemical and annealing of the deposited sample.

I would like to thank the authority of Pilot Plant & Process Development Center of Bangladesh Council for Scientific & Industrial Research, Dhaka, for their excellent cooperation by allowing me to use the available facilities in that laboratory.

I am grateful to the Department of Glass and Ceramic engineering, BUET for permitting me to use the scanning electron microscope for surface morphological measurements. I would like to thank Mr. Rana Ahmed for helping me to take the SEM micrographs.

I would like to thank Mrs. Nasima Banu, Mrs. Afruja Nasreen, Mrs. Rahima Nasrin, Dr. Sonjit Sen Roy, Ahaduzzaman Deeraz, Mrs. Kishwar-E Hasin, Ms. Rabeya Rahman, Mohammad Fahim, Md. Aminul Islam, Ms. Meherun nesa, and Md. Abdul Momin and also all the other research workers of the Materials Science Laboratory for their cooperation.

I am also thankful to all the staff members, Department of Physics, BUET for their sincere help.

Finally, I would like to express my gratitude to my beloved parents and all other family members for their multifaceted support through all these years during my work.

Tanvir Ahmmed

October, 2014

A b s t r a c t

A Chemical Bath Deposition system is set up to deposit zinc selenide (ZnSe) thin films on glass substrate. Zinc acetate and sodium selenosulfate aqueous alkaline medium are used as zinc and selenium source, respectively. Films were deposited by varying concentration of sodium selenosulfate and for different deposition times. The surface morphology, structural and optical properties of the ZnSe thin films were investigated by using scanning electron microscopy (SEM), X-ray diffraction, UV–visible spectroscopy. The SEM observation revealed non-uniform distribution of spherical ZnSe crystallites. The elemental compositions of the films were confirmed by energy dispersive X-ray spectroscopy. The results showed that the deposition time had a strong influence on the morphology. The optical band gap also observed to vary with increasing deposition time and concentrations of the sodium selenosulfate. The thickness of the films deposited at different concentrations of Se and different time durations were 140–225 nm and 175–375 nm, respectively. The SEM micrographs show that ZeSe thin films prepared at different time duration are not compact but have good coverage of glass substrate. These films revealed that grains were very small in size with well defined grain boundaries. X-ray diffraction studies show that though the as–deposited ZnSe thin films do not show crystalline nature but, annealed ZnSe thin films are polycrystalline in nature with preferential orientation along the (111), (220), and (311). The films also have ZnO and Na_2SeSO_3 phase. The average crystallite size is found to be 23.21±3.61 nm. The strain and dislocation density are found to be 1.62×10^{-3} lines^{-2} m^{-4} and 2.18×10^{15} m^{-2}, respectively. The number of crystals per unit area is 2.633×10^{16} m^{-2}. All the diffraction peaks can be assigned to face centered cubic with lattice constants (a = 5.670 Å) which are in good agreement with the previous work. Various optical parameters such as absorbance, transmittance, refractive index, extinction coefficient and dielectric constant of the films have been studied for the as-deposited ZeSe thin films and are recorded in the wavelength range from 250 to 1100 nm. The films prepared for 60 min exhibit higher absorption as compared to other deposition times. The maximum transmittance is 65% for the ZnSe thin film deposited at 0.5 M concentration of Se. The direct optical band gap of the films deposited at different time duration and different molar concentration of Se source show wide band gap energies of 3.50–3.55 eV and 2.70–3.55 eV, respectively. The band gap of the ZnSe thin film deposited for 40 min of 1.0 M concentration have been increased from

3.5 to 3.75 eV after annealing effect. It is observed that the refractive index decreases, as the wavelength increase. However, the transmittance and extinction coefficient increases with the increase of wavelength. The electrical properties of the as–deposited and annealed ZnSe thin films have been observed. The resistivity decreases with the increase of temperature and the conductivity increases with the increase of temperature which reveals the semiconducting nature of the films. The maximum resistivity of the ZnSe Films deposited for 30 min is 2.2×10^3 Ω–m. The activation energy of the ZnSe thin film deposited at 0.3M concentration for 40 min is 0.093863 which supports the values of previous research.

CHAPTER 1

GENERAL INTRODUCTION

CHAPTER 1

1.1 Introduction

Thin films and its devices play an important role in the development of modern technology. Thin films are three dimensional form of solid material, whose one dimension, called the thickness, is much smaller than the other two dimensions. Thin films are formed by atom to atom or molecule to molecule condensation process. Semiconductor thin films have been the basis of the development of a wide variety of applications such as high-speed transistors, solar cells, solid-state lighting devices, sensors, information storage devices, etc [1]. Fundamental knowledge of the basic properties of compound semiconducting thin films and understanding their interfaces with other device are very important for the recent technological progress. There are various methods to deposit semiconducting thin films such as chemical bath deposition (CBD) [3], vacuum evaporation [4], electrodeposition [5], chemical vapor deposition [6], molecular beam epitaxy [7], pulsed laser deposition [8], thermal evaporation [9], etc. Among them CBD appears to be very suitable method for a large scale fabrication of the semiconducting thin films. The main advantages of this method are that it is a low cost method and do not require any sophisticated instruments, and films can be prepared at low processing temperature. In CBD a direct reaction occurs between the precursors species in the solution [10]. It has been reported that type II–VI semiconductors are important in optoelectronic applications for their high optical transparency, low dark electrical resistivity, high photoconductivity and better crystallinity [12]. For example, PbS thin films due to its narrow band gap are employed to produce photo resistors, photodetectors, solar cells and photoemitters in the IR range [13]. CdS thin films deposited by CBD have demonstrated numerous beneficial attributes to the copper indium gallium sulfate device. ZnSe is used as a window layer in heterojunction solar cells together with some narrow band gap semiconductors. It is also a key material for the applications to other optoelectronic devices such as blue-green laser diodes, white light emitting diodes, optically controlled switches, tunable mid-IR laser sources for remote sensing applications, photovoltaic and photo electro-chemical devices [15]. In this work zinc selenide (ZnSe) thin film is obtained using the CBD technique and its different properties are studied.

1.2 Deposition Methods of Film

Thin film can be prepared by many physical and chemical techniques. In this section, some of the commonly used methods for depositing large area thin film on a variety of commercially available substrates are described briefly. The physical techniques are vacuum evaporation, sputtering, spraying and painting while vapor deposition, oxidation, immersion plating, chemical bath deposition and electroplating are called chemical techniques.

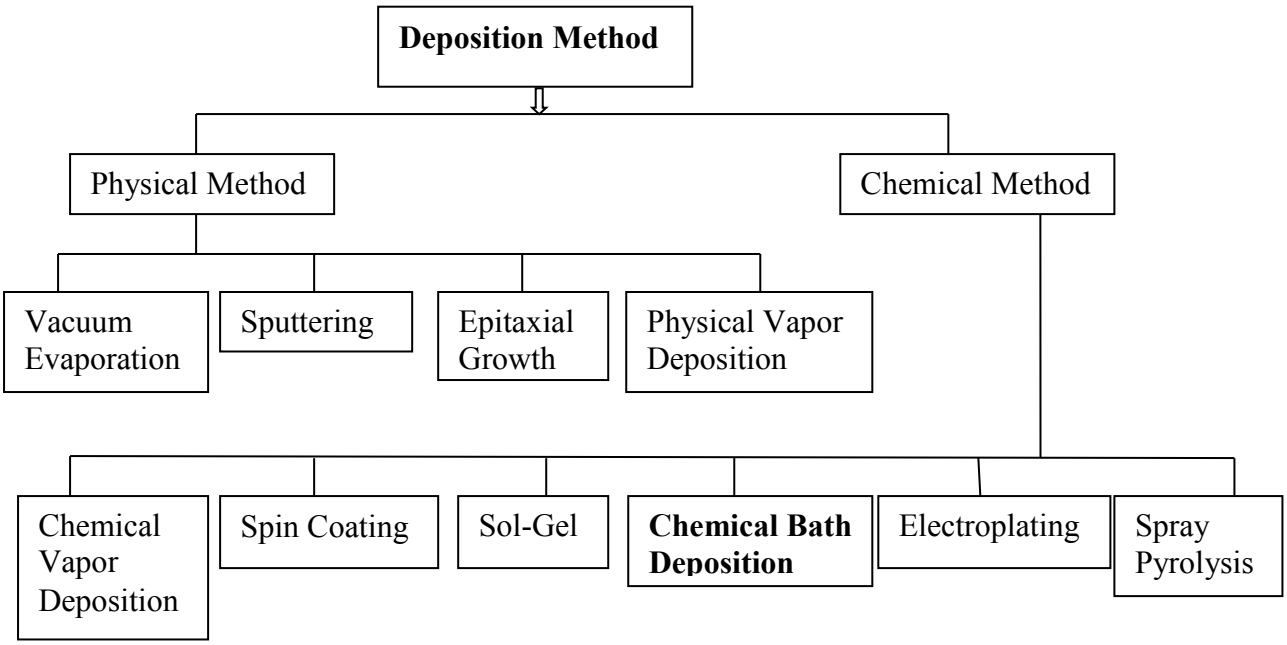

Figure 1.1: Types of deposition techniques

1.2.1 Physical Techniques

Physical deposition uses mechanical, electromechanical or thermodynamic means to produce a thin film of solid. An everyday example is the formation of frost. Since most engineering materials are held together by relatively high energies, and chemical reactions are not used to store these energies, commercial physical deposition systems tend to require a low-pressure vapor environment to function properly.

1.2.1.1 *Vacuum Evaporation*

In this method, material is first thermally vaporized and then condensed on a substrate. Among the numerous deposition parameters substrate temperature, evaporation rate and the vacuum quality affect the microstructure and surface morphology of the coatings [16].

Vapor species may be created by kinetic ejection from the surface of a material (called target of cathode) by bombardment with energetic and nonreactive ions. The ejection process, known as sputtering, takes place as a result of momentum transfer between the impinging ions and the atoms of the target surface. The sputtered atoms are condensed on a substrate to form a film.

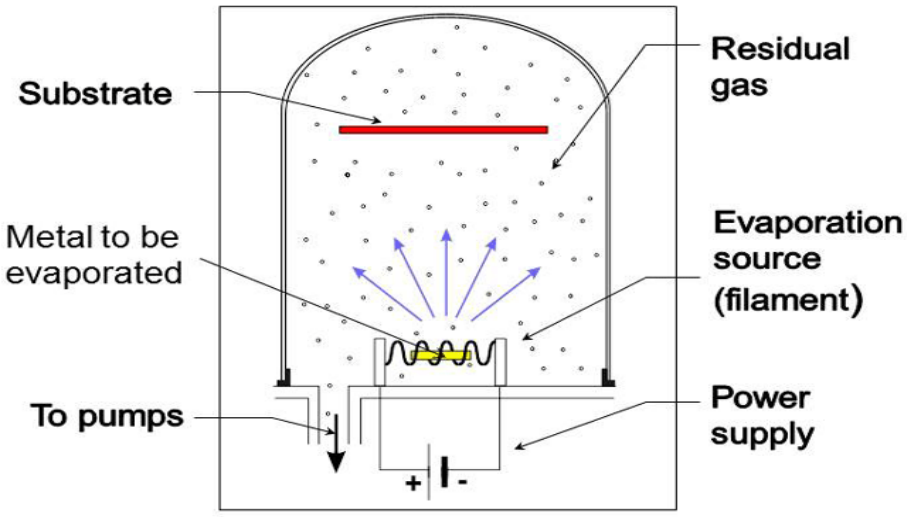

Figure 1.2: Schematic diagram of thermal or vacuum evaporation coating system

An arrangement of vacuum chamber is shown in Fig. 1.2. The material to be evaporated lies in high melting point metallic filament through which a high current is passed and the evaporated material is deposited on substrate attached to a heater. This arrangement chamber is pumped to high vacuum.

1.2.1.2 *Spray Pyrolysis*

The spray pyrolysis technique involves spraying a solution, usually aqueous, containing soluble salts of the constituent atom of the desired compound onto a heated substrate maintained at elevated temperatures [17]. The sprayed droplet reaching the hot substrate surface undergoes pyrolytic (endothermic) decomposition and forms a single crystallite or a cluster of crystallites of the product. The other volatile byproducts and the excess solvent escape in the vapor phase. The substrate provides the thermal energy for the thermal decomposition and subsequent recombination of the constituent species followed by sintering and recrystallization clusters of crystallites giving rise to a coherent film.

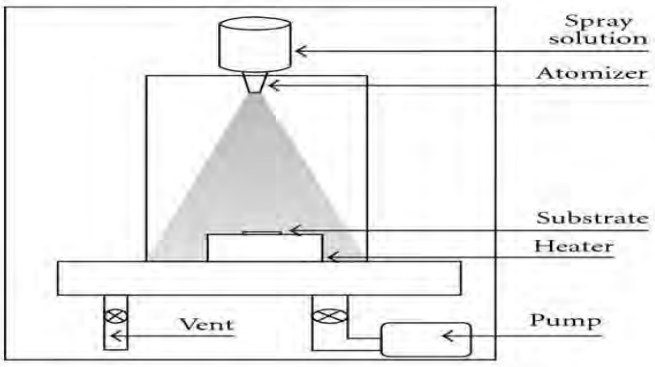

Figure 1.3: A diagram of Spray Pyrolysis system.

1.2.1.3 *Sputtering*

If a surface of target material is bombarded with energetic particles, it is possible to cause ejection of the surface atom: this is the process known as sputtering. The ejected atoms can be condensed on to a substrate to form a thin film. This method has various advantages over normal evaporation techniques in which no container contamination will occur. It is also possible to deposit alloy films which retain the composition of the parent target material. DC sputtering, radio frequency sputtering and magnetron sputtering methods are the oldest types of sputtering used [18]. High pressure oxygen sputtering and facing target sputtering are the two new methods introduced for deposition of thin films for applications in superconducting and magnetic films.

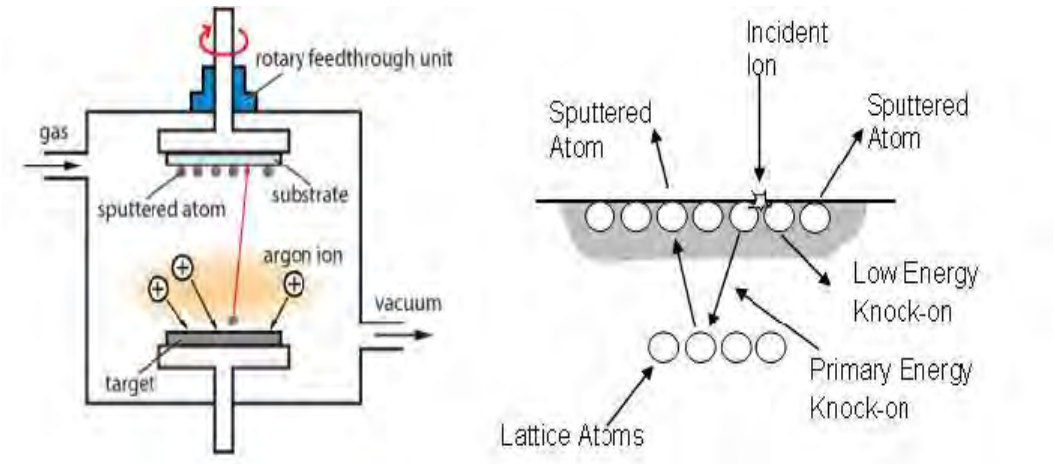

Figure 1.4: A diagram of sputtering system.

1.2.1.4 *Epitaxial growth*

Epitaxy means the growth of a single crystal film on top of a crystalline substrate. Epitaxial films may be grown from gaseous or liquid precursors [19]. Because the substrate acts as a seed crystal, the deposited film may lock into one or more crystallographic orientations with respect to the substrate crystal. If the overlayer either forms a random orientation with respect to the substrate or does not form an ordered overlayer, it is termed non-epitaxial growth. If an epitaxial film is deposited on a substrate of the same composition, the process is called homoepitaxy; otherwise it is called heteroepitaxy. Among the various Epitaxial growth methods, Molecular Beam Epitaxy (MBE) is frequently used for its advantages over other methods.

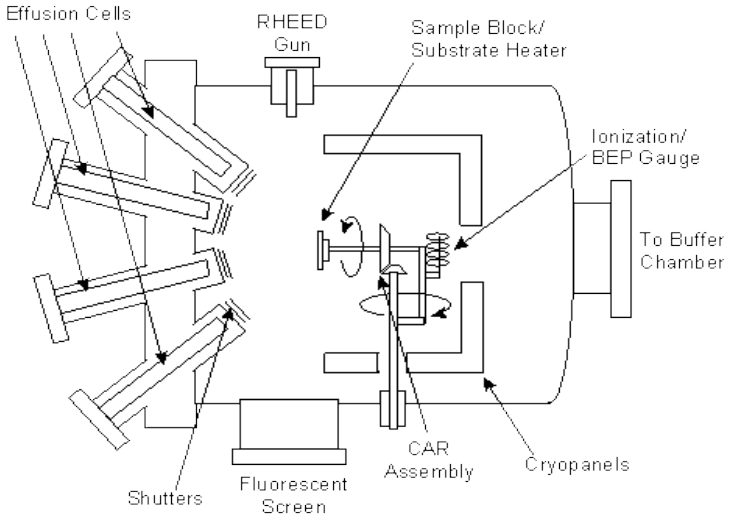

Figure 1.5: Diagram of a typical MBE system growth chamber

1.2.2 Chemical Techniques

1.2.2.1 *Chemical Vapor Deposition (CVD)*

Chemical vapour deposition can be defined as a material synthesis method in which the constituents of vapour phase react together to form a solid film at surface. The chemical reaction is an essential characteristic of this method [20]; therefore, besides the control of the usual deposition process variables, the reactions of the reactants must be well understood.

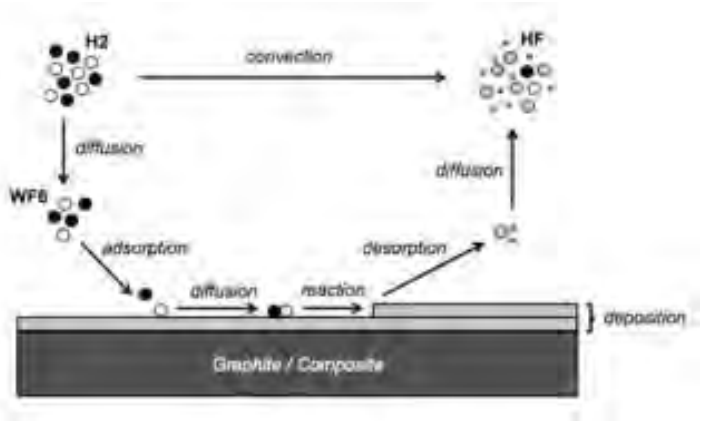

Figure 1.6: Diagram of a chemical vapor deposition process

1.2.2.2 *Spin Coating*

Spin coating process involves depositing a small puddle of a fluid material onto the center of a substrate and then spinning the substrate at high speed (typically around 3000 rpm) [21]. Centripetal acceleration will cause most of the resin to spread to, and eventually off, the edge of the substrate, leaving a thin film of material on the surface. Factors such as final rotation speed, acceleration, and fume exhaust affect the properties of the coated films. One of the most important factors in spin coating is repeatability, as subtle variations in the parameters can result in drastic variations in the coated film.

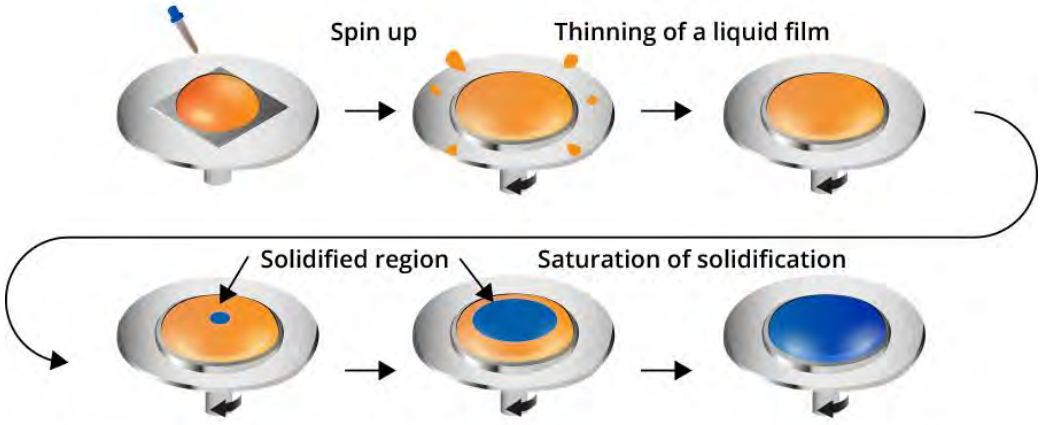

Fig.1.7: Schematic representation of the spin coating method

A machine used for spin coating is called a spin coater, or simply spinner. Rotation is continued while the fluid spins off the edges of the substrate, until the desired thickness of the film is achieved. The applied solvent is usually volatile, and simultaneously evaporates. So,

the higher the angular speed of spinning, the thinner the film. The thickness of the film also depends on the viscosity and concentration of the solution and the solvent.

1.2.2.3 *Electroplating*

Electrophoresis is the migration of charged particles in an electric field. Electrophoretic deposition, or electrocoating, is the electro deposition of large charged particles from a solution [22]. The particles may be charged dielectric particles (glass particles, organic molecules, paint globules, etc.) which are non soluble in the aqueous electrolyte. Alternatively some of the components can be treated so that they are soluble in water but will chemically react in the vicinity of an electrode and their solubility is decreased. Particles are usually deposited on the anode but sometimes on the cathode. Electroplating is the deposition on the cathode of metallic ions from the electrolyte of an electrolysis cell [18, 19]. Only selective elements and some alloy composition can be commercially deposited from aqueous solutions. Typically, the anode of the electrolytic cell is of the material to be deposited and is consumed in the deposition process. Displacement plating is the deposition of ions in solution on a surface and results from the difference in electro negativity of the surface and the ions. Electrophoresis is the migration of charged particles in an electric field. Electrophoretic deposition, or electrocoating, is the electro deposition of large charged particles from a solution. The particles may be charged dielectric particles (glass particles, organic molecules, paint globules, etc.) which are non soluble in the aqueous electrolyte. Alternatively some of the components can be treated so that they are soluble in water but will chemically react in the vicinity of an electrode and their solubility is decreased. Particles are usually deposited on the anode but sometimes on the cathode.

1.2.2.4 *Sol-Gel Technique*

The sol-gel processing consists of the formation of an amorphous gel from solutions followed by dehydration at relatively low temperatures. Since it starts from a solution of all components in the form of soluble precursor compounds, the mixing at a molecular level is retained through gel formation. Metal alkoxides or salts are partially hydrolysed which leads to branching and cross linking. Then the rigid coherent gel is dried and heated at temperatures dramatically lower than with other techniques. The sol-gel method can produce high quality fine electroceramic powders with excellent homogeneity but the process is tedious and expensive because of the scarce raw materials used and the need to calcine the amorphous powder at high temperature to obtain the desired crystallinity. Furthermore, large shrinkages

will normally occur during processing. Therefore, this technique is not suitable for bulk component fabrication, but applicable for films. The typical steps that are involved in sol-gel processing are shown in the schematic diagram below [23].

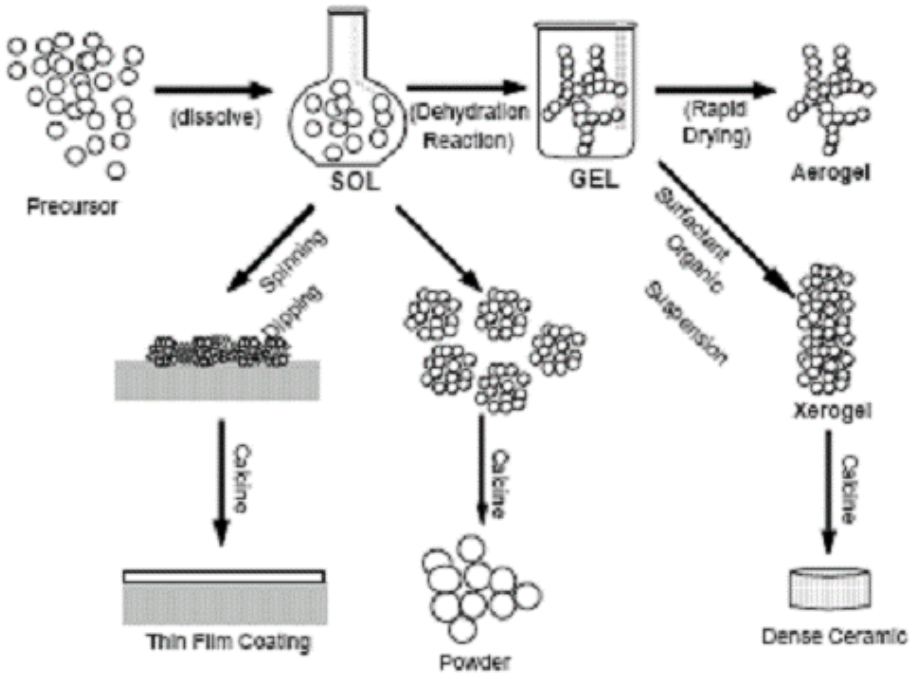

Fig 1.8: Schematic representation of sol-gel process of synthesis of nanomaterials.

1.2.2.5 *Chemical Bath Deposition*

Chemical bath deposition (CBD) is also called chemical solution deposition. It is a solution-based technique for thin film deposition. It provides a simple and low cost method to produce uniform, adherent, and reproducible large area thin films that are suitable for fabricating large area electronic devices. It is also capable of producing nanocrystalline, microcrystalline or even epitaxial thin films [3-4]. Many compound semiconductors (II-VI, IV-VI, V-VI, I-III-VI) have been deposited by CBD techniques and these techniques are primarily used in the process of fabricating Cu (In, Ga) Se_2 and CdTe based thin film photovoltaic [5, 6]. In the case of the batch CBD process, the heat needed for chemical reaction is supplied from the solution bath to the sample surface, resulting in both heterogeneous nucleations at the surface as well as homogeneous particle formation in the bath. For a better understanding and optimization of the CBD processes, it is necessary to find a method to de-couple the homogeneous particle formation and deposition from the molecular level heterogeneous surface reaction. Furthermore, the continuous process has resulted in a minimization of waste production and led

to more uniform films with negligible occurrence of pinholes. Uniform, smooth, and highly oriented nanocrystalline thin films can be successfully deposited on glass substrates at a low temperature (~90ºC) using this technique.

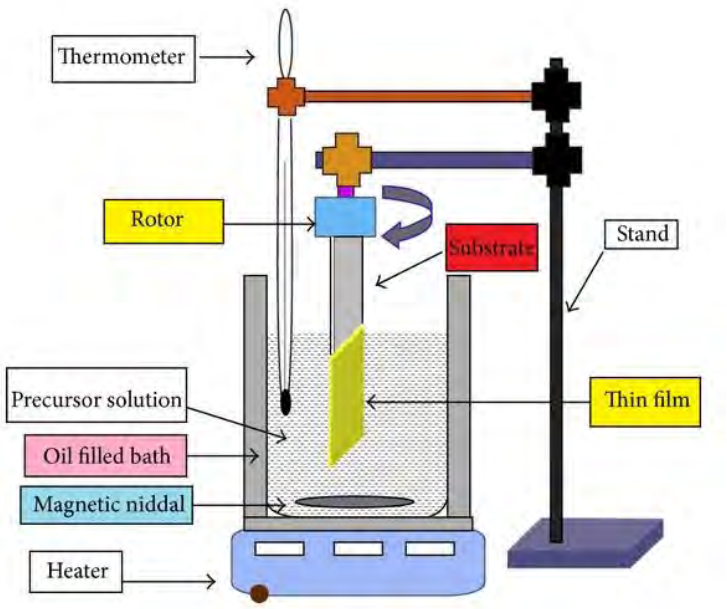

Fig. 1.9: A schematic diagram of CBD system

1.3 Advantages of CBD

The advantages of chemical bath deposition method are as follows.

- CBD is a simple and low cost technique.
- The method does not require sophisticated instrumentation.
- It is applicable for large area deposition.
- Electrical conductivity of the substrate materials is not an important criterion.
- The deposition is easy even at low temperature and avoids the oxidation or corrosion of the metallic substrate.
- Intertype conversion possible by this easy methods
- It is a safe procedure with minimum environmental hazards
- An intimate contact between reacting solution and substrate gives pinhole free and uniform deposition.
- Stoichiometry of the deposit can be easily maintained.

- The process is slow that facilitates better orientation of crystallites with improved grain structure.
- The method can be used to deposit a large number of metal chalcogenides.
- As very dilute solutions are used in the process, the method offers minimum toxicity and occupational hazards.
- Reproducibility is high and wastage can be minimized.
- Chemical bath deposition method has been used for formation of II-VI, III-V and IV-VI semiconducting thin film materials.

1.4 Applications of ZnSe Thin Films

Zn based nanostructures have been widely investigated recently due to its different potential applications [30]. Zinc selenide (ZnSe) shows unique optical properties exhibiting some potential applications, such as blue-green light emitting diodes, photo-luminescent and electro-luminescent devices, lasers, thin film solar cell, nonlinear optical crystal and infrared optical material. ZnSe and its lattice matched ternary alloys have been regarded as useful II–VI compound semiconductors for optoelectronic and photo electronic devices. For the energy ranges from visible to ultraviolet, ZnSe based materials are structured the first manifestation of the blue-green laser in 1991 [1]. ZnSe has been a material of choice for blue diode lasers and photovoltaic solar cells since its bulk band gap is 2.67 eV (460 nm) which can be tuned by adding impurities [3]. Out of varieties of applications, ZnSe can be used as optically controlled switching devices [1, 2]. Hence it is of great interest as a model material as thin film, quantum wells, bulk crystals and nanodots [3]. Since last few decades the nanosized materials have been subject of great interest due to their unique physical and chemical properties. Thus the strong, size-dependent optical emission of many semiconductor nanostructures makes them promising candidates for use as fluorescent tags in the study of biological systems.

1.5 Literature Review

A brief review of research on ZnSe thin films are given below:

Al-Mamun et al. investigated $Cu_{2-x}Se$ thin films deposited on glass substrates using a low cost chemical bath deposition (CBD) technique [35]. XRD study of the $Cu_{2-x}Se$ films annealed at 523 K suggested a cubic structure with a lattice constant of 5.697 Å. Both as-deposited and annealed films show very low resistivity in the range of (0.04–0.15) × 10^{-5}Ω-

m. Transmittance and Reflectance were found in the range of 5–50% and 2–20% respectively. Optical absorption of the films results from free carrier absorption in the near infrared region with absorption coefficient of ~108 m^{-1}. The band gap for direct transition, direct E_g, varied in the range of 2.1–2.3 eV and that for indirect transition E_g, was in the range of 1.25–1.5 eV.

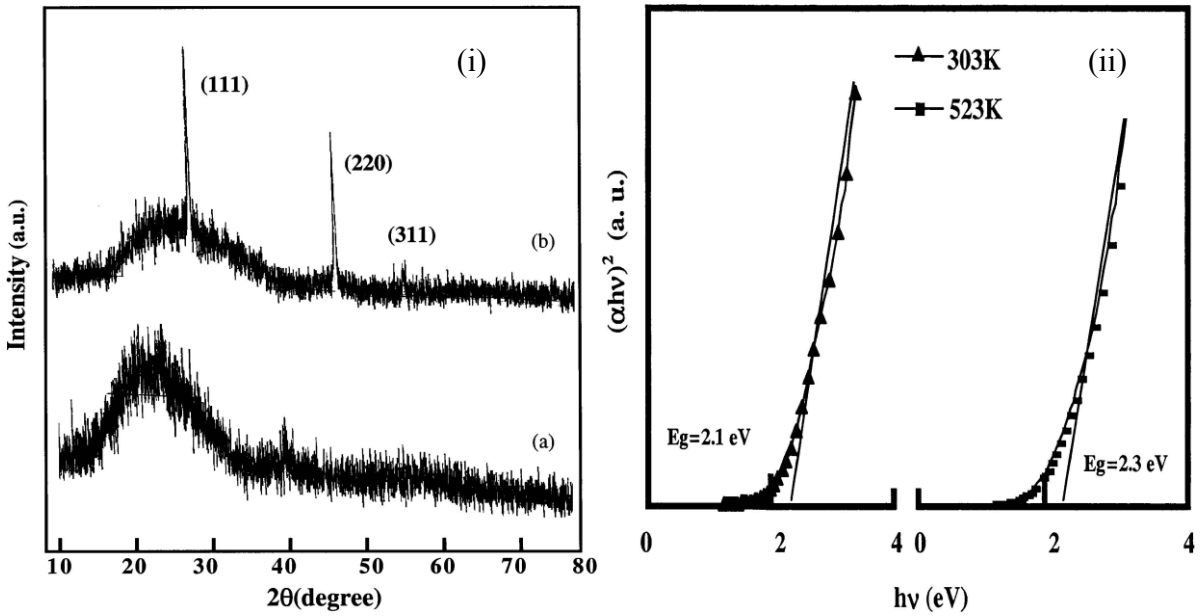

Fig. 1.10 : (i*)* X-ray diffraction patterns of (a) as-deposited Cu_{2-x} Se thin film and (b) Cu_{2-x}Se thin film annealed at 523 K in air for 1 h. (ii) $(\alpha hv)^2$ vs hv plots of Cu_{2-x} Se thin film (a) as-deposited, (b) annealed at 523 K for 1 h.

Alam et al. studied that CdSe layers were grown by electrodeposion method and deposited layers showed n-type conductivity, high transmittance and low absorbance in infrared region [36], band gap lied in the range 1.75–2.14 eV, polycrystalline structure with (111) preferential orientation, crack free surface with spherical grains. CdTe layers were grown by electrodeposition method and deposited layers showed p-type conductivity, band gap lies in the range 1.44–1.50 eV, polycrystalline structure with (1 1 1) preferential orientation, crack free surface with granular shaped grains. After getting the good quality CdSe and CdTe layers, a fabrication of CdTe/CdSe heterojunction solar cell structure was performed. I–V behavior of the metal contacts on CdTe films in dark condition showed anticipated rectifying behavior indicating a diode character. Current vs. voltage measurements confirmed the ability to deposit a p–n junction by electrodepositing CdTe thin film on a previously electrodeposited n-type CdSe film.

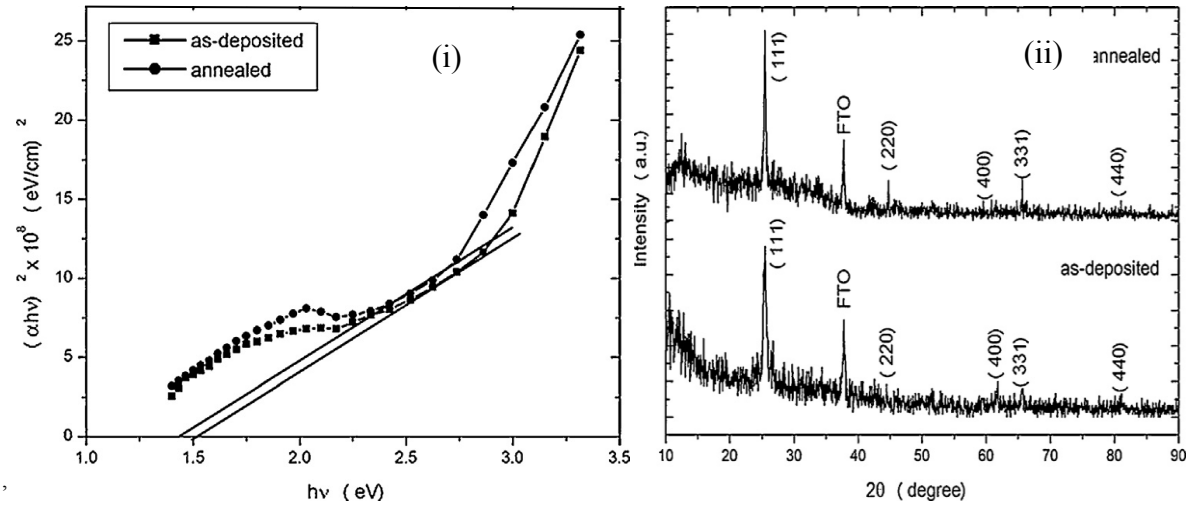

Fig. 1.11: (i) $(\alpha h\upsilon)^2$ as a function of photon energy ($h\upsilon$) of as-deposited and annealed CdTe film (ii) XRD pattern of as-deposited and annealed CdSe thin film.

Bakiyaraj et al. observed the flower-like ZnSe nanostructured thin films prepared by a CBD method on non-conducting glass substrate in an aqueous alkaline medium using sodium selenosulphate as Se^{2-} ion source [29]. XRD spectrum of the flower-like ZnSe thin they observed peak intensity of the (111) plane was relatively higher than those of other reflections. Peaks were relatively broadened indicating that the nanoflowers have very small crystallite size. The average grain size and strain were 2.70 nm and 10.34 $\times 10^{-2}$ respectively. The quantification calculation shows that the atomic ratio of Se:Zn is about 47.88 : 46.58. The size of each nanoflower is approximately in the range 100–200 nm. The band-gap values were estimated to be 2.80 eV for ZnSe thin films.

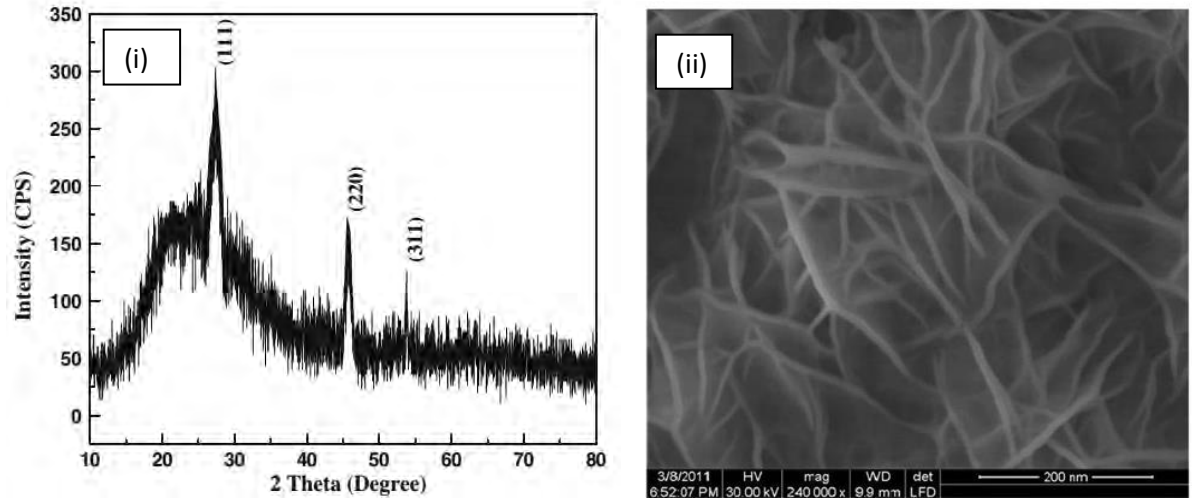

Fig. 1.12: (i) The X-ray diffraction pattern of flower-like ZnSe nanostructured thin films. (ii) Image of flowerlike ZnSe nanostructure allows high magnification view.

Wei et al. investigated ZnSe thin films deposited onto glass substrates by CBD method at different hydrazine hydrate concentrations and different concentrations of zinc sulfate solution [10]. For this, the zinc sulfate solution was used as the Zn^{2+} ion source, and the sodium selenosulfate solution was used as the Se^{2-} ion source, ammonia was used as a complexing agent. The crystal structure of ZnSe thin films was reported to be the zinc-blende structure, and the grain size of the ZnSe nanocrystals was about 6–10 nm. The optical transmittance of the ZnSe thin films reported over 80% in the wavelength range of 450–800 nm. The optical band-gaps of all the samples calculated from the transmission spectra were found to be 2.95–3.14 eV.

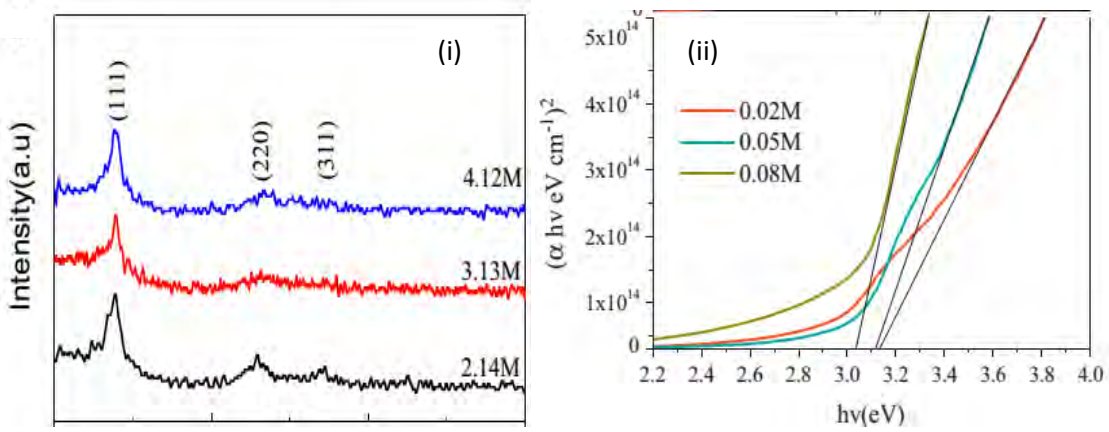

Fig. 1.13: (i) XRD patterns of the ZnSe nanocrystalline thin films and (ii) $(\alpha hv)^2$ vs. (hv) plots of the ZnSe nanocrystalline thin films deposited at different hydrazine hydrate concentrations.

Mehta et al. studied the effect of deposition parameters on structural, optical and electrical properties of nanocrystalline ZnSe thin films by CBD on non-conducting glass substrates [15]. The size of the nanoparticles was found of the order of 6-7 nm and the shape of the nanoparticles was spherical in nature. Structure of the nanoparticles observed by XRD technique was obtained both cubic and hexagonal. The band gap decreases from 3.5 eV to 3.0 eV with the increase in temperature and decrease in concentration of the bath. Electrical parameters like dark and photoconductivity increased as the particle size increasesd.

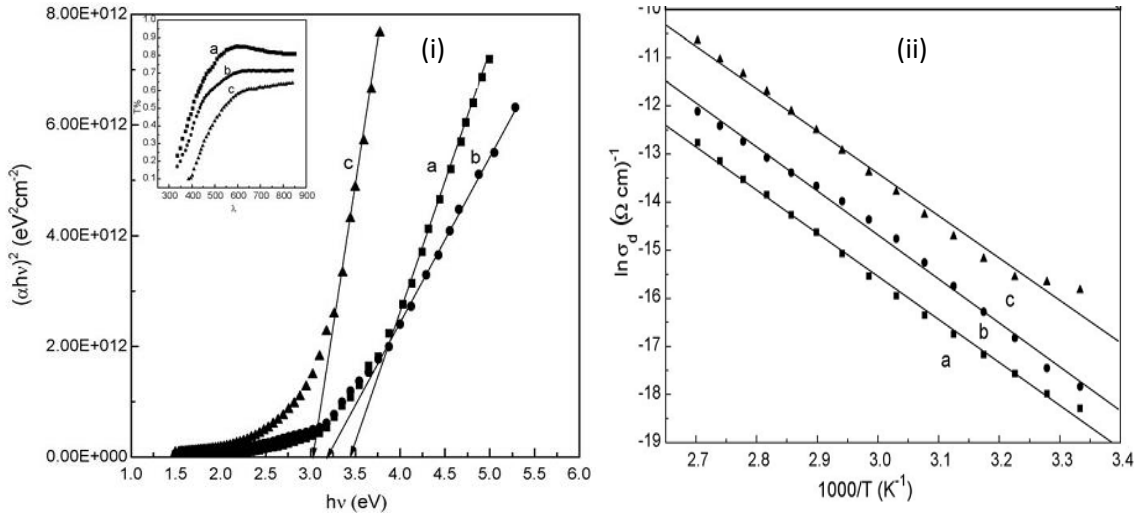

Fig. 1.14: (i) Plot of $(\alpha hv)^2$ vs. (hv) for n-ZnSe films deposited at pH 13 at temperatures (a) 318 K (b) 333 K (c) 353 K. (ii) Plot of log (σ_d) vs. $(1000/T)$ of n-ZnSe films deposited at different temperatures: (a) 318 K (b) 333 K (c) 353 K.

Hankare et al. investigated the Photo electrochemical applications of ZnSe synthesized by CBD method onto stainless steel plate [30]. Then reported that the ZnSe was a n-type conductor. The junction ideality factor of the film was 3.85. The flat band potential value found to be −0.530V (SCE) for ZnSe–polysulphide redox electrolyte. The barrier height was determined by measuring the reverse saturation current (I_o) through the junction at different temperature from 363 to 303 K. The barrier height value was found to be 0.171 eV. The power conversion efficiency was found to be 0.13%. The spectral response of a cell was recorded in the 400–900 nm wavelength range. The maximum current was obtained corresponding to λ= 440 nm gives band gap value 2.81 eV.

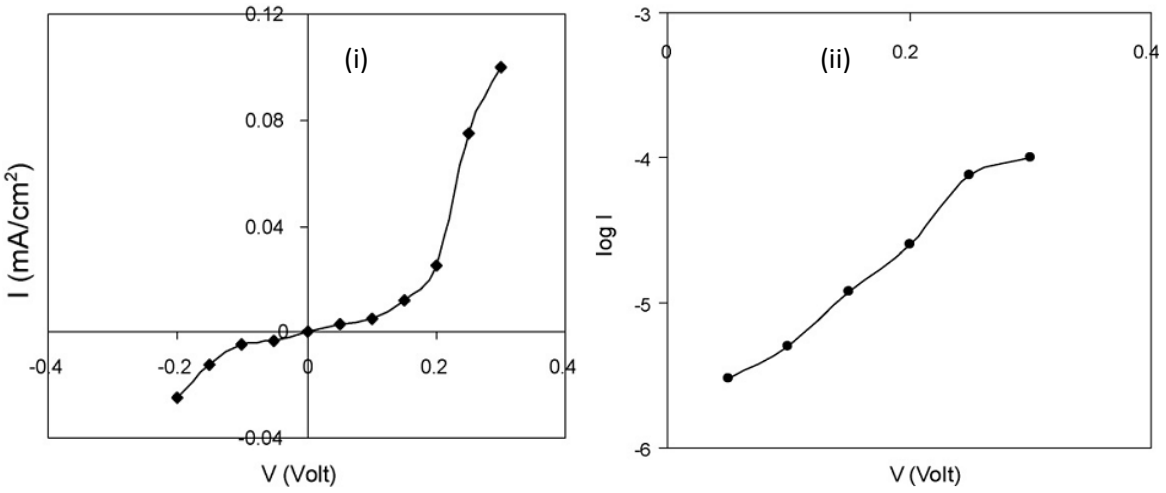

Fig.1.15: (i) *I–V* characteristics of ZnSe photoelectrode (in dark) (ii) Determination of junction ideality factor of ZnSe photoelectrode.

Deshmukh et al**.** observed the role of reducing environment in the chemical growth of ZnSe thin films with various Zn/Se ratio ($0.57 \leq x \leq 0.99$) obtained from an aqueous alkaline chemical bath at the optimized conditions (70^{o} C; 210mins and pH = 10±0.2) onto the glass substrates [11]. The XRD analysis of thin films were shown the crystalline and wurtizite structure with preferred <101> orientation. SEM micrographs revealed distinguishable spherical crystallites and non-uniformly distribution. The optical band gap (E_g) was determined for various Zn/Se ratio using $(\alpha hv) = A(hv\text{-}E_g)^n$ equation.

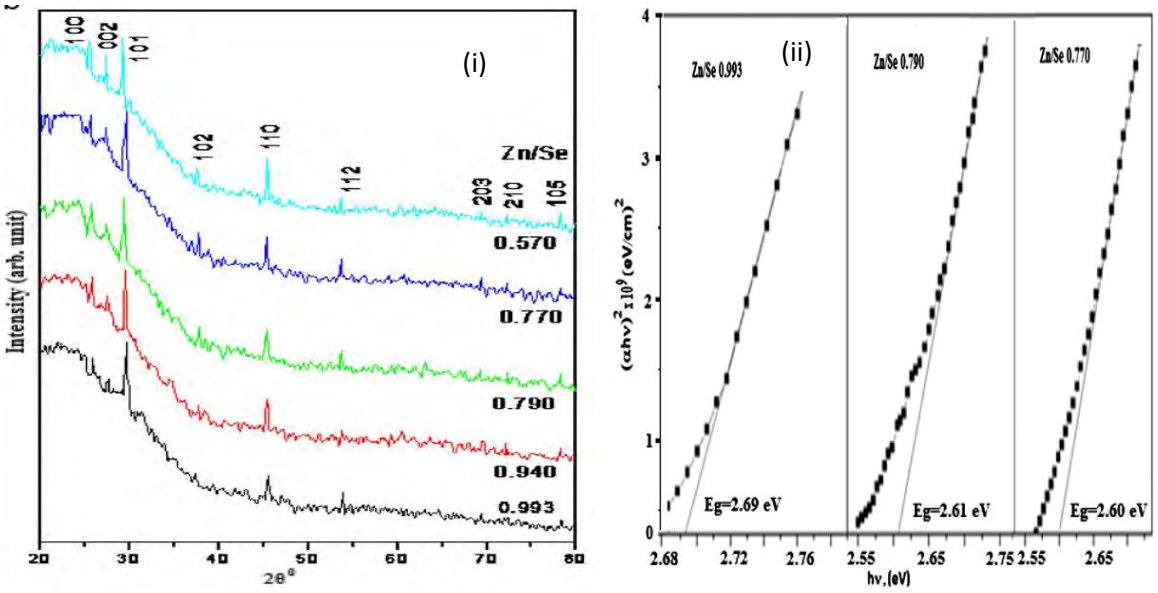

Fig. 1.16: (i) X-ray diffractograms of the as-deposited ZnSe thin films (ii) Variation of $(\alpha hv)^2$ versus hv for as-prepared ZnSe thin films.

Agawanea et al. reported the synthesis of CBD zinc selenide (ZnSe) thin films using a mixture of non-toxic complexing agent tri-sodium citrate (Na_3-citrate) and hydrazine hydrate at 80^{o}C. The effects of different amounts of Na_3-citrate and hydrazine hydrate on the morphological, structural, chemical, compositional and optical properties of CBD-thin films were investigated [24]. It's reported that the grain size of ZnSe thin films decrease with the increase of Na_3-citrate concentration. The XRD pattern for the ZnSe was to be cubic phase. The transmission of light range between 200-800nm observed to be 55-88% with variation of Na_3-citrate and hydrazine hydrate quantity and also observed varied absorption edge in the near ultraviolet wave – length region from 370 to 270 nm. The direct band gap energies of the ZnSe thin films varied from 2.65 to 3.55 eV depending upon the solution.

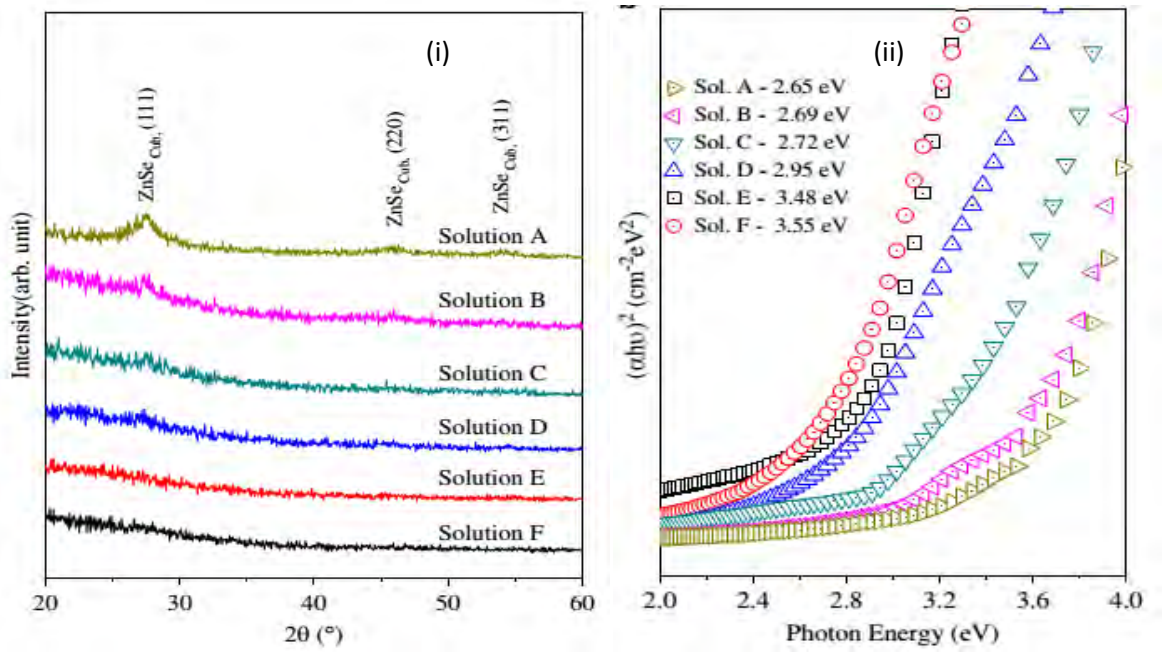

Fig. 1.17: (i) XRD patterns of the ZnSe thin films deposited using different solutions (ii) the plot of $(\alpha h\upsilon)^2$ vs. $h\upsilon$ of the ZnSe thin films deposited using various solutions.

Lohar et al. investigated the Structural, optical, photoluminescence, electrochemical, and photo electrochemical properties of Fe doped ZnSe hexagonal nanorods synthesized via the galvanostatic mode of deposition [32]. X-ray diffraction patterns were recorded for ZnSe, 1%, 3%, 5% Fe doped ZnSe thin films respectively suggested that the deposited films were polycrystalline in nature with hexagonal structure. The sphere like morphology of ZnSe were obsrerved but after Fe doping surface morphology was changed and 200 nm hexagonal nanorods were also observed for 1%, 3% and 5% Fe doped ZnSe thin films. The band gap energy of ZnSe was observed to be increasing after addition of Fe content. photoluminescence spectra exhibit peaks at 675.95 nm after the addition of Fe content. Only the peak intensity was observed to be increasing. For 5% Fe doped ZnSe hexagonal nanorods show an efficiency of 0.15%.

Dhanasekarana et al. studied the structural and optical properties of electro synthesized ZnSe thin films [40]. ZnSe thin films were prepared using an electrolyte containing $ZnSO_4$ and SeO_2. X-ray diffraction studies revealed that as-deposited films were polycrystalline nature. X-ray diffraction patterns of the films showed face centered cubic phase of ZnSe. The transmittance increased with wavelength from 40 to 80%. Optical absorption measurements represented that the deposited films have a direct band gap in the range between 2.52 and

2.61 eV which in turn confirms the stoichiometric formation of well crystallized ZnSe thin films.

Sadekar et al. investigated the nanocrystalline ZnSe thin films were deposited onto the glass substrates by solution growth technique [1]. The XRD peaks indicated that the film was nanocrystalline in nature. Crystallite size (*D*) of the film was calculated using Scherrer's formula and found to be ~10 nm. The as deposited films presented excellent adherence, uniform deposition, smooth morphological and nanocrystalline properties, confirmed by SEM, AFM and XRD analysis. The EDX study showed almost stoichiometric deposition. Energy band gap of the as-deposited ZnSe film reported to be 2.71 eV, which shows a blue emission. From *I–V* study with different illumination intensity showed almost linear photoresponse. The study of physical, optical and electrical properties reveal that the ZnSe thin film can be suitably employed in photosensor and/or optoelectronic applications.

Yücel et al. investigated the PbS thin films onto glass substrates grown by chemical bath deposition varying synthesis parameters including amount of tri-sodium citrate (0.2-0.8 mL), deposition time (14-34 h) and deposition temperature (26.6–43.4 °C). The XRD pattern of the thin film sample fabricated under the optimum deposition conditions revealed the polycrystalline nature of the film [34]. No characteristic peaks of impurity phases such as PbO or $PbSO_4$ were detected. The SEM image was showed that the surface of the film was compact, smooth, and uniform with no observed cracks or defects. Under optimal conditions, experimental band gap and predicted value were 2.20 eV and 1.98 eV, respectively.

1.6 Objectives of the Present Study

Objectives of this research are-

i. Development of the CBD system for the preparation of ZnSe thin films.
ii. Preparation of ZnSe thin films at different concentrations and for different time duration.
iii. Investigation of the structural information and surface morphology of the deposited thin films.
iv. Investigation of the optical properties to reveal the absorption, refractive index, dielectric constant, optical conductivity and band gap of the deposited thin films
v. The electrical properties have been studied to understand the *I-V* nature, temperature dependent resistivity, conductivity and activation energy of annealed ZnSe thin films.

References

[1] Sadekar, H. K., Ghule, A. V., Sharma, R., 'Nanocrystalline ZnSe thin films prepared by solution growth technique for photosensor application', Composite Part B, vol. 44, p. 553–557, (2013).

[2] Pardo, A. P., Gonzalez, H. G., Castro-Lora, López-Carreño, L. D., Martínez, H. M, Salcedo, N. J. T., 'Physical properties of ZnSe thin films deposited on glass and silicon substrates', J. Phys. Chem. Solid, vol.75, p.713–725, (2014).

[3] Akhtar, M. S., Malik, M. A., Riaz, S., Naseem, S., O'Brien, P., 'Optimising conditions for the growth of nanocrystalline ZnS thin films from acidic chemical baths', Mater. Sci. Semicond. Process., vol. 30, p. 292–297, (2015).

[4] Chander, S. and M. S. Dhaka, 'Physical properties of vacuum evaporated CdTe thin films with post-deposition thermal annealing', J. Physica E, vol. 73, p. 35-39, (2015).

[5] Xu, J., Wang, W., Zhang, X., Chang, X., Shi, Z., Haarberg, G. M., 'Electro deposition of ZnSe thin film and its photocatalytic properties', J. Alloys Compd., vol. 632, p.778–782, (2015).

[6] Mlowe, S., Nyamen, L. D., Ndifon, P. T., et al., 'Aerosol assisted chemical vapor deposition (AACVD) of CdS thin films from heterocyclic cadmium (II) complexes', Inorg. Chim. Acta, vol. 434, p.181–187, (2015).

[7] Wu, X. J., Zhang, Z. Z., Zhang, J. Y., et al., 'Growth of FeSe on general substrates by metal-organic chemical vapor deposition and the application in magnet tunnel junction devices', Thin Solid Film, vol. 516, p. 6116–6119, (2008).

[8] Tseng, Y. H., Yang, C. S., Wu, C. H., et al., 'Growth mechanism of $CuZnInSe_2$ thin films grown by molecular beam epitaxy', J. Cryst. Growth, vol. 378, p. 158–161, (2013).

[9] Khan, T. M., Zakria, M., Ahmad, M., Shakoor, R. I., 'Optoelectronic study and annealing stability of room temperature pulsed laser ablated ZnSe polycrystalline thin films', J. Lumin., vol. 147, p. 97–106, (2014).

[10] Wei, A., Zhao, X., Liu, J., Zhao, Y., 'Investigation on the structure and optical properties of chemically deposited ZnSe nanocrystalline thin films', Physica B, vol. 410, p. 120–125, (2013).

[11] Deshmukh, L. P., Pingale, P. C., Kamble, S. S., Mane, S.T., Pirgonde, B. R., Sharonb, M., Sharon, M., 'Role of reducing environment in the chemical growth of zinc selenide thin films', Mater. Lett., vol. 92, p. 308–312, (2013),

[12] Ghosh, B., Kumar, K., Singh, B. K., Banerjee, P., Das, S., 'Growth of CdS thin films on indium coated glass substrates via chemical bath deposition and subsequent air annealing', Appl. Sur. Sci., vol. 320, p. 309–314, (2014).

[13] Hone, F. G., Ampong, F. K., Abza, T., Nkrumah, I., Paal, M., Nkum, R. K., Boakye, F., 'The effect of deposition time on the structural, morphological and optical band gap

of lead selenide thin films synthesized by chemical bath deposition method', Mater. Lett., vol. 155, p. 58–61, (2015).

[14] Aguileraa, M. L. A., Márqueza, J. M. F., Trujillob, M. A. G., Morales, G. R., Galán, O. V., 'Influence of CdS thin films growth related with the substrate properties and conditions used on CBD technique', Energy Procedia. vol. 44, p. 111 – 117, (2014).

[15] Mehta, C., Saini, G. S. S., Abbas, J. M., Tripathi, S. K., 'Effect of deposition parameters on structural, optical and electrical properties of nanocrystalline ZnSe thin films', Appl. Surf. Sci., vol. 256, p. 608–614, (2009).

[16] Chopra K. L. and Das S. R., Thin film Solar Cells, Plenum Press, New York (1983).

[17] Morales, J., Sanchez, L., Martin, F., Ramos-Barrado, J. R., and Sanchezz, M., 'Use of low- temperature nano structured CuO thin films deposited by spray-pyrolysis in lithium cells', Thin Solid Film, vol. 474, p. 133-140, (2005)

[18] Behrisch, R., 'Sputtering by Particle Bombardment', Springer, Berlin (1981).

[19] Vispute, R. D., Narayan, J., Wu, H., and Jagannadham, K., 'Epitaxial growth of AIN thin films on silicon (111) substrates by pulsed laser deposition', J. Appl. Phy., vol. 77, p. 4724 - 4728, (1995).

[20] Mahalingam, T., Kathalingam, A., Lee, S., Moon, S., Kim, Y. D., 'Studies of Electrosynthesized Zinc Selenide Thin Films', J. New Mater. Electrochemi. Sys., vol. 10, p. 15-19, (2007).

[21] Jacob, A. A., Balakrishnan, L., Meher, S. R., Shambavi, K., Alex, Z. C., 'Structural, optical and photodetection characteristics of Cd alloyed ZnO thin film by spin coating', J. Alloy. Compound., vol. 695, p. 3753–3759, (2016)

[22] Slonopas, A., Ryan, H., Foley, B., Sun, Z., Sun, K. el al., 'Growth mechanisms and their effects on the opto-electrical properties of CdS thin films prepared by chemical bath deposition', Mater. Sci. Semi. Process., vol. 54, p. 24-31, (2016).

[23] Huang. F., Hou, J., Wang, H., Tang, H., et al., 'Impacts of surface or interface chemistry of ZnSe passivation layer on the performance of CdS/CdSe quantum dot sensitized solar cells', Nano Energy, vol. 32, p. 433–440, (2016).

[24] Rana, T. R., Kim, J., 'Phase engineering of CBD grown tin sulfide films by post-sulfurization and solar cell application', Current. App. Phy., vol. 16, p. 1666-1673, (2016).

[25] Ma, L., Ai, X., Wu, X., 'Effect of substrate and Zn doping on the structural, optical and electrical properties of CdS thin films prepared by CBD method', J. Alloy Compound., vol, 691, p. 399–406, (2016).

[26] Aguilera, M. L. A., Márquez, J. M. F., Trujill, M. A. G., Kuwahara, Y. M., et al., 'Influence of CdS thin films growth related with the substrate properties and conditions used on CBD technique', Erg. Proce. vol. 44, p. 111 – 117, (2014).

[27] Massaccesi, S., Sanchez, S. and Vedel, J., J. Electrochem. Soc., vol.140**,** p. 2540-2544, (1993).

[28] Lyons, L. E., Morris, G. C., Horton, D. H., Keyes, J. G., J. Electranal. Chem., vol. 168, p. 101-105, (1984)

[29] Bakiyaraj G., Dhanasekaran, R., 'Synthesis and characterization of flower-like ZnSe nano structured thin films by chemical bath deposition (CBD) method', Appl. Nanosci. vol. 3. p. 125-131, (2013).

[30] Hankare, P. P., Chate, P. A., Chavan, P. A., Sathe, D. J., 'Chemical deposition of ZnSe thin films: Photoelectrochemical applications', J. Alloys Compd., vol. 461, p. 623–627, (2008).

[31] Agawanea, G. L., Shin, S. W., Gurav, K. V., Moholkar, A. V., Lee, J. Y., Patil, P. S., Yun, J. H., Kim, J. K., 'Novel reduced toxic route synthesis and characterization of chemical bath deposited ZnSe thin films', Ceramic. Int., vol. 40, p. 367–374, (2014).

[32] Lohar, G. M., Shinde, S. K., Rath, M. C., Fulari, V. J., 'Structural, optical, photoluminescence, electrochemical, and photoelectrochemical properties of Fe doped ZnSe hexagonal nanorods', Mater. Sci. Semicond. Process. vol. 26, p. 548–554, (2014).

[33] Dhanasekaran, V., Mahalingam, T., Rhee, J., Chu, J. P., 'Structural and optical properties of electrosynthesized ZnSe thin films', vol. 124, p. 255-260, (2013).

[34] Yücel, E., Yücel, Y., Beleli, B., 'Optimization of synthesis conditions of PbS thin films grown by chemical bath deposition using response surface methodology', J. Alloy. Compound., vol. 642, p. 63–69, (2015).

[35] AL-Mamun, Islam, A. B. M. O., Bhuiyan, A. H., 'Structural, electrical and optical properties of copper selenide thin films deposited by chemical bath deposition technique', J. Mater. Sci.: Mater. Electronic., vol. 16, p**.** 263– 268, (2005).

[36] Alam, S., Pathan, M. A. K., Siddiquee, K. A. M. H., Islam, A. B. M. O., Gafur, M. A., Saha, D. K., Mori, M., Tambo, T., 'Optical and structural characterization of CdSe and CdTe layers and fabrication of a CdTe/CdSe structure', Optik, vol. 124, p. 2165–2170, (2013).

CHAPTER 2

Theoretical Background

2.1 CBD Process in Details

There are three different possibilities for the process of thin film deposition in CBD technique. First possibility is the ion-by-ion process in which the ions condense at the reacting surface to form the film [1]. The second is the cluster-by-cluster process in which colloidal particles that are formed in the solution as a result of homogenous reaction gets adsorbed at the substrate surface to form thin layers. Usually both these processes may occur or may interact each other, leading to films in which colloidal material is included in the growing films. The predominance of one mechanism over the other is governed by the extent of heterogeneous and homogeneous nucleation. Heterogeneous nucleation is a result of reaction occurring at the surface of the substrate while homogeneous nucleation is a result of reaction occurring within the bulk of the solution.

2.2 Factors Influencing the Deposition Process

The various factors that influence the deposition process in CBD technique are described below [2].

2.2.1 Nature of the Reactants

Nature of the reactants influences the composition of the products. In the preparation of copper selenide it is observed that when sodium selenosulfate is used as the selenium source, the final phase is usually Cu_2Se, while the use of dimethylselenourea results is CuSe phase. The growth kinetics also depends on the nature of reactants. For example, when metal sulfate is employed to deposit metal selenide films using sodium selenosulfate, the rate of deposition decreases and the terminal thickness increases. Here the SO_4^{2-} ions obtained from the metal sulfatereduce the concentration of Se^{2-} ions.

2.2.2 Concentration of Reactants

The deposition rate and terminal thickness initially increases with an increase in the ionic concentration of the reactants. However, at high concentration the precipitation becomes very fast, leading to decrease in film thickness on the substrate.

2.2.3 Nature of Complexing Agent

Nature of complexing agents may influence the final products. For example, when ammonia is used as a complexing agent for the preparation of ZnS thin film, it is found to result in

$ZnO/Zn(OH)_2$ phase rather than ZnS. However when two complexants ammonia and hydrazine are used, the oxide and hydroxide phases could be avoided to a great extend [2].

2.2.4 Concentration of Complexing Agent

In a general reaction, the metal ion concentration decreases with increasing concentration of the complexing ions. Consequently the rate of reaction and hence precipitation are reduced leading to a larger terminal thickness of the film. Such behavior has been observed for CdSe, CdS, PbSe and ZnS films.

2.2.5 Reaction Temperature

Temperature of deposition is another factor that influences the rate of reaction. As temperature increased dissociation of the complex increases. The kinetic energy of the molecules also increases leading to greater interaction between ions. This will result in increase or decrease of terminal thickness, depending on the extent of super saturation of the solution.

2.2.6 Reaction pH

When the pH value of the reaction bath increases, the metal complex usually becomes more stable, reducing the availability of free metal ions. This will decrease the reaction rate resulting in higher terminal thickness. Recently there was a report by Yücel et al. [3], on a novel approach to the deposition of CdS by CBD. He succeeded in depositing CdS from an acidic bath for the first time. It was observed that the film properties were very much different in the case of such films when compared with that of films deposited from alkaline bath.

2.2.7 Duration of Reaction

The dependence of film thickness on the duration of deposition (all the other factors remaining the same) has been studied in detail for different semiconductor thin films obtained by CBD technique [4]. In general, the growth of good quality semiconductor thin films proceeds at a slow rate. This technique of CBD is ideally suited for producing uniform films with thickness in the 0.05–0.3 μm range in most cases and rarely to an extend of few microns.

2.2.8 Nature of Substrates

This factor plays a major role in the reaction kinetics and in the adhesion of the deposited film. Hence cleaning of substrate surface form the first important step in the thin film deposition

procedure. Higher deposition rates and terminal thickness are observed for those substrates whose lattices and lattice parameters match well with those of the deposited material. During deposition of PbSe thin films under similar conditions, higher rates and thickness have been observed on Ge rather than on Si because of matching of the lattice parameters of PbSe with those of Ge [5]. On a pre-sensitised substrate surface, no incubation period for nucleation is observed since nucleation centers already exist on the substrate. Also when the substrates are suspended in the container before forming the complex in the solution, film thickness increases in a manner similar to that of the sensitised surface.

2.2.9 Spacing of Substrates

Recently Ma et al. [6] studied the film thickness as a function of separation between substrates in batch production. It was observed that film thickness reach "an asymptotic maximum with increase in substrate separation. This behavior is explained on the basis of the existence of a critical layer of solution near the substrate, within which the relevant ionic species have a higher probability of interacting with "the thin film layer that contribute to precipitate formation. The critical layer depends on the solution composition, the temperature of the bath, as well as the duration of deposition. In the case of CdS thin film, this critical layer is found to extend from 0.5 to 2.5 μm from the substrate surface, depending on the deposition conditions. The above mentioned influencing factors do not actually affect the chemical reaction individually, but the final result is due to the cumulative effect of inter dependence of all these factors.

2.3 Surface Morphological Characterization

Scanning Electron Microscopy (SEM)

SEM utilizes an electron beam to scan and produce a magnified image of the specimen sample. SEM is similar to optical microscopy; the exception is that electrons are used instead of photons. Much larger magnifications are, therefore, possible with a SEM since electron wavelengths are much smaller than photon wavelengths and the depth of field is much larger.

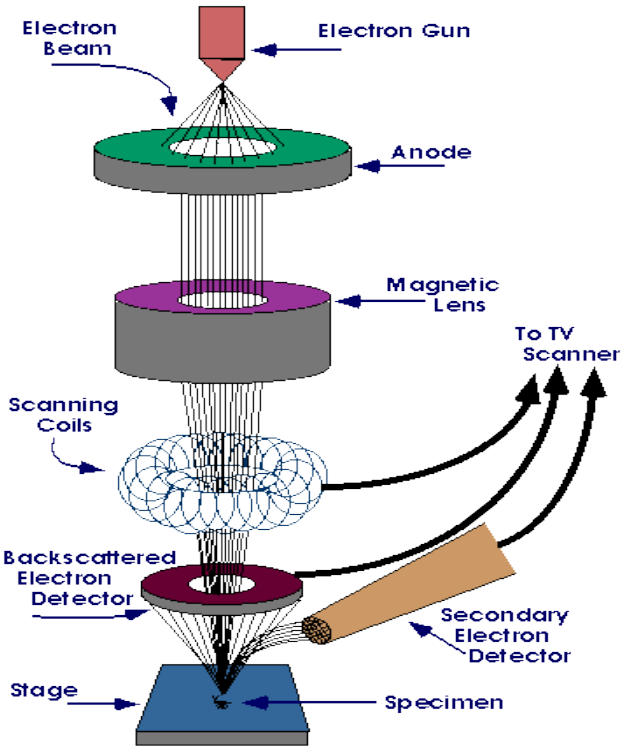

Figure 2.1: Schematic representation of SEM and EDX operation.

The resolution of the SEM can approach a few nm and it can operate at magnifications that are easily adjusted. Not only is topographical information produced in the SEM, but information concerning the composition near surface regions of the material is provided as well. In the SEM, a source of electrons is focused (in vacuum) into a fine probe that is rastered over the surface of the specimen. The main operation of the instrument is shown in Fig.2.1. An electron beam is generated by an electron gun at the top of the column. This beam is focused by two magnetic lenses and deflected by two scanning coils before hitting the sample in a very small spot. To avoid undue scattering and absorption of the electrons, the column and sample chamber is operated under vacuum. When the electrons penetrate into the sample, several processes take place as they are being absorbed. Some are reflected (back scattered electron, BSE) out of the sample and are collected by a suitable detector. These electrons can be used to obtain information on the mean atomic number in the part of the sample from which they originate. Secondary electron (SE), with very low energy, is also released from the sample from an area close to the spot where the primary electrons enter. Collected by a suitable detector, these are used to obtain information on the topography of the sample. Thus, this signal is used to modulate the intensity on a viewing screen, which is scanned synchronously with the primary beam in the column. Thereby an image is generated on the viewing screen with high brightness in areas with a strong signal from the detector,

and darker areas, where weak signal are detected. To select an area of investigation, the sample is mounted on a special stage, with allows translation, tilt and rotation of the sample. This stage can be controlled from outside the vacuum chamber.

Energy Dispersive X-Ray (EDX)

Energy dispersive x-ray spectrometer (EDX or EDS) is one of the most common analytical attachments to the SEM. The high energy primary electron beam causes emission of a core electron which leaves the atom in an excited state. The atom undergoes deexcitation by x-ray emission (Fig. 2.1) which is characteristic of the elements from which they originate and thus it helps for elemental analyses of the solid under probe. The emitted X-rays are detected by a solid state detector which is positioned in the vicinity of the sample. The detector is a Li-doped Si crystal which is biased at a high voltage. X-rays interacting with the detector create electron-hole pairs which are swept through the detector due to the high voltage bias. The charge pulse is converted to a voltage pulse by a charge sensitive preamplifier. The useful energy range for EDX systems is from 1.0 to 220 k eV which limits the analysis to elements with $Z > 9$. EDX detectors with thin protective layers or no protective layer, when used in ultra-high vacuum systems, permit analysis of the lighter elements down to boron. The analysis depth is dependent on the path length of the X-rays, not the primary electron beam. As a result, EDX signals may originate from depths of 0.5 m or more. The major advantage of EDX is its utility in the pulse counting mode and in the detection of the characteristic X-rays for all elements above F in the periodic table.

2.4 Structural Characterization

X-ray Diffraction (XRD)

X-ray diffraction [7, 8] is the most precise technique for studying the structure of solids, generally requiring no elaborate sample preparation and is essentially non-destructive. Thin surface films, up to about 1000 Å thick, can be investigated using X-ray diffraction [9, 10]. Thicker films can be characterized by reflection high-energy electron diffraction (RHEED). Analysis of the diffraction patterns obtained by these techniques and comparison with standard ASTM data can reveal the existence of different crystallographic phases in the film, their relative abundance, the lattice parameters, and any preferred orientations. From the width of the diffraction line, it is possible to estimate the average grain size in the film [11].

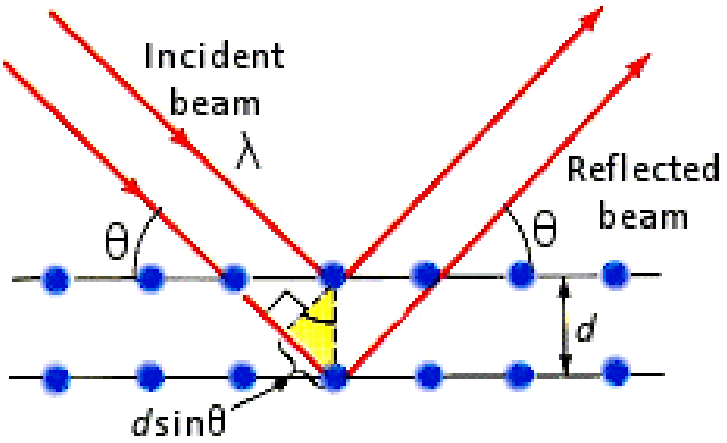

Figure 2.2**:** Schematic diagram of X-ray diffraction process.

The technique of XRD is based on Bragg‟s law

$$n\lambda = 2d\sin\theta \qquad (2.1)$$

where n is the order of diffraction, λ is the wavelength of the x-rays, d is the distance between two neighboring planes, θ is the angle between the incident x-ray and the crystalline plane (in radians). As shown in Fig. 2.2 when a monochromatic X-ray beam of wavelength λ is incident on the lattice planes of a crystal at an angle θ, diffraction occurs only when the distance traveled by the rays reflected from successive planes differs by a complete number n of wavelengths. In polycrystalline materials, several d values satisfy Bragg‟s law by varying the angle θ.

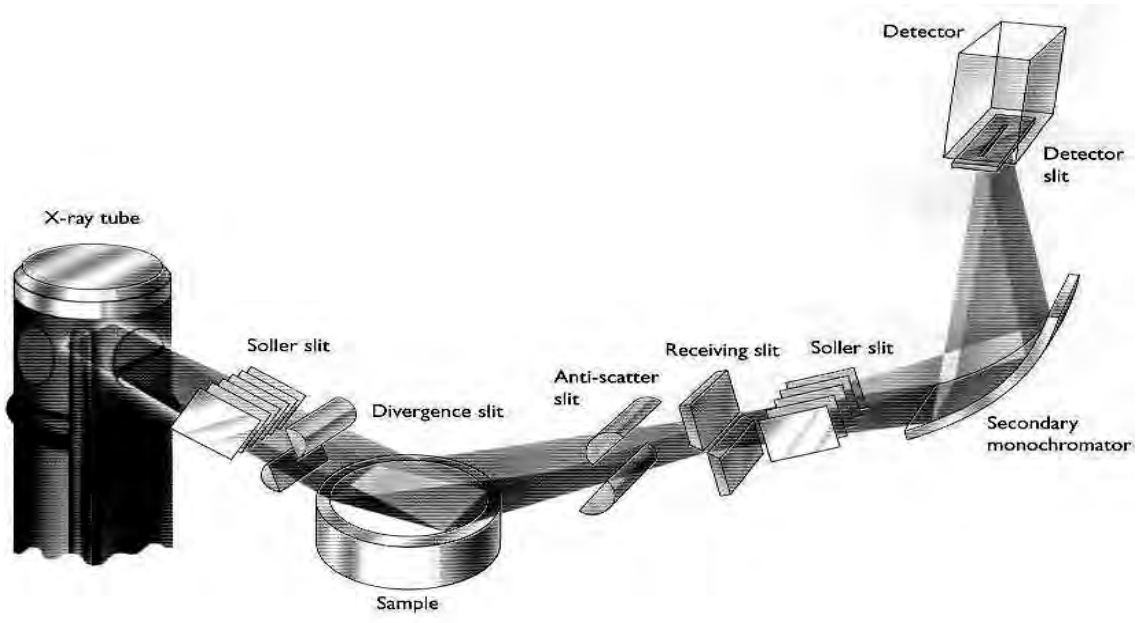

Figure 2.3: Schematic of the X-ray powder diffractometer.

The x-ray source provides a polychromatic radiation produced from a copper target source. The monochromator positioned in front of the detector is tuned to select only the CuK_α emission line from the source. The system can then be viewed as operating with a monochromatic source whose wavelength is 1.5406 Å. The sample is rotated around an axis. As the scanning proceeds, the detector is rotated around the same axis to detect the diffracted beam. The instrument is fully computer controlled. Fig. 2.3 shows a schematic of the X-ray powder diffractometer. The x-rays detected from the sample surface have been diffracted by families of planes, according to Bragg‟s law. The result of XRD measurements is a diffractogram, which is a plot of the intensity (number of counts) versus the angle. The different phases in the crystal (from peak positions), phase concentrations (from peak heights), crystallite sizes (from peak widths) and amorphous content (from background hump) can be deduced from a diffractogram.

2.5 Optical Measurement

2.5.1 Beer-Lambert law

The Beer-Lambert law (or Beer's law) [12] is the linear relationship between absorbance and concentration of an absorbing species. The general Beer-Lambert law is usually written as:

$$A = \alpha \times b \times c \qquad (2.2)$$

Where A is the measured absorbance, $\alpha(\lambda)$is a wavelength-dependent absorbance coefficient, b is the path length, and c is the analyzed concentration. When working in concentration units of molarity, the Beer-Lambert law is written as

$$A = \varepsilon \times b \times c \qquad (2.3)$$

Where ε is the wavelength-dependent molar absorptivity coefficient with units of $M^{-1}cm^{-1}$. Experimental measurements are usually made in terms of transmittance (T), which is defined as:

$$T = I / I_o \qquad (2.4)$$

Where I is the light intensity after it passes through the sample and I_o is the initial light intensity. The relation between A and T is:

$$A = -\log T = -\log (I / I_o) \qquad (2.5)$$

Modern absorption instruments can usually display the data as transmittance, %transmittance, or absorbance. An unknown concentration of an analyte can be determined by measuring the amount of light that a sample absorbs and applying Beer's law. If the absorptivity coefficient

is not known, the unknown concentration can be determined using a working curve of absorbance versus concentration derived from standards.

Derivation of the Beer-Lambert law

The Beer-Lambert law can be derived from an approximation for the absorption coefficient for a molecule by approximating the molecule by an opaque disk whose cross-sectional area,σ, represents the effective area seen by a photon of frequency ν. If the frequency of the light is far from resonance, the area is approximately 0, and if ν is close to resonance the area is a maximum. Taking an infinitesimal slab, dz, of sample (Figure 2.4)

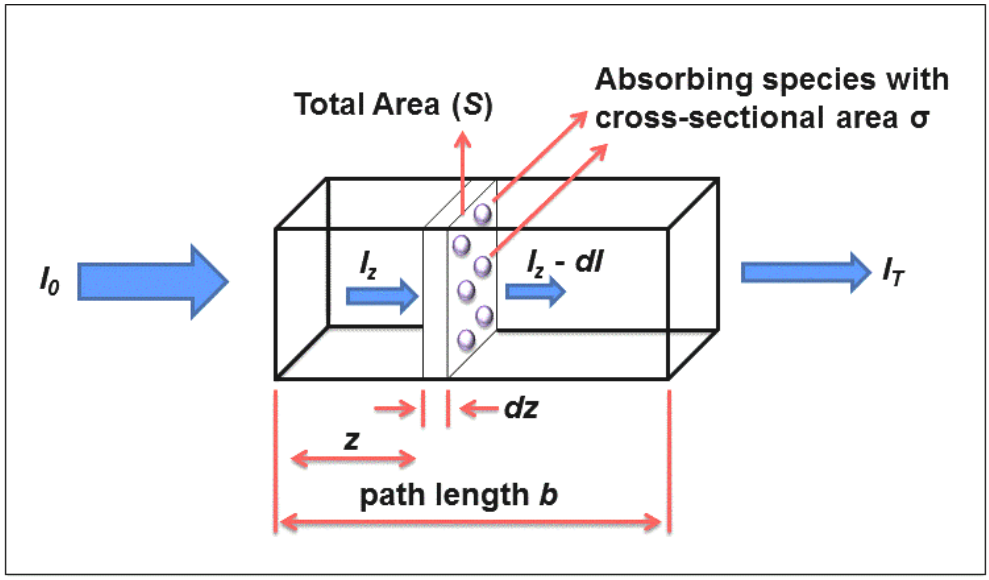

Figure 2.4: Absorption of light by a sample

I_o is the intensity entering the sample at $z = 0$, I_z is the intensity entering the infinitesimal slab at z, dI is the intensity absorbed in the slab, and I is the intensity of light leaving the sample. Then, the total opaque area on the slab due to the absorbers is $\sigma \times N \times A \times dz$. Then, the fraction of photons absorbed will be $\sigma \times N \times A \times dz / A$ so,

$$dI / I_z = - \sigma \times N \times dz \qquad (2.6)$$

Integrating this equation from $z = 0$ to $z = b$ gives:

$$\ln(I) - \ln(I_o) = - \sigma \times N \times b$$

$$\text{or, } - \ln(I / I_o) = \sigma \times N \times b.$$

Since,c (moles/liter), N (molecules/cm^3)×(1 mole / 6.023x10^{23} molecules)×1000 cm^3 / liter and 2.303 × log(x) = ln(x) then,

$$- \log(I / I_o) = \sigma \times (6.023 \times 10^{20} / 2.303) \times c \times b$$

$$\text{Or, } - \log(I / I_o) = A = \varepsilon \times b \times c$$

Where $\varepsilon = \sigma \times (6.023 \times 10^{20} / 2.303) = \sigma \times 2.61 \times 10^{20}$, and ε is called absorptivity. Thus the intensity of the transmitted light can be expressed as $I = I_o\, e^{-\alpha d}$ where d is the path length through the sample and α is the absorbance coefficient. This equation can be written as,

$$ln\,(I/I_o) = -\alpha \times d$$

$$\text{or, } 2.303 \log (I/I_o) = -\alpha \times d$$

$$\text{or, } \alpha = \frac{2.303\ (\log (I/I_o)}{d}$$

$$\text{or, } \alpha = \frac{2.303\ A}{d} \qquad (2.7)$$

Electronic transitions

The absorption of UV or visible radiation corresponds to the excitation of outer electrons. There are three types of electronic transition which can be considered;

1. Transitions involving π, σ, and *n* electrons
2. Transitions involving charge-transfer electrons
3. Transitions involving *d* and *f* electrons (not covered in this Unit)

When an atom or molecule absorbs energy, electrons are promoted from their ground state to an excited state. In a molecule, the atoms can rotate and vibrate with respect to each other. These vibrations and rotations also have discrete energy levels, which can be considered as being packed on top of each electronic level (Figure 2.5).

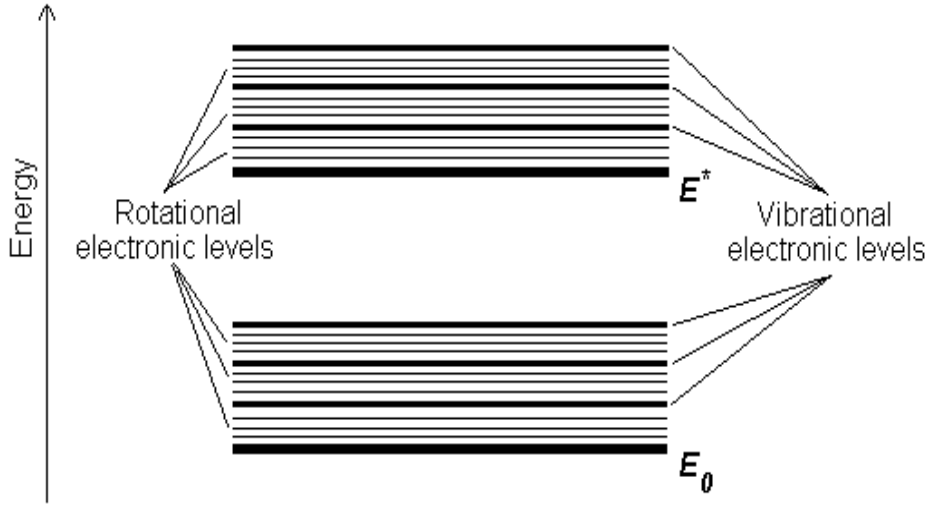

Figure 2.5: Vibrational and rotational energy level

Absorbing species containing π, σ, and *n* electrons

Absorption of ultraviolet and visible radiation in organic molecules is restricted to certain functional groups (chromophores) that contain valence electrons of low excitation energy. The spectrum of a molecule containing these chromophores is complex. This is because the superposition of rotational and vibrational transitions on the electronic transitions gives a combination of overlapping lines. This appears as a continuous absorption band. Possible electronic transitions of π, σ, and *n* electrons are;

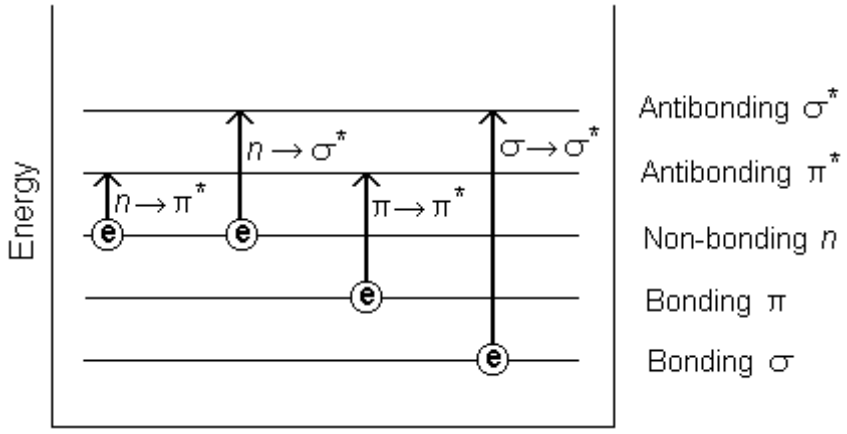

Figure 2.6: Transition of electron into different energy level

σ→ σ* Transitions

An electron in a bonding σ orbital is excited to the corresponding anti bonding orbital. The energy required is large. For example, methane (which has only C-H bonds, and can only undergo σ→ σ* transitions) shows an absorbance maximum at 125 nm. Absorption maxima due to σ→ σ* transitions are not seen in typical UV-Vis. spectra (200 - 700 nm).

***n*→σ* Transitions**

Saturated compounds containing atoms with lone pairs (non-bonding electrons) are capable of $n \rightarrow \sigma^*$ transitions. These transitions usually need less energy than $n \rightarrow \sigma^*$ transitions. They can be initiated by light whose wavelength is in the range 150 - 250 nm. The number of organic functional groups with $n \rightarrow \sigma^*$ peaks in the UV region is small.

***n*→σ* and π→π* Transitions**

Most absorption spectroscopy of organic compounds is based on transitions of *n* or π electrons to the π^* excited state. This is because the absorption peaks for these transitions fall

in an experimentally convenient region of the spectrum (200 - 700 nm). These transitions need an unsaturated group in the molecule to provide the π electrons. Molar absorbtivities from $n \rightarrow \sigma^*$ transitions are relatively low, and range from 10 to 100 L mol^{-1} cm^{-1}. $\pi \rightarrow \pi^*$ transitions normally give molar absorbtivities between 1000 and 10,000 L mol^{-1} cm^{-1}. The solvent in which the absorbing species is dissolved also has an effect on the spectrum of the species. Peaks resulting from $n \rightarrow \sigma^*$ transitions are shifted to shorter wavelengths (blue shift) with increasing solvent polarity. This arises from increased solvation of the lone pair, which lowers the energy of the *n* orbital. Often (but not always), the reverse (i.e. red shift) is seen for $\pi \rightarrow \pi^*$ transitions. This is caused by attractive polarization forces between the solvent and the absorber, which lower the energy levels of both the excited and unexcited states. This effect is greater for the excited state, and so the energy difference between the excited and unexcited states is slightly reduced - resulting in a small red shift. This effect also influences $n \rightarrow \sigma^*$ transitions but is overshadowed by the blue shift resulting from solvation of lone pairs.

2.5.2 Direct and Indirect optical Transitions

The equilibrium situation in semiconductor can be disturbed by generation of carriers due to optical photon absorption. Optical photon incident on any material may be reflected, transmitted or absorbed. The phenomena of radiation absorption in a material is all together considered to be due to (1) inner shell electrons, (2) valence band electrons, (3) free carriers including electrons and (4) electrons bound to localized impurity centers or defects of some type. In the study of fundamental properties of the semiconductors, the absorption by the second type of electrons is of great importance. In an ideal semiconductor, at absolute zero temperature the valence band would be completely full of electrons, so that electron could not be excited to higher energy state from the valence band. Absorption of quanta of sufficient energy tends to transfer of electrons from valence band to conduction band. The optical absorption spectra of semiconductors generally exhibits a sharp rise at a certain value of the incident photon energy which can be attributed to the excitation of electrons from the valence band to conduction band (may also involve acceptor or donor impurity levels, traps, excitons, etc). The conservation of energy and momentum must be satisfied in optical absorption process. Basically there are two types of optical transitions that can occur at the fundamental edge of the crystalline semiconductor, direct and indirect. Both involve the interaction of an electromagnetic wave with an electron in the valence band, which is rose across the fundamental gap to the conduction band. However, indirect transition involves simultaneous interaction with lattice vibration. Thus the wave vector of the electron can change in the

optical transition. The momentum change being taken or given up by phonon. Direct inter band optical transition involves a vertical transition of electrons from the valence band to the conduction band such that there is no change in the momentum of the electrons and energy is conserved as shown in Fig. 2.6. The optical transition is denoted by a vertical upward arrow. The forms of the absorption coefficient ‚α' as a function of photon energy $h\upsilon$ depend on energy of $N(E)$ for the bands containing the initial and final states. For simple parabolic bands and for direct transitions [7].

$$\alpha = A\,(h\upsilon - E_g)^n / h\upsilon \qquad (2.8)$$

where A is a constant depending upon the transition probability for direct transition, n =1/2 or 3/2 depending on whether the transition is allowed or forbidden in the quantum mechanical sense. E_g is the optical gap. Let"s visualize a situation given in Fig. 2.7 where inter band transition takes place between different k–states. Since these must satisfy the momentum conservation laws, the only way such transition can take place is through the emission or absorption of a phonon with wave vector q i.e.

$$k' \pm q = k + K \qquad (2.9)$$

The transitions defined by Equation (2.11) are termed as indirect transitions. For indirect transitions [22]

$$\alpha h\upsilon = A\,(h\upsilon - E_g)^n \qquad (2.10)$$

For allowed transition n = 2 and for forbidden transitions n = 3.The band gap energy ‚E_g" is determined by extrapolating the linear portion of the plot of $(\alpha h\upsilon)^n$ against $h\upsilon$ to the energy axis at α = 0.

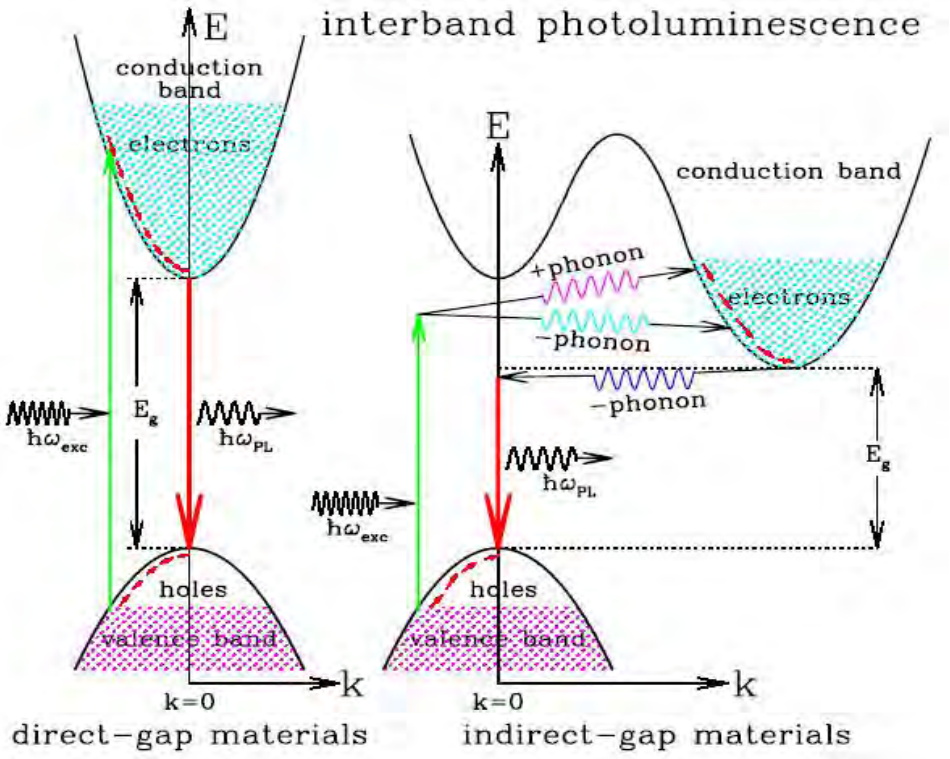

Fig. 2.7: "Direct inter band optical transitions" for direct band and indirect band semiconductors. The transitions are represented by vertical arrow.

While discussing the optical absorption edges observed in amorphous semiconductors the following assumptions are made: (a) the matrix elements for the electronic transitions are constant over the range of photon energies of interest and (b) *K*–conservation selection rule is relaxed. This assumption is made in amorphous semiconductors because near the band edges at least, $\Delta k \sim k$ and thus k is not a good quantum number. On E– k diagram such transitions would be non–vertical. However, no phonon absorption or emission processes are invoked to conserve momentum and all the energy required is provided by the incident photons. Such transitions are termed non–direct as opposed to indirect. Without knowledge of the form of $N(E)$ at the band edges, and under the assumption of parabolic bands, the absorption in many amorphous material is observed to obey the relation (2.10) with $n = 2$. Thus absorption edge of many amorphous semiconductors can be described by a simple power law, at least over a limited range of the absorption coefficients, which enables an optical gap „E_g" to be defined.

2.5.3 UV-Vis Spectrophotometer

In this work a dual-beam UV-Vis. spectrophotometer is used and a schematic diagram of the dual-beam UV-Vis. spectrophotometer is given in Fig. 2.8. The functioning of this instrument

is relatively straightforward. A beam of light from a visible and/or UV light source is separated into its component wavelengths by a prism or diffraction grating. Each monochromatic (single wavelength) beam in turn is split into two equal intensity beams by a half-mirrored device. One beam, the sample beam (colored magenta), passes through a small transparent container (cuvette) containing a solution of the compound being studied in a transparent solvent. The other beam, the reference (colored blue), passes through an identical cuvette containing only the solvent. The intensities of these light beams are then measured by electronic detectors and compared. The intensity of the reference beam, which should have suffered little or no light absorption, is defined as I_0. The intensity of the sample beam is defined as I. Over a short period of time, the spectrometer automatically scans all the component wavelengths in the manner described. The ultraviolet (UV) region scanned is normally from 200 to 400 nm, and the visible portion is from 400 to 800 nm.

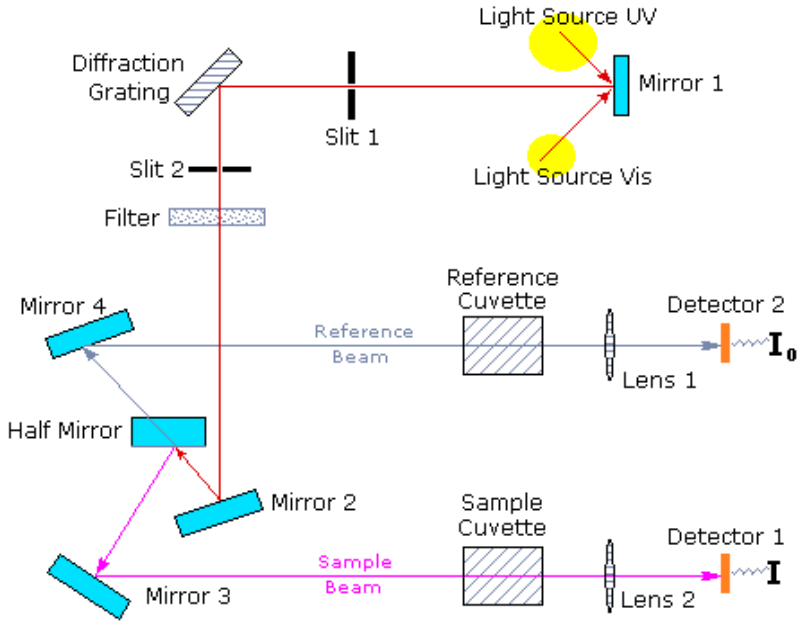

Fig. 2.8: Schematic diagram of a dual-beam UV-Vis. spectrophotometer

If the sample compound does not absorb light of a given wavelength, $I = I_0$. However, if the sample compound absorbs light then I is less than I_0, and this difference may be plotted on a graph of absorption versus wavelength. Absorption may be presented as transmittance ($T = I/I_0$) or absorbance ($A = log\ I_0/I$). If no absorption has occurred, T = 1.0 and A= 0. Most spectrometers display absorbance on the vertical axis, and the commonly observed range is from 0 (100% transmittance) to 2 (1% transmittance). The wavelength of maximum absorbance is a characteristic value, designated as λ_{max}.

2.5.4 Refractive Index and Extinction Coefficient

One of the most important optical constants of a material is its refractive index, which in general depends on the wavelength of the electromagnetic wave, through a relationship called dispersion. In materials where an electromagnetic wave, can be lose its energy during its propagation, the refractive index become complex. Refraction of light at the interface between two media of different refractive indices n_1 and n_2 are shown in Fig.2.9.

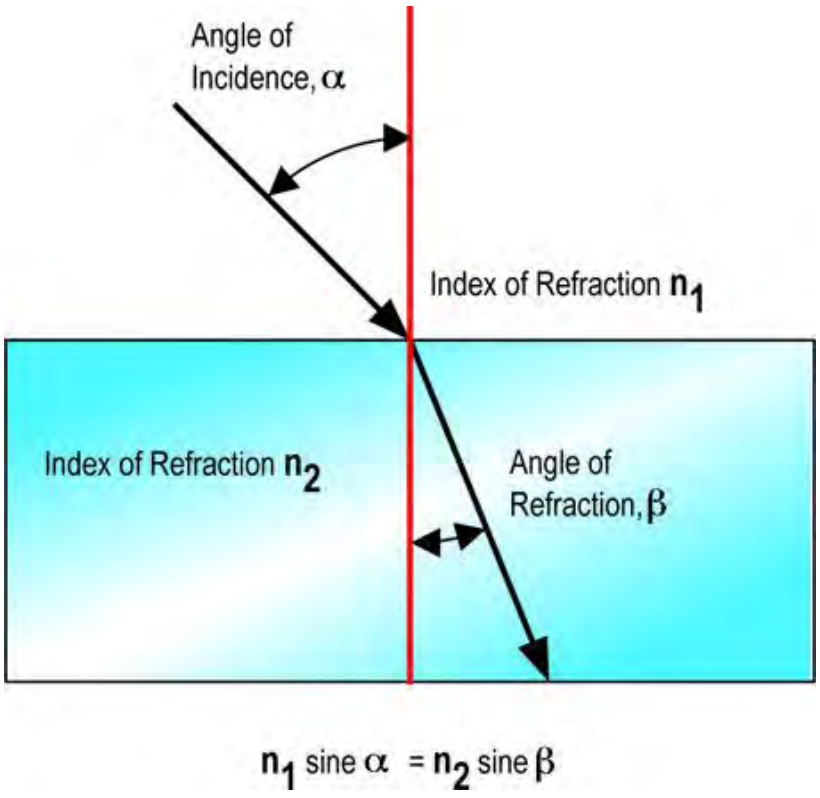

Fig. 2.9: Refraction of light at the interface between two media of different refractive indices

The real part is usually the refractive index (*n*) and the imaginary part is called the extinction coefficient (*k*). In this section, *n* and *k* will be presented in detail along with some common dispersion relations. *N* of an optical or dielectric medium, is the ratio of the velocity of light *(c)* in vacuum to its velocity *v* in the medium, $n = c/v$. Using the Maxwell‟s equations, one obtains the well known Maxwell‟s formula for the refractive index of substance as $n=\sqrt{\varepsilon}\mu_r$ where ε is the static dielectric constant or relative permittivity and μ_r the relative permeability. As $\mu_r = 1$ for nonmagnetic substrate, one gets, $n=\sqrt{\varepsilon}$, which is very useful in relating the dielectric property to optical properties of materials at any particular frequency of interest. As ε depends on the wavelength of light, n also depends on the wavelength of light, and this dependence is called dispersion. In addition to dispersion, an electromagnetic wave

propagating through a medium, which means it loses its energy, due to various loss mechanisms such as the generation of phonons (lattice wave), photo generation, free carrier absorption, scattering, etc. In such materials, the refractive index becomes a complex function of the frequency of light wave. The complex refractive index, denoted by n^*, with real part n, and imaginary part k, called the extinction coefficient, is related to the complex relative permittivity (ε) by:

$$n^* = n - jk = \sqrt{\varepsilon} = \sqrt{(\varepsilon_r - j\varepsilon_i)} \quad (2.11)$$

where ε_r and ε_i are, respectively, the real and imagination parts of ε. Equation gives

$$n^2 - k^2 = \varepsilon_r \text{ and } 2nk = \varepsilon_i \quad (2.12)$$

In explicit terms, n and k can be obtained as:

$$n = \sqrt{\frac{1}{2}}\sqrt{[\sqrt{(\varepsilon_r^2 + \varepsilon_i^2)} + \varepsilon_r]} \quad (2.13)$$

$$k = \sqrt{\frac{1}{2}}\sqrt{[\sqrt{(\varepsilon_r^2 + \varepsilon_i^2)} - \varepsilon_r]} \quad (2.14)$$

the optical constants n and k can be determined by measuring the reflectance from the surface of a material as a function of polarization and the angle of incidence. For normal incidence, the reflective coefficient, r, is obtained as

$$r = \frac{1-n^*}{1+n^*} = \frac{1-n+jk}{1+n+jk} \quad (2.15)$$

the reflectance R is then defined by:

$$R = |r|^2 = \left|\frac{1-n+jk}{1+n+jk}\right|^2 = \frac{(1-n)^2+k^2}{(1+n)^2+k^2} \quad (2.16)$$

And refractive index can be calculated by using following equation

$$n = \left(\frac{1+R}{1-R}\right) + \sqrt{\frac{4R}{(1-R)^2} - k^2} \quad (2.17)$$

Notice that whenever k is large, for example over a range of wavelength, the absorption is strong, and the reflectance is almost unity. The light is then reflected, and any light in the medium is highly attenuated. Extinction coefficient can be determined from the relation as follows

$$k = \frac{\alpha\lambda}{4\pi} \quad (2.18)$$

Optical conductivity of thin films is calculated by using the following equation

$$\sigma_{0pt} = \frac{\alpha nc}{4\pi} \quad (2.19)$$

Where c is the speed of light in vacuum.

2.6 Measurement of Film Thickness

Multiple-Beam Interferometry method utilizes the resulting interference effects when two silvered surfaces are brought close together and are subjected to optical radiation. This interference technique, which is of great value in studying surface topology in general, may be applied simply and directly to film-thickness determination. When a wedge of small angle is formed between unsilvered glass plates, which are illuminated by monochromatic light, broad fringes are seen arising from interference between the light beams reflected from the glass on the two sides of the air wedge. At points along the wedge where the path difference is an integral and odd number of wavelengths, bright and dark fringes occur respectively.

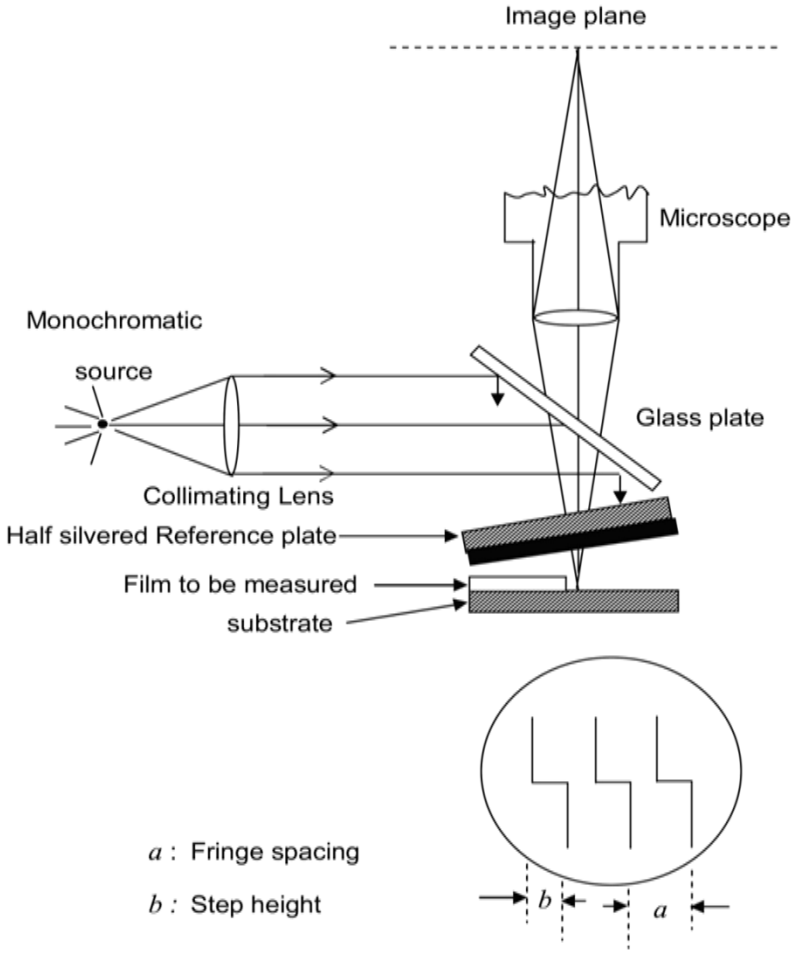

Fig. 2.10: Interferometer arrangement for producing reflection Fizeau fringes of equal thickness.

If the glass surfaces of the plates are coated with highly reflecting layers, one of which is partially transparent, then the reflected fringe system consists of very fine dark lines against a bright background. A schematic diagram of the multiple-beam interferometer along with a

typical pattern of Fizeau fringes from a film step is shown in Fig. 2.10. As shown in this figure, the film whose thickness is to be measured is over coated with a silver layer to give a good reflecting surface and a half-silvered microscope slide is laid on top of the film whose thickness is to be determined. A wedge is formed by the two microscope slides, and light multiply reflected between the two silvered surfaces forms an interference pattern with a discontinuity at the film edge as shown in Fig. 2.10. The thickness of the film *d* can then be determined by the relation,

$$d = \frac{\lambda}{2} \times \frac{b}{a} \qquad (2.20)$$

Where, λ is the wavelength and *b/a* is the fractional discontinuity identified in the figure.
In general, the sodium light is used, for which λ= 5893Å. In conclusion, it might be mentioned that the Tolansky method of film-thickness measurement is the most widely used and in many respects also the most accurate and satisfactory one.

2.7 Electrical Characterization

Electrical characterization of a material involves the measurement of the resistivity (ρ). The technique for measuring ρ is very well known and has been documented in several literatures [13, 14]. Some methods of resistivity measurement are as follows:

Linear four point probe method

Four probe apparatus is one of the standard and most widely used apparatus for the measurement of resistivity of semiconductors. This method is employed when the sample is in the form of a thin wafer, such as a thin semiconductor material deposited on a substrate. The sample is nanometer in size and having a thickness *d*. It consists of four probe arranged linearly in a straight line at equal distance *S* from each other. A constant current is passed through the two probes and the potential drop *V* across the middle two probes is measured. An oven is provided with a heater to heat the sample so that behavior of the sample is studied with increase in temperature.

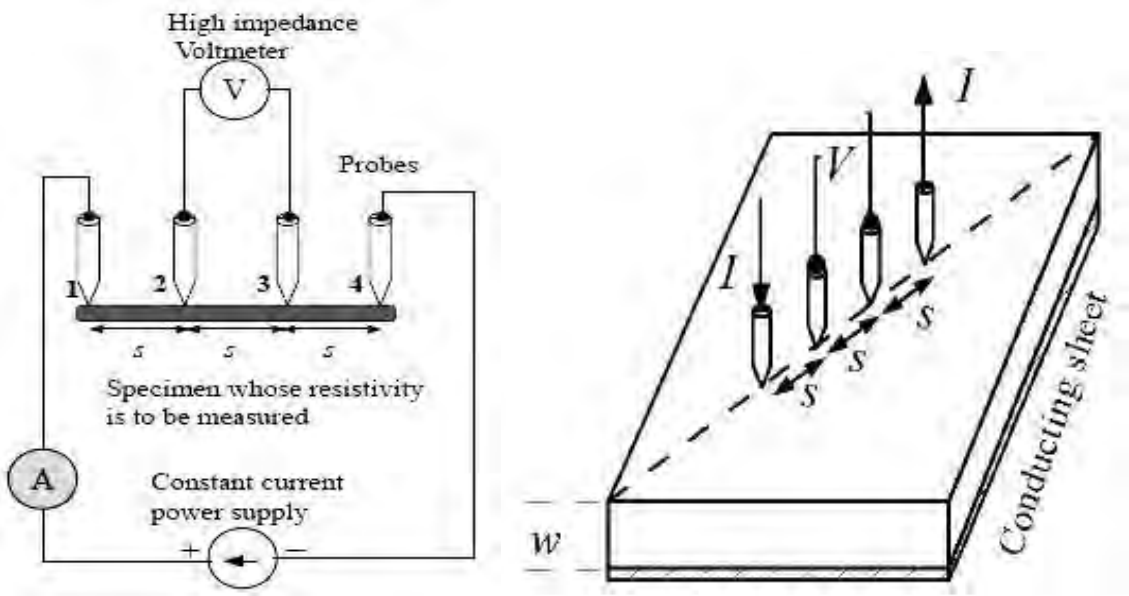

Figure 2.11: The arrangements of four probes that measure voltage (V) and supply current (I) to the surface of the crystal.

At a constant temperature, the resistance, R of a conductor is proportional to its length L and inversely proportional to its area of cross section A.

$$R = \rho\frac{L}{A} \qquad (2.\ 21)$$

Where ρ is the resistivity of the conductor and its unit is Ω-m.

A semiconductor has electrical conductivity intermediate in magnitude between that of a conductor and insulator. Semiconductor differs from metals in their characteristic property of decreasing electrical resistivity with increasing temperature. According to band theory, the energy levels of semiconductors can be grouped into two bands, valence band and the conduction band. In the presence of an external electric field it is electrons in the valence band that can move freely, thereby responsible for the electrical conductivity of semiconductors. In case of intrinsic semiconductors, the Fermi level lies in between the conduction band minimum and valence band maximum. Since conduction band lies above the Fermi level at O K, when no thermal excitations are available, the conduction band remains unoccupied. So conduction is not possible at O K, and resistance is infinite. As temperature increases, the occupancy of conduction band goes up, thereby resulting in decrease of electrical resistivity of semiconductor.

Resistivity of semiconductor by four probe method

1. The resistivity of material is uniform in the area of measurement.

2. If there is a minority carrier injection into the semiconductor by the current- carrying electrodes most of the carriers recombine near electrodes so that their effect on conductivity is negligible.
3. The surface on which the probes rest is flat with no surface leakage.
4. The four probes used for resistivity measurement contact surface at points that lie in a straight line.
5. The diameter of the contact between metallic probes and the semiconductor should be small compared to the distance between the probes.
6. The boundary between the current carrying electrodes and the bulk material is hemispherical and small in diameter.
7. The surface of semiconductor material may be either conducting and non-conducting. A conducting boundary is one on which material of much lower resistivity than semiconductor has been plated. A non-conducting boundary is produced when the surface of the semiconductor is in contact with insulator.

Adequately far from the probes, the die may be considered to be identical to a slice. For this case of a slice of thickness *w* and the resistivity is computed as

$$\rho = \frac{\rho_o}{f\left(\frac{w}{s}\right)} \qquad (2.22)$$

The function, *f(w/S)* is a divisor for computing resistivity which depends on the value of *w* and *S.* It is assumed that the size of the metal tip is infinitesimal and sample thickness is less than the distance between the probes,

$$\rho = 2\pi s\left(\frac{V}{I}\right) \qquad (2.23)$$

Where *V* is the potential difference between inner probes in volts.
I is the current through the outer pair of probes in ampere.
S is the spacing between the probes in meter.

Temperature dependence of resistivity of semiconductor

Total electrical conductivity of a semiconductor is the sum of the conductivities of the valence band and conduction band carriers. Resistivity is the reciprocal of conductivity and its temperature dependence is given by

$$\rho = A\, exp\, \frac{E_g}{2KT} \qquad (2.24)$$

Where E_g is the band gap of the material

T – Temperature in kelvin

k – Boltzmann constant, $k = 8.6\times10^{-5}$ eV/K

the resistivity of a semiconductor rises exponentially on decreasing the temperature.

References

[1] Schwartz, M., Deposition from Aqueous Solutions: An overview. In: Handbook of Deposition Technologies for Film and Coatings (Ed. R. F. Bunshah), Noyes Publications, (1994).

[2] Ariyakkani, P., Suganya, L., Sundaresan, B., „Investigation of the structural, optical and magnetic properties of Fe doped ZnO thin films coated on glass by sol-gel spin coating method", J. Alloy. Compound, vol. 695, p. 3467–3475, (2016).

[3] Aguilera, M. L. A. Márquez, J. M. F., Trujillo, M. A. G., Kuwahara, Y. M., Morales, G. R., Galán, O. V., „Influence of CdS Thin Films Growth Related with the Substrate Properties and Conditions Used on CBD Technique", Enrg. Procedi., vol. 44, p. 111–117, (2014).

[4] Dinni, J. W., Electrodeposition: The Material Science of Coatings and Substrates, Noyes Publications, (1993).

[5] Brewer, G. E. F. (Ed.), Electrodeposition of Coatings. In: Advances in Chemistry, Series No. 119, American Chemical Society, (1973).

[6] O'Brien, P. and McAleese, J., „Developing an understanding of the processes controlling the chemical bath deposition of ZnS and CdS", J. Mater. Chem., vol. 8, p. 2309-2313, (1998).

[7] Binnig, G., Rohrer H., Gerber Ch. and Weibel E., „Surface studied by scanning tunneling microscope", Phy. Rev. Lett., vol. 49, p. 57-61, (1982).

[8] Hansma, P. K., and Tersoff J., „Scanning tunneling microscopy", J. Appl. Phys., vol. 61, p. 823-828, (1987).

[9] Binnig, G., Quate C. and Gerber Ch., „Atomic force microscope", Phy. Rev. Left., vol. 56, p.930-934, (1986).

[10] Magonov, S. N., and Whangbo M. H., „Surface Analysis with STM and AFM-Experimental and Theoretical Aspects of Image Analysis", (VCH, 1996).

[11] Howland, R., and Benatar, L., „A Practical Guide to Scanning Prob Microscopy", (Park Scientific Instruments, 1997).

[12] Bouguer, P., „Essai d‟optique sur la gradation de la lumière“, claude Jombert: Paris, (1729).

[13] Cullity, B. D., „Elements of X-ray Diffraction“, Addison-Wesley, Inc., USA, (1959).

[14] McCarter, W. J., Starrs, G., Kandasami, S., Jones, R., Chrisp, M., „Electrode configurations for resistivity measurements on concreate“, ACI Mater. J., vol. 106(3), p. 258-264, (2009).

[15] Lataste, J. F., „Electrical resistivity measurement“, in Non-Destructive Assessment of concrete structures, springer, (2012).

CHAPTER 3

EXPERIMENTAL DETAILS

3.1 Introduction

In the advancement of science and technology the discovery of novel materials those are having varied characteristics and applications have played an important role. Characterization is an important step in the development of exotic materials. The complete characterization of any material consists of surface characterization, compositional characterization, structural analysis, optical study, and electrical measurement, which have strong bearing on the properties of materials. This has led to the emergence of variety of advanced techniques in the field of materials science. In this section different analytical instrumental techniques used to characterize our thin films are described with relevant principles of their operation and working.

3.2 Chemicals

The different chemicals were used as follows;

i) Sodium Sulfate (Anhydrous), BDH Lab. Supply, England ≥ (98.0%).
ii) Zinc Acetate. BDH Lab. Supply, England (99.5%)
iii) Selenium Powder, BDH Lab. Supply, England (99.5%)
iv) Sodium Hydroxide. D Lab. Chemical, Dhaka
v) Hydrazine Hydrate, Merck, Germany (80%)
vi) Acetone, Merck, Germany (99.9%)

3.3 Experimental Set-up

Chemical bath deposition (CBD) which is also known as solution growth, controlled precipitation or simply chemical deposition, recently has emerged as a method for the deposition of metal chalcogenides as well as metal dichalcogenides thin films. It is an analogue, in the liquid phase, of the well known chemical vapor deposition in gaseous phase. The reactions take place between the dissolved precursors generally in aqueous solution at low temperature. Physical methods and chemical methods are use for deposition thin film. Physical methods have been classified into vapor deposition and sputtering. The various chemical deposition methods are chemical bath deposition, spray pyrolysis, anodization, electrodeposition, screen printing, chemical vapor deposition, sol-gel, etc. Chemical bath deposition is simple, low cost, economically viable and convenient for large area deposition, without use of sophisticated instrumentation and low temperature process control. This method is better than any other for deposition cost intensive [1]. A schematic diagram of

CBD system is shown in Fig. 3.1 and the photograph of the chemical bath deposition system is shown in Fig.3.2.

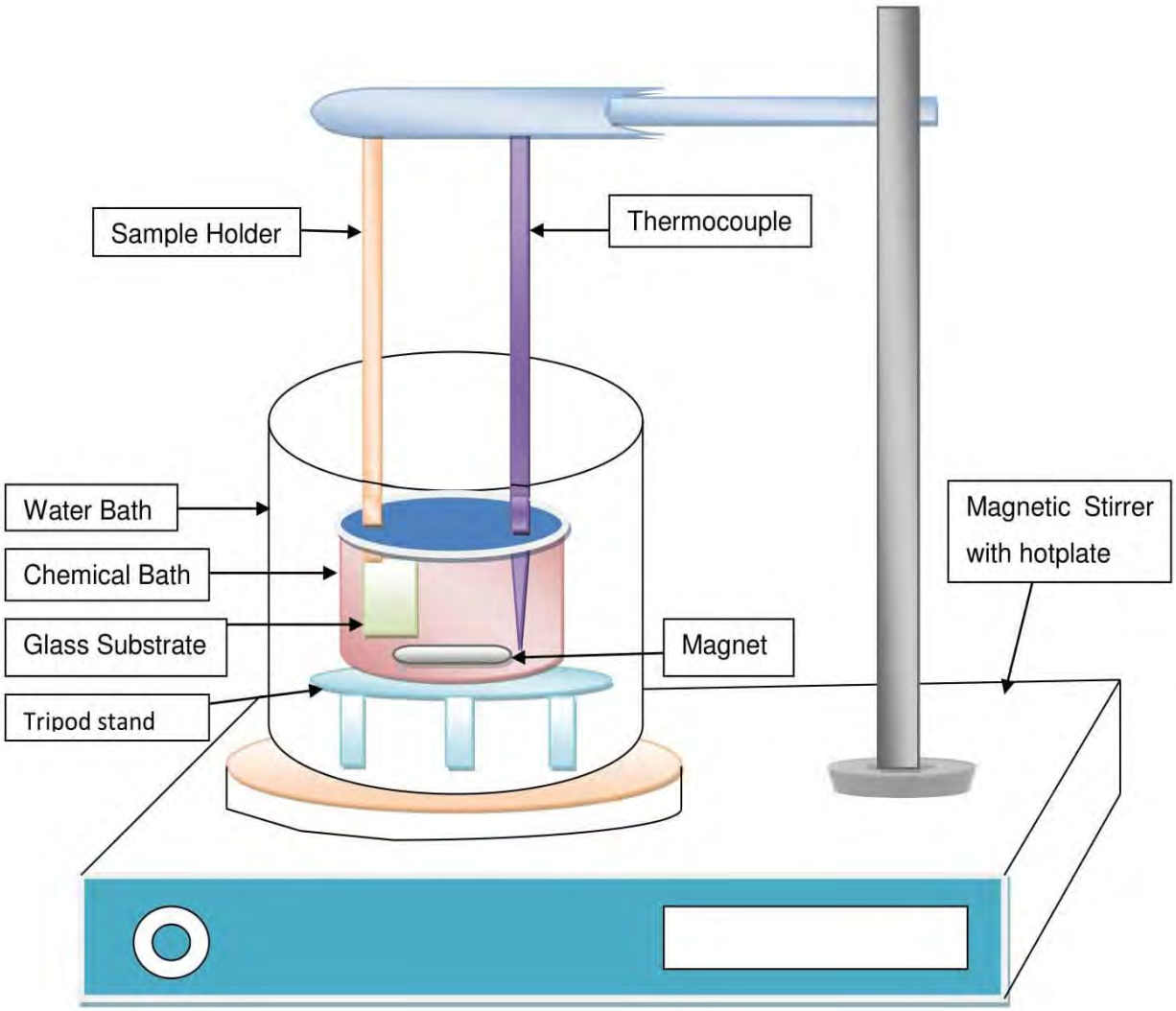

Figure 3.1: A schematic diagram of the CBD system

Fig. 3.2: Chemical bath deposition system and films deposition process

3.3.1 Magnetic Stirrer with Thermostat

The reaction mixture is continuously stirred using a magnetic stirrer with heater at its top. The preparation of the zinc selenide thin films is carried out while the stirring is continuous.

The temperature of the solution can be controlled by the thermostat of the stirrer with an accuracy of $\pm 0.5^0$C.

3.3.2 Water Bath

A 500 ml quartz beaker containing water/ paraffin oil was used as a bath. The container was insulated with thermocol in order to prevent the thermal loss to surroundings.

3.3.3 The chemical bath

It consists of glass vessel containing the reaction mixture of required proportions of precursor and complexing agent solutions commonly known as bath.

3.3.4 The substrate holder

The substrate holder can hold the substrates of $38.1 \times 25.4 \times 1.2$ mm^3, which are partially dipped in the solution in study vertical position. The probe of the digital temperature meter is immersed in to the bath to measure the temperature of the bath.

3.3.5 Substrate cleaning

Non uniformity and poor adhesion were the common problems occurred when the thin films were deposited on smooth substrates by chemical bath deposition method. Hence, much attention was paid on the cleaning and activating the substrate surface. The selection of the substrate and methods used for the cleaning of the surface of the substrate are very important in the formation of thin films with reproducible process. Nature of the material, size, surface roughness and cleanliness of the substrate play an important role in the formation of the film and its properties such as adhesion, pin-hole density, porosity, film microstructure, morphology and mechanical properties. Substrate cleaning usually involves removing surface contaminations like greasy particles, dust, metals etc. The cleaning process varies with the substrate being cleaned. The contaminants present in the surface of the substrate can be broadly categorized into two types, namely organic and inorganic. Organic contaminants can be easily removed by emulsifying the surface of the substrate with washing solutions. However, for the removal of inorganic contaminants a direct mechanical approach is needed when they are in particle form. A number of procedures are available for this purpose such as immersing in solvents, ultrasonic cleaning, electronic discharge etc [2]. The systematic procedure used for cleaning the substrates is outlined here.

- The substrates were initially wiped with acetone and cotton to remove the visible contaminations like dust particles.
- The substrates were washed with ultrasonic bath in acetone and distilled water. The substrates were dried in a hot oven before mounting them on the substrate holder

3.4 Reaction Mechanism in CBD

The reaction into the chemical bath takes place between a slowly released selenide anion (Se^{2-}) with a free metal zinc cation (Zn^{2+}). Sodium selenosulfate (Na_2SeSO_3) was used as a precursor for Se^{2-} ions [3]. It was obtained by adding selenium (Se) powder to a hot solution of sodium sulfite (Na_2SO_3), which was magnetically stirred for several hours at 80 ^oC and excess of the Se is removed. As this solution was relatively unstable it will be prepared freshly prior to film deposition. The main solution for the film deposition were obtained by mixing an appropriate amount of 1 M zinc acetate ($Zn(O_2CCH_3)_2$) with 2 M NaOH and with 80% hydrazine hydrate (H_6N_2O) in a 100 ml beaker. Afterwards, 20 ml of 1 M Na_2SeSO_3 will be added slowly with constant stirring to this mixture. The solution was stirred for few seconds and transferred to another beaker containing substrates. Then the reactant vessel will be kept in a constant temperature water bath maintained at 45 ^oC to provide external heat energy for ZnSe formation. During the film formation the solution was kept at ~90 ^oC.

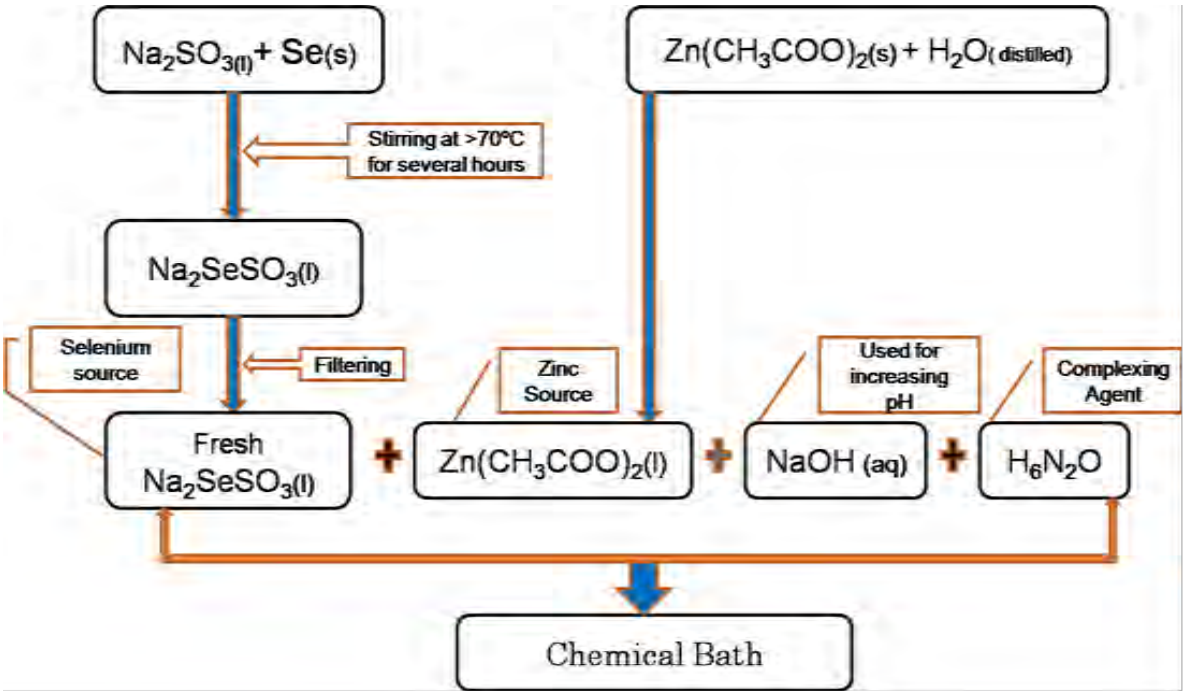

Figure 3.3: A flow-chart of CBD reaction process

3.5 Preparations of Thin Films

Flow-chart of the CBD technique

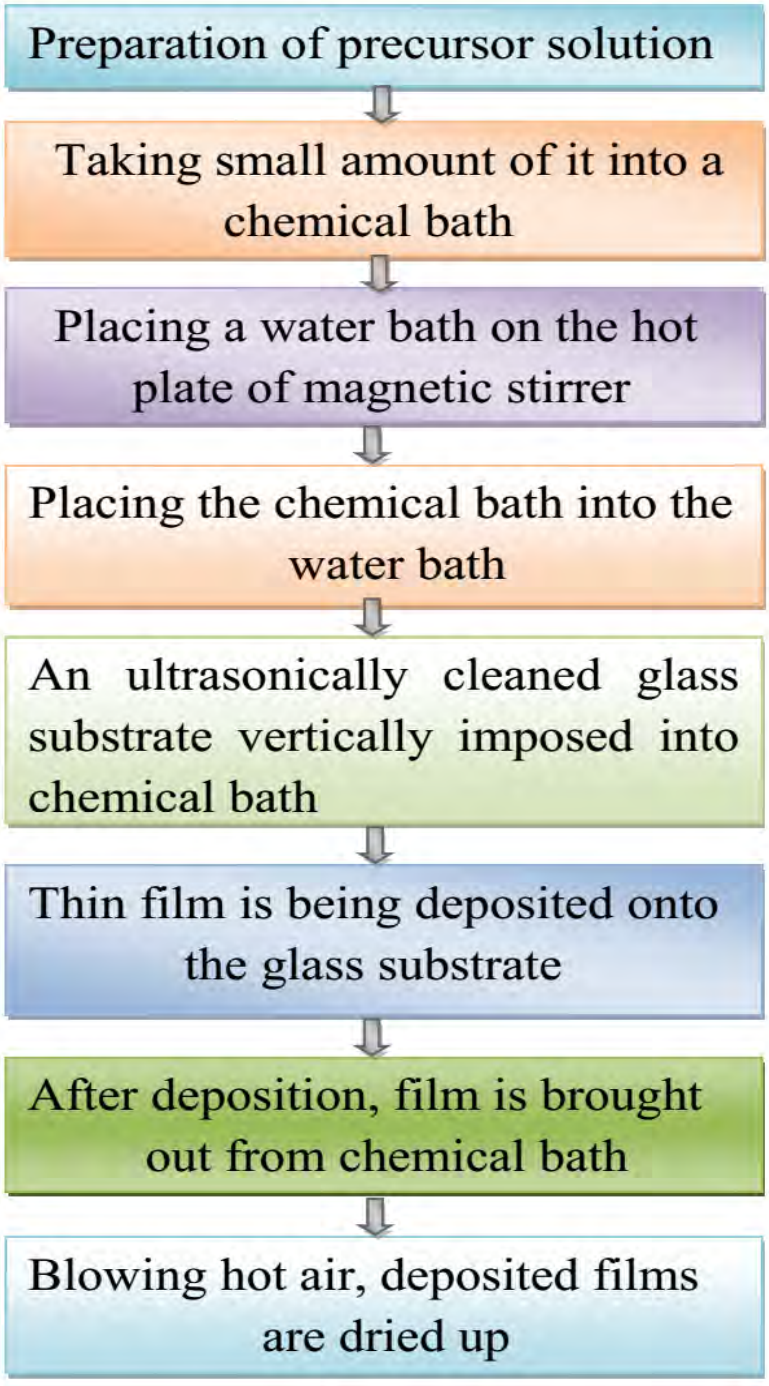

Fig.3.4: Flow-chart of CBD deposition process.

3.5.1 Preparation of Substrates for Deposition

The substrates used for depositing the films were non-conducting amorphous and approximately 100% transmitting glass slides of the size 76.2 x 25.4 x 1.2 mm (Sail Brand, CAT.NO. 7101, China). The films deposited on the glass substrates were used to study the characterization of the films. Substrate cleaning plays a vital role in the deposition of thin films. The properly cleaned substrates are required for the deposition. The contaminated substrate surface provides nucleation sites facilitating the growth, which results non-uniform film growth. The glass substrates were cleaned in ultrasonic bath with acetone and distilled water about 15 min. by turn.

3.5.2 Preparations of the Solutions

All the solutions were exclusively prepared in double-distilled water and the basic chemicals used were of AR grade. The main solution for the film deposition were obtained by mixing an appropriate amount of 1 M 20 ml zinc acetate ($Zn(O_2CCH_3)_2$) with 1 M 10 ml NaOH and with 10 ml 80% hydrazine hydrate (H_6N_2O) in a 100 ml beaker. Afterwards, 20 ml of 1 M Na_2SeSO_3 will be added slowly with constant stirring to this mixture.

3.5.3 Chemical Reaction in CBD

The solution was stirred for few seconds and transferred to another beaker containing substrates. Then the reactant vessel will be kept in a constant temperature water bath maintained at 45 ^{o}C to provide external heat energy for ZnSe formation. During the film formation the solution was kept at ~90 $^{\circ}$C. After deposition the deposited films were removed from chemical bath and dried by using hot air blow.

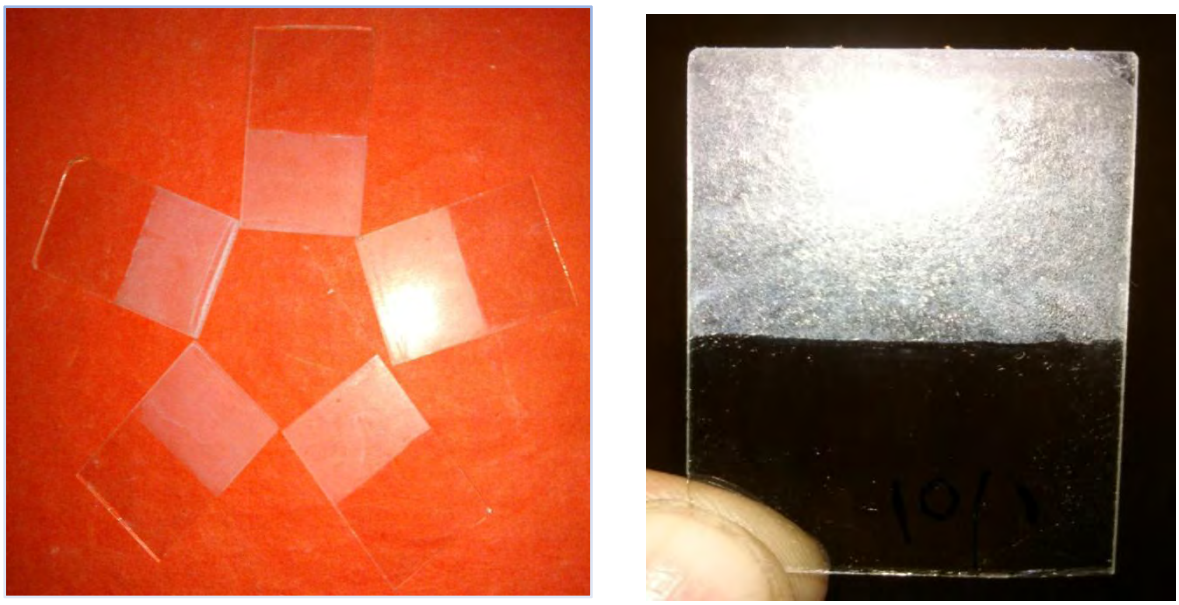

Fig. 3.5: Photographs of CBD deposited films

3.6 Characterization of Thin Films

This section describes experimental details of the various characterization techniques.

3.6.1 Thickness Measurement

The film thickness is the most important factor because most of the properties of thin film depend upon the thickness. There are various methods to determine the thickness of the film. But, the most suitable and convenient method is multiple beam interferometry method. It can also be measured accurately from interference fringes using multiple beam interferometry and also from the fringes of equal chromatic order (FECO) techniques. In the former case two reflecting surfaces are brought in close proximity such that a small wedge with a small air gap in between them is formed. If a monochromatic light is now incident on them at normal incidence, then an interference of light due to interactions of multiple reflected beams in air gap will take place resulting in a series of fringes which can be observed in the back reflected light. The distance between the fringes or lines depends on the air gap as well as one the wave length of the monochromatic light. This principle is adopted and suitably modified for the multiple beam interferometric method of the measurement of film thickness. A Multi Beam Interferometer is shown in Fig. 3.6.

Fig.3.6. A Multi Beam Interferometer

After obtaining a set of sharp fringes, the thickness (*d*) can be determined using the relation (2.20)

$$d = \frac{\lambda}{2} \times \frac{b}{a}$$

Where *b* is the displacement of the fringes at the step and *a* is the distance between consecutive fringes. The fringe displacements which are in the form of parallel lines, however, occur at the film edge.

3.6.2 Scanning Electron Microscope (SEM)

The surface morphology of the semiconductor electrode plays an important role in the performance of Photo electrochemical cell. Therefore it was essential to study a surface analysis of the ZnSe thin films. The surface nature of thin films was observed through scanning electron microscope (SEM), *JEOL-JSM 7600F (Japan*). The accelerating voltage was kept at 20 kV. All the SEM micrographs were obtained at the same magnification so as to have comparative study for the variation of composition of the ZnSe thin films.

Fig.3.7: A Scanning Electrical Microscopy

3.6.3 Compositional Analysis by Energy Dispersive X-ray Analysis

The quantitative analysis of the films was carried out using Energy Dispersive X-ray Analysis (EDX) for the thin films to study the stoichiometry of the film. This unit is attached to the SEM. When a beam of electrons strikes the specimen, some of the incident electrons excite the atom of the specimen which emits X-ray on returning to the ground state. The energy of the X-ray is related to the atomic number of the excited element. Lithium drifted Si-diode, held at liquid nitrogen temperature is used as a detector of the X-rays. *JEOL-JSM 7600F* Japan was employed in the present investigation.

3.6.4 X-ray Diffraction (XRD)

Crystallographic studies of the ZnSe thin film were characterized by *Bruker D8 Advance X-ray diffractometer* with Cu K_α line (λ = 1.54056 Å) in 2θ range from 10° to 80°. The X-ray tube was operated at 20 kV, 20 mA with a scanning speed of 0.25 sec per step. For comparative purpose, the standard JCPDS data were used. The indexing of spectra as well as lattice parameters of the samples was also examined.

Fig.3.8: A Bruker D8 Advance X-ray diffractometer

3.6.5 Optical Absorption Measurement

The optical absorption technique was utilized to estimate the absorption coefficient (α), band gap energy (E_g) and the type of optical transition. The optical absorption was measured for various wavelengths (λ). The optical properties were studied by taking absorption spectrum of film using a *Shimadzu-1601* (Japan) double-beam spectrophotometer in the range of 200–1100 nm at BCSIR. A substrate absorption correction was made by placing an identical uncoated glass slides in the reference beam.

Fig. 3.9: A Uv-visible spectrophotometer

3.6.6 Electrical Characterization

Electrical parameters such as resistivity, conductivity, activation energy, etc. of the ZnSe thin films deposited by CBD onto glass substrate were measured by the four points probe method. DC electrical resistivity measurements were made in air for the ZnSe thin films from room temperature, 303 K to 423 K. During the measurement, data were taken by slowly increasing the temperature of the films. Variation of current and voltage with corresponding temperature were recorded and then electrical parameters were calculated. For dc conductivity measurements, a 20 V dc fixed bias was maintained. A power supply (*Model: GPR-3060D*) was used to pass a constant dc current through the test sample. An electrometer (Model: UT 393) was used to monitor the current through the sample and a digital multimeter (*Model: GDB-450 A*) was used to measure the potential differences across each sample. The glass substrate was heated by a specially heater and the temperature was measured by a chromel-alumel thermocouple placed under the sample.

Fig: 3.10: A four point probe set-up

Reference

[1] Hankare P. P., Chate P. A., Chavan P. A., Sathe D. J., 'Chemical deposition of ZnSe thin films: Photoelectrochemical applications', J. Alloy. Compd., vol. 461, p. 623–627, (2008).

[2] Agawanea, G. L., Shin S. W., et al,'Novel reduced toxic route synthesis and characterization of chemical bath deposited ZnSe thin films', Ceramic. Int. vol. 40, p. 367–374, (2014).

[3] Mehta, C., Saini, G. S. S., Abbas, J. M., Tripathi, S. K., 'Effect of deposition parameters on structural, optical and electrical properties of nanocrystalline ZnSe thin films', Appl. Surf. Sci., vol. 256, p. 608–614, (2009).

CHAPTER 4

RESULTS AND DISCUSSION

4.1 Introduction

The outcome of this study is the deposition and characterization of ZnSe thin films using CBD technique. In this chapter, the results and discussion on all the experimental studies such as surface morphology, structural, optical, and electrical properties, etc. of the ZnSe thin films have been presented.

4.2 Surface Morphology

The surface morphology of the as-deposited ZnSe thin films deposited at ~90 ^{o}C for different time durations viz. 30 min, 40 min, and 50 min are shown in Fig. 4.1(a–c) and for different molar concentration of selenium source viz. 0.3 M, 0.5M, 1.0 M and 1.5 M are shown in Figs. 4.2 (a–d). Surface morphological analysis of the as-deposited and annealed ZnSe thin films also have been studied and shown in Fig. 4.3 (a, b) and 4.4 (c, d).

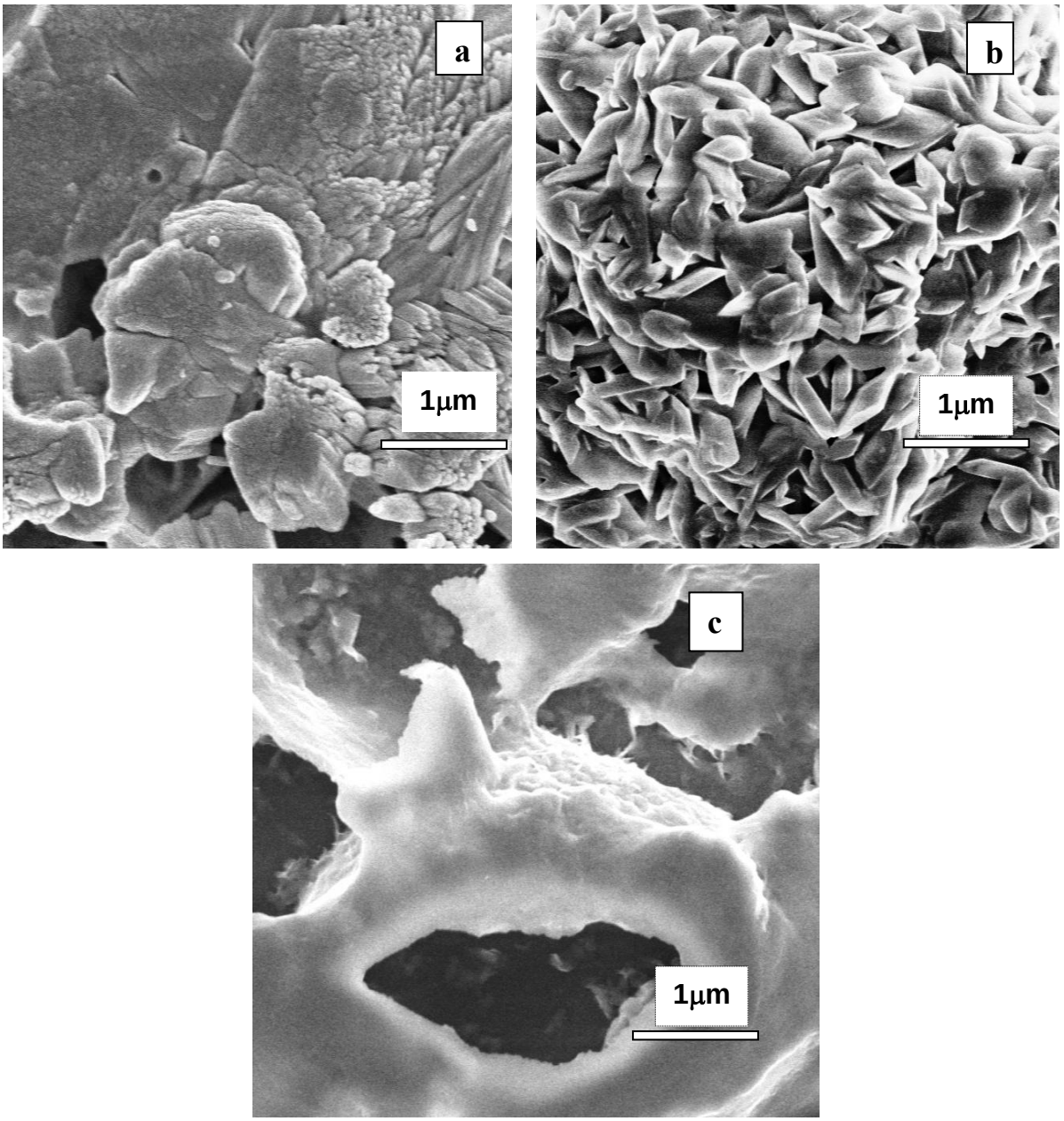

Fig. 4.1 (a–c): SEM images at ×10 K magnification of the ZnSe (1M) thin films deposited for 30, 40, 50 min at 90 ^{o}C.

From the Figs. 4.1(a–c), it is observed the ZnSe thin films have fiber type nature as observed by others [1]. Amalgamation occurs for the as-deposited ZnSe thin film onto the glass substrate showing porous type nature, which is increasing with deposition time. The SEM micrograph shows that ZnSe thin films prepared at different time duration are not so compact but have good coverage of glass substrate shown in Fig. 4.1(a–c). These films revealed that grains were very small in size with no well defined grain boundaries. It may occur due to increase Zn particle into the ZnSe thin film.

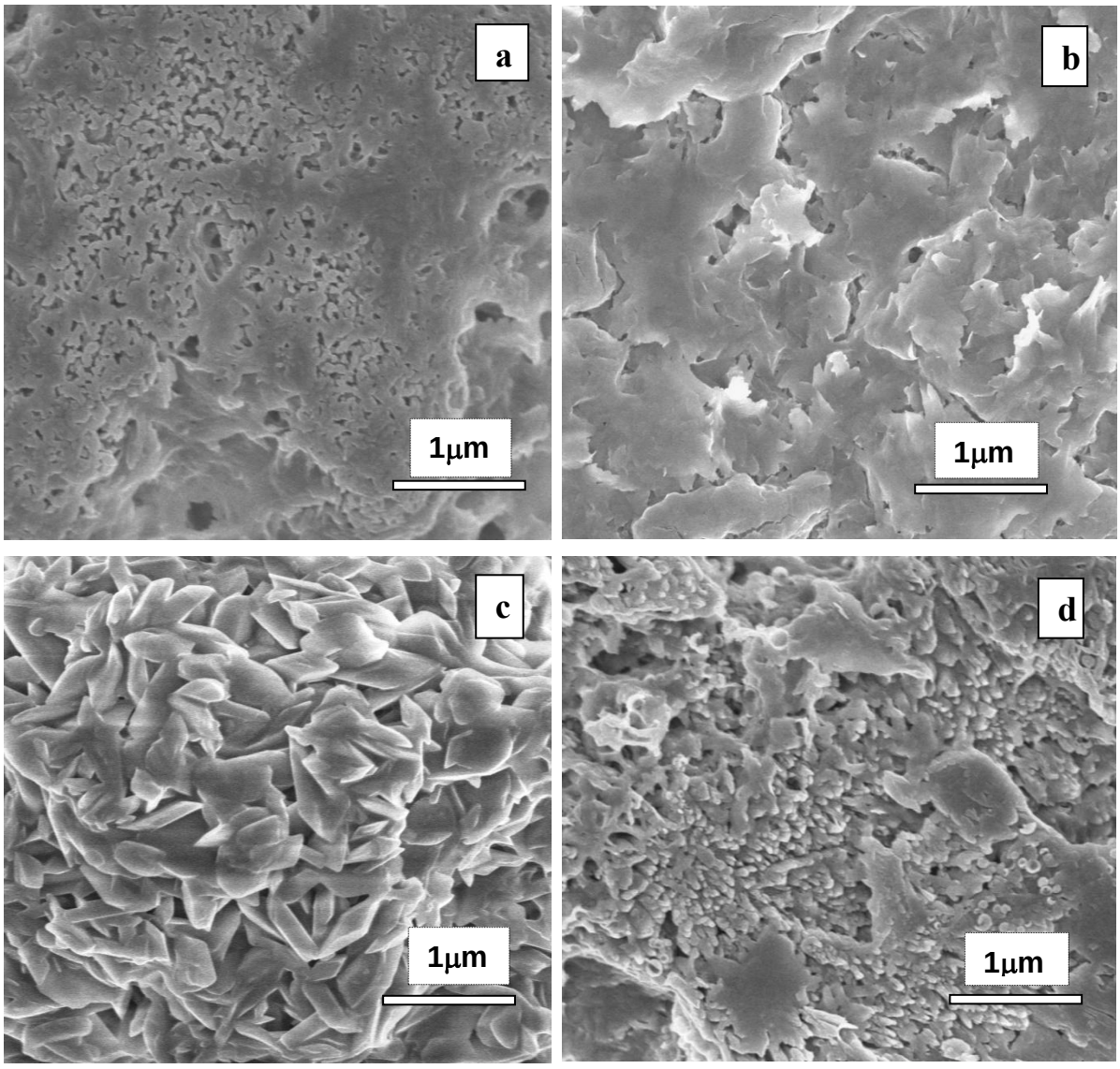

Fig. 4.2: SEM images at ×10 K magnification of ZnSe thin film deposited at (a) 0.3, (b) 0.5, (c) 1.0, and (d) 1.5 M concentration of Se source for 40 min at 90 ^{o}C.

ZnSe thin films grown on glass substrate at different concentration of Se source exhibit dense flakes and needle like growth of film onto the surface of glass substrate, as can be seen in Fig. 4.2 (a–d) and this observation is similar with previous research.

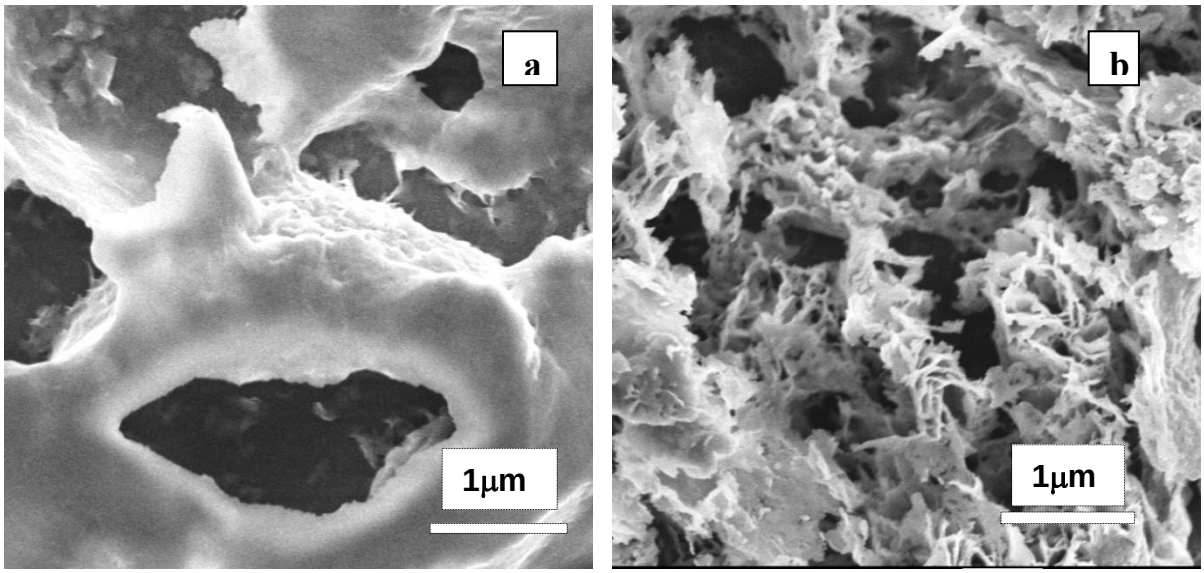

Fig. 4.3: SEM image at ×10 K magnification of ZnSe (1M) thin film deposited for 40 min at 90 ^{o}C. (c) As-deposited and (d) annealed at 300 ^{o}C for 1 hr

.

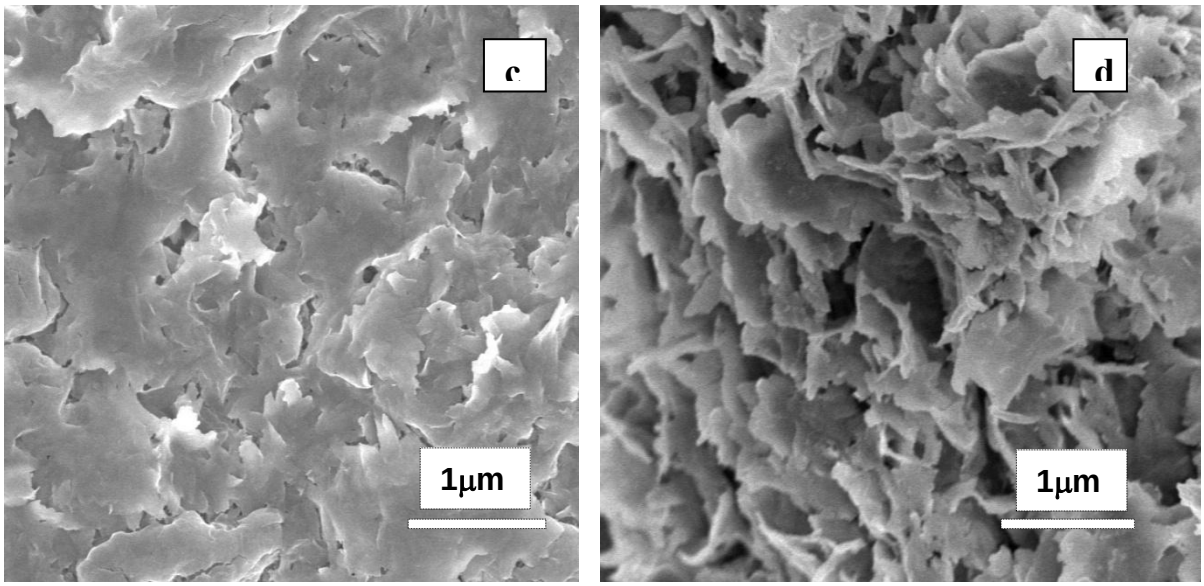

Fig. 4.4: SEM image at ×10 K magnification of ZnSe thin film deposited of 0.5 M concentration of Se source for 40 min at 90 ^{o}C (c) As-deposited and (d) annealed at 300 ^{o}C for 1 hr

From SEM micrographs shown in Figure 4.3 (a, b) and 4.4 (c, d), we observe that the annealing effect makes films more fibrous and porous in nature.

4.3 Elemental Analyses

The elements that present in ZnSe thin films are confirmed by EDX spectroscopic analyses and are shown in Figs. 4.5 and 4.6. It has been observed that the peaks of Se increase for the samples with concentration and the strong peaks of Zn also have been observed. A strong peak of O has been observed which may due to the formation of ZnO [2]. Agawane et al. [3] reported that the chalcogenide based materials synthesized by chemical bath deposition in basic mediums suffer from the presence of the metal–OH compounds and these metal–OH compounds are grounds of different characteristics such as poor crystallinity, low growth rate and meta stable band gap energy and they also reported that an inadequate amount of the strong complexing agent in chemical bath may be the another cause for present of excess oxygen in the deposited thin films by CBD.

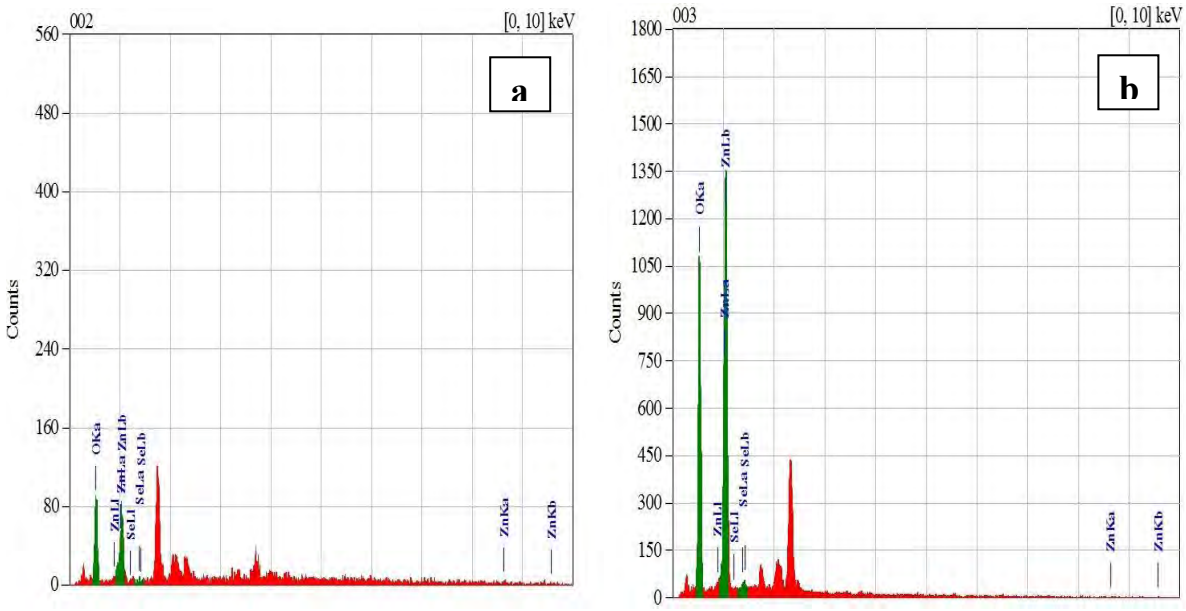

Fig 4.5: EDX spectra of ZnSe thin film deposited of (a) 0.3 M and (b) 0.5 M concentration of Se source for 40 min at 90 ^{o}C.

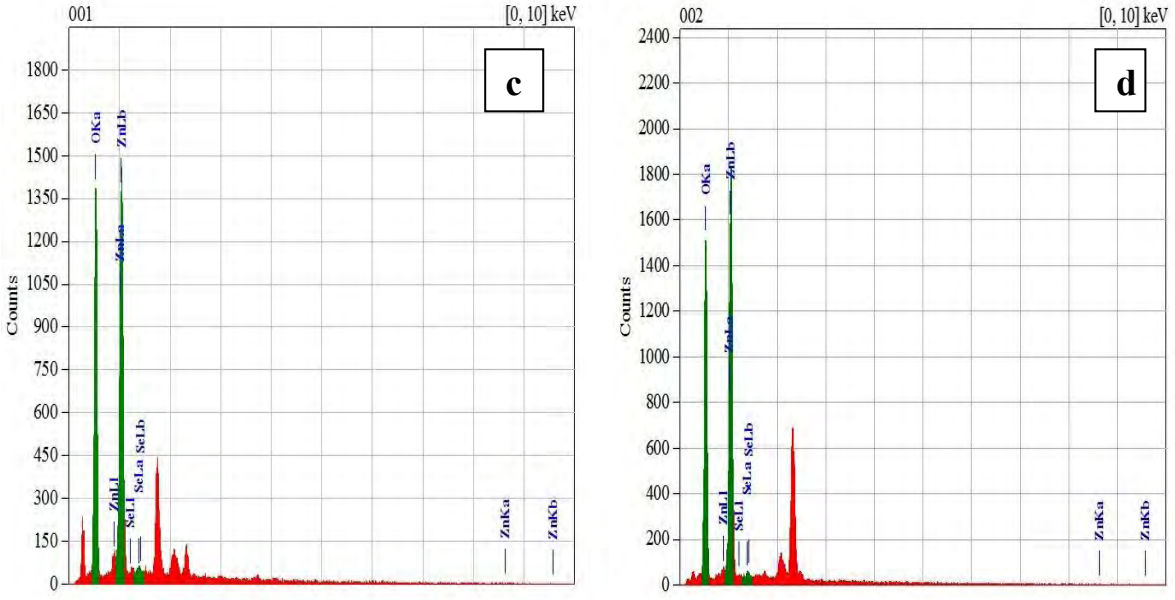

Fig 4.6 (c, d): EDX spectra of ZnSe thin film deposited of (a) 1.0 M and (b) 1.5 M concentration of Se source for 40 min at 90 ^{o}C.

Table 4.1: Data of elemental analysis for ZnSe thin films

Sample	Mass Percentage of Elements		
	Zn	Se	O
ZnSe (0.3 M, 40 min, 140±10 nm)	45.07	1.74	53.19
ZnSe (0.5 M, 40 min, 165±10 nm)	38.24	2.53	59.23
ZnSe (1.0 M, 40 min, 200±10 nm)	46.60	1.89	51.51
ZnSe (1.5 M, 40 min, 225±10 nm)	40.56	1.13	58.31

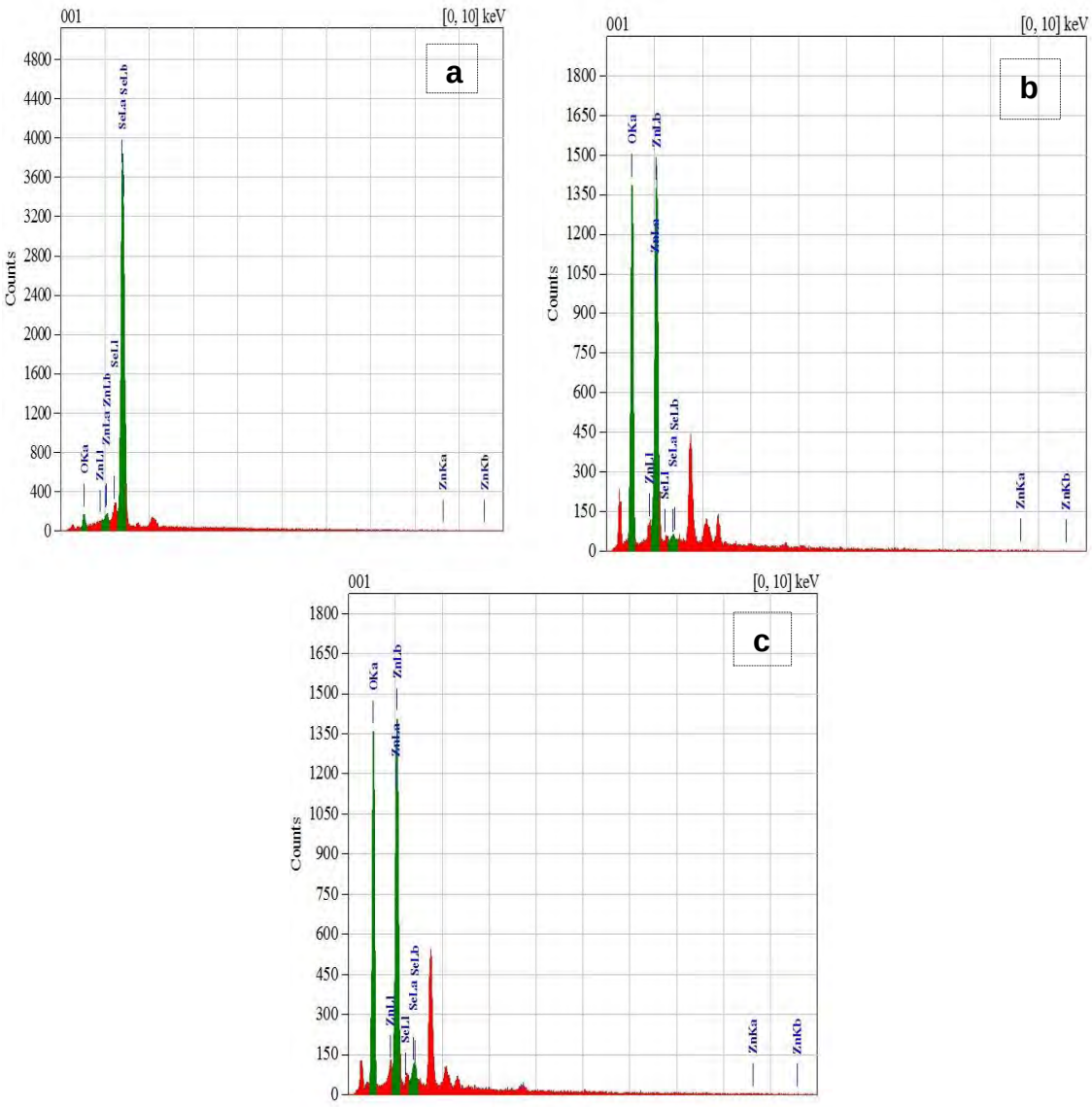

Figs 4.7 (a-c): EDX spectra of ZnSe thin film deposited for (a) 30 min (b) 40 min (c) 50 min time duration.

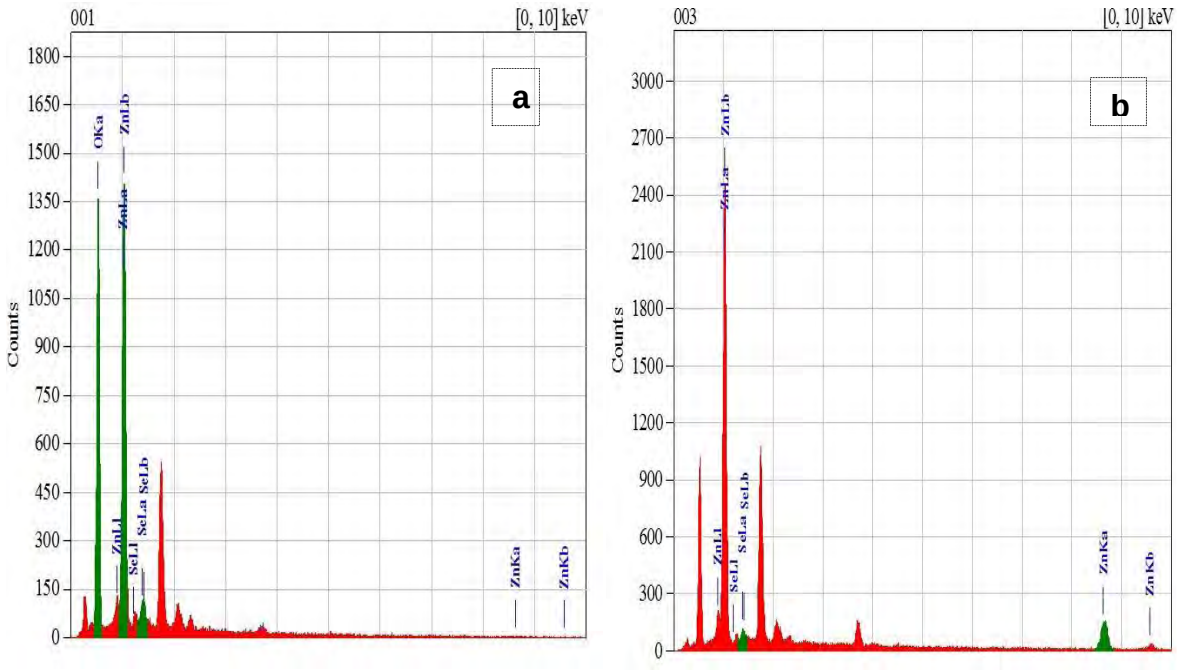

Fig: 4.8**:** Spectra of elemental analysis for the ZnSe thin films (a) as-deposited and (b) 40 min time durational film.

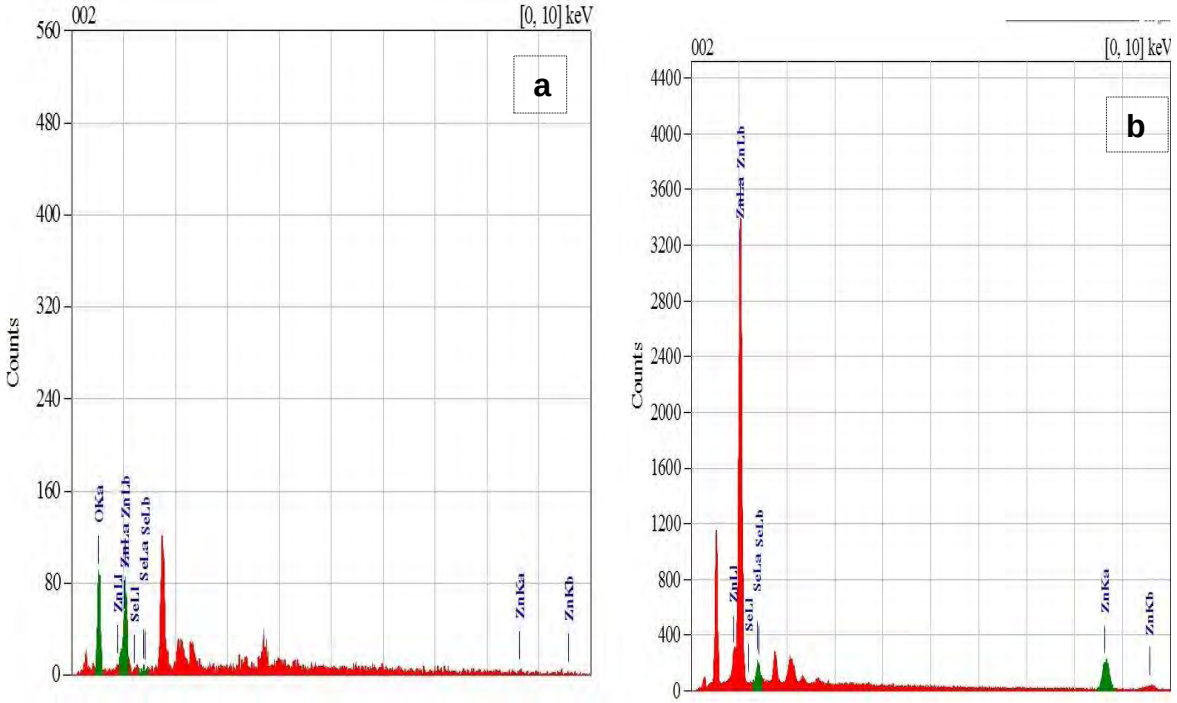

Fig: 4.9**:** Spectra of elemental analysis for the ZnSe thin films of 1.0 M concentration. (a) as-deposited and (b) annealed

Table 4.2: Data of elemental analysis for the ZnSe thin films deposited in different time duration

Sample		Mass Percentage of Elements		
		Zn	**Se**	**O**
ZnSe (30 min; 1 M, 175±15 nm)	As-deposited	1.61	94.45	3.94
ZnSe (40 min; 1 M, 200±20 nm)	As-deposited	46.60	1.89	51.51
	Annealed	87.57	12.43	
ZnSe (50 min; 1 M, 300±10 nm)	As-deposited	48.94	5.00	46.06
	Annealed	92.60	7.40	

Table 4.1 and 4.2 show the data of the elemental analysis for ZnSe thin films prepared at different concentration of Se on glass substrate and different time duration, respectively. From Table 4.1, it is observed that the stoichiometric ratio of elements show irregular nature. The percentage of Zn and O are high and Se is small. It may be due to low concentration of the Se source or the low concentration of the complexing agent. The pH of the chemical bath plays a vital role during the film formation. It is observed that high pH reduces the rate of formation of ZnSe thin film. During the deposition of the ZnSe thin films, the pH of the chemical bath was ≈ 12±1.

4.4 XRD Studies

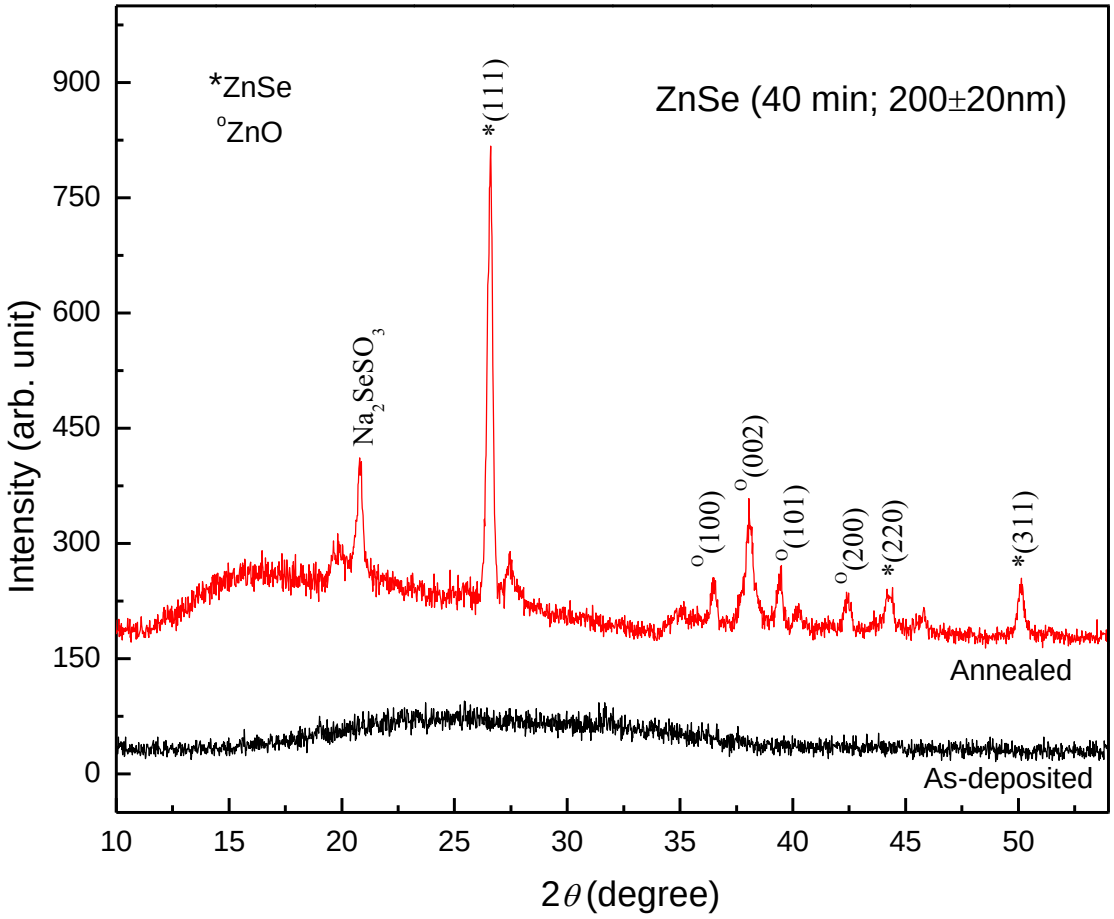

Figure 4.10: XRD patterns for the as-deposited and annealed ZnSe thin films at1M concentration and deposited for 40 min at 300 °C for 1 hr.

Figure 4.10 shows the XRD patterns for the as-deposited ZnSe thin films from 1M concentration of Se source deposited for 40 min that annealed at 300 °C for 1 h. The appearance of the 2θ peaks at 26.57, 44.27, and 50.13 correspond to peaks from (1 1 1), (2 2 0) and (3 1 1) planes, respectively [4, 5] However, in addition to Zn and Se, there are other peaks corresponding to Si, O, Ca, etc. and can be attributed to those originating from amorphous glass substrate. The (111) plane is the preferred orientation, and it is the close-packing direction of the zinc-blende structure of cubic ZnSe phase. Crystallite size (D) of the film was calculated using Scherrer's formula from the full width at half maximum (β) of the peaks expressed in radians,

$$D = \frac{K\lambda}{\beta \cos\theta}$$

where 'K' is constant dependent on crystallite shape (0.9), 'λ' is wavelength of CuK_α radiation, and 'θ' is angle between the incident and scattered X-ray. The strain, ε values were evaluated by the following relation:

$$\varepsilon = \frac{\beta \, Cos \, \theta}{4}$$

The dislocation density was determined using the following relation:

$$\delta = \frac{15\beta \, Cos \, \theta}{4aD}$$

The number of crystallites per unit area (N) of the films was determined with using formula

$$N = \frac{d}{D^3}$$

Where, a is the lattice constant, δ is dislocation density, and d is the thickness (200 nm) [6]. The average crystallite size is found to be 23.21±3.61 nm. The strain and dislocation density are found to be 1.62×10^{-3} (lines^{-2}m^{-4}) and 2.18×10^{15} m^{-2}, respectively. The number of crystallites per unit area is 2.63×10^{16} m^{-2}. All the diffraction peaks can be assigned to face centered cubic with lattice constants (a = 5.670 Å) which are in good agreement with the JCPDS card no: 01-071-5977 [7]. As-deposited films show weak peaks but after annealing the thin films show several peaks which show the crystalline nature.

4.5 Optical Properties

When a ray of light passes through the material or a thin film, different phenomena are observed such as absorbance, transmittance, reflectance, scattering, refraction, luminescence, etc. In this portion of Chapter 4, using the data collected from the UV-visible spectroscopy various optical properties of the chemical deposited ZnSe thin films have calculated and the revealed properties have discussed comparing with the previous research.

4.5.1 Absorbance

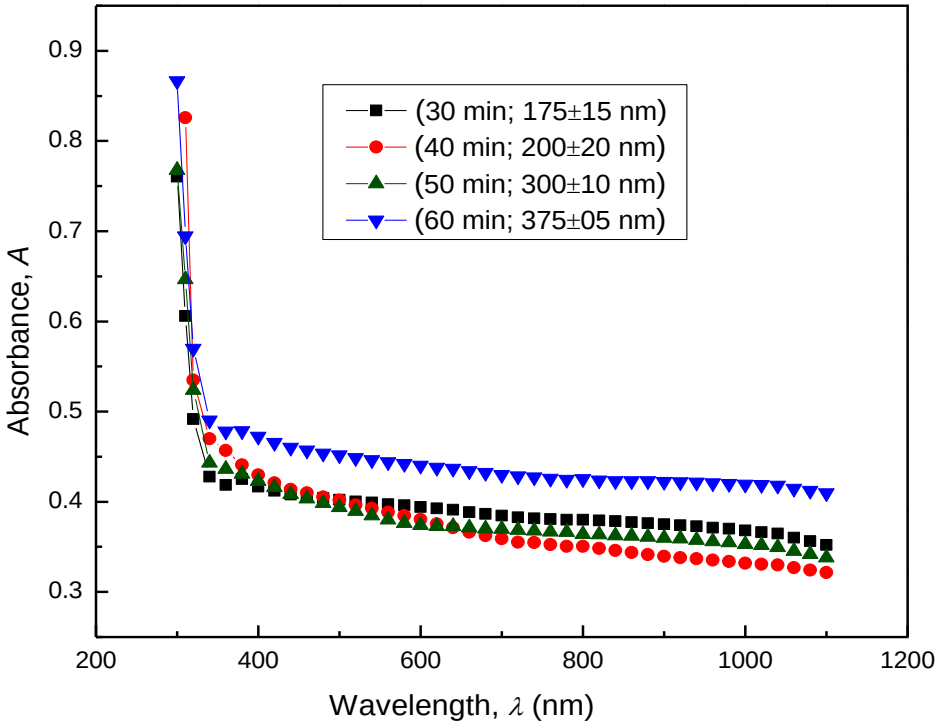

Fig. 4.11: Absorbance vs. wavelength graph of the ZnSe thin films obtained in different time duration.

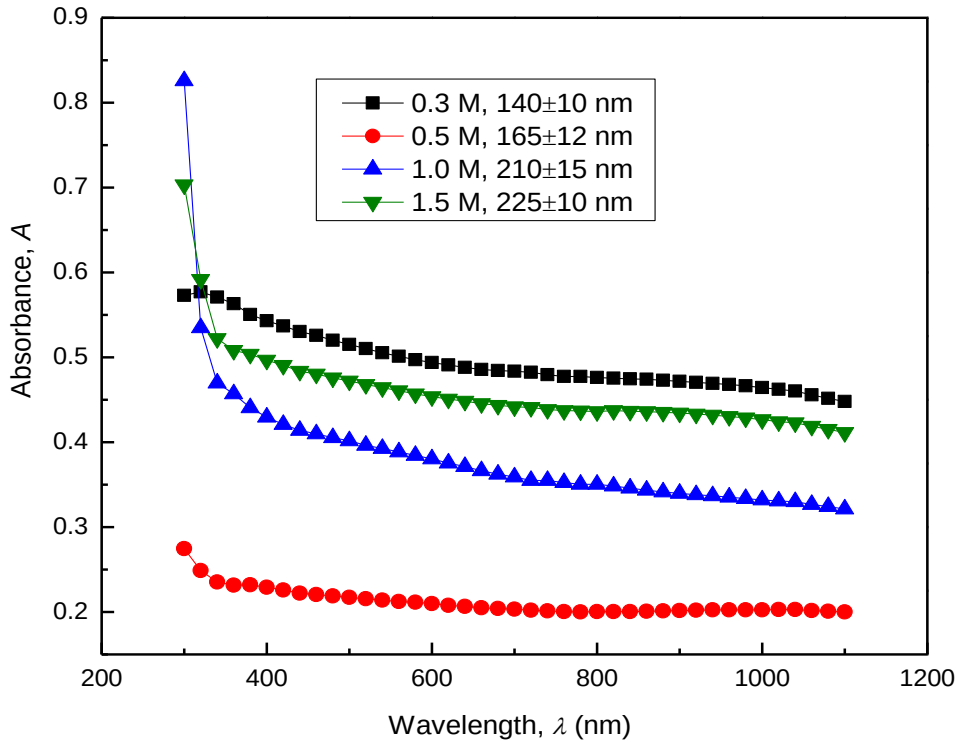

Fig. 4.12: Absorbance vs. wavelength graph of the ZnSe thin films obtained in different concentration of Se source.

It is observed that the as-deposited ZnSe thin films were semi–transparent and white in color. Figure 4.10 shows the variation of absorbance (A) with wavelength, λ, of the ZnSe thin films deposited at 90 ^{o}C for 30, 40, 50, and 60 min. The absorbance spectra for the films deposited under various deposition times and for different Se source were recorded in the wavelength of 250–1100 nm which are shown in Figs. 4.11 and 4.12. All the films indicate a gradually increasing absorbance throughout the visible region, which makes it possible for this material to be used in a photo electrochemical cell [3]. Based on the Figs. 4.11 and 4.12, it is observed that the films prepared for 60 min exhibits higher absorption characteristic as compared to other deposition times, indicating more molecules are deposited onto the substrate. As the film grows thicker, there is more ZnSe particulate absorption at the film surface giving rise to scattering losses, which increases with the decrease of wavelength [8].

4.5.2 Transmittance

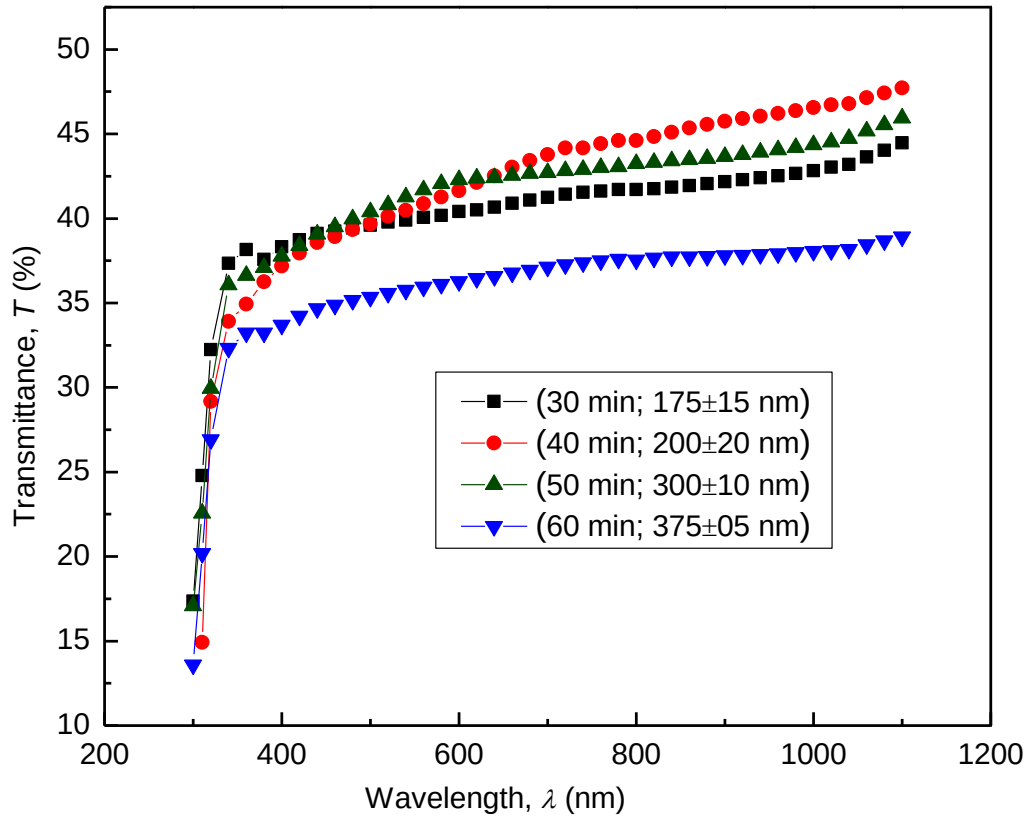

Figure 4.13: Transmittance (%) vs. wavelength graph of the ZnSe thin films in different time duration.

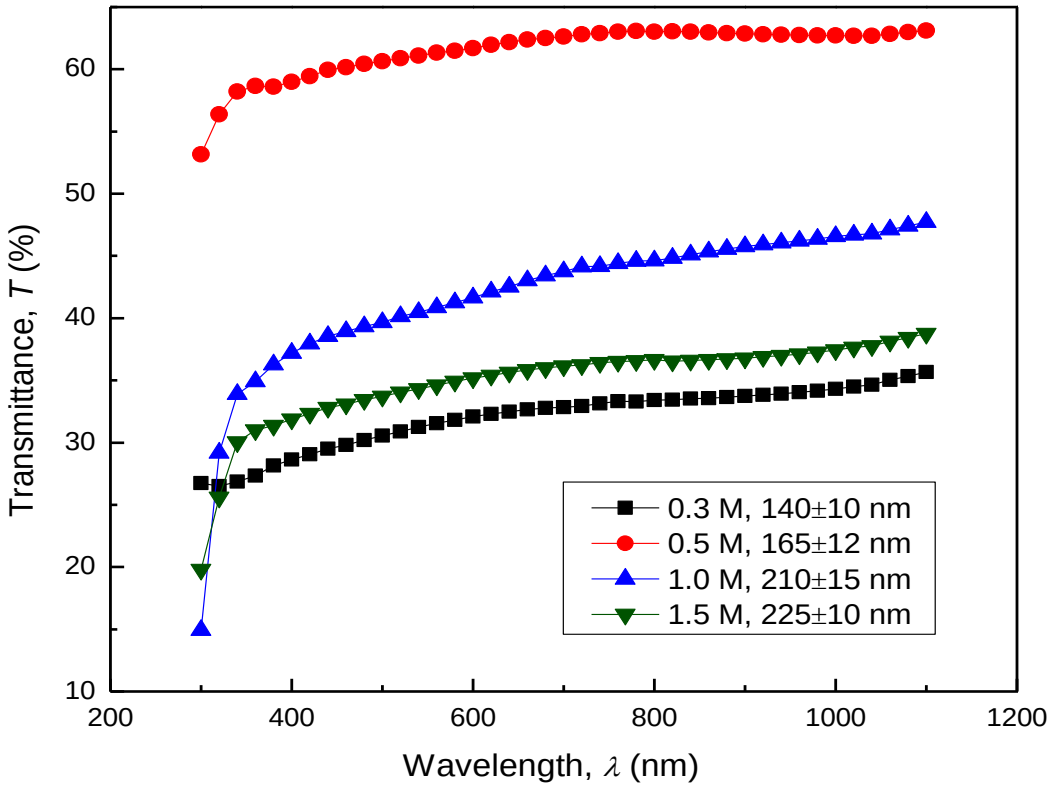

Figure 4.14: Transmittance (%) vs. wavelength graph of the ZnSe thin films at different concentration of Se source.

The plot of the spectral transmittance (%) of the deposited films versus wavelength is shown in Figs. 4.13 and 4.14.The transmittance spectra showed minimum transmission at shorter wavelengths whereas maximum transmission in the higher wavelength range and the transmission edge is not sharp as expected for thin films. The transmittance spectra reveal transmission between 40% – 53% in the visible region for all the films deposited at different time duration and between 40% – 65% for all the films deposited at different concentration of Se source. The higher transmittance in the visible region makes it a strong candidate for use in optoelectronic devices. The wide transmission range of ZnSe film makes the material useful in manufacturing optical components, windows, mirrors, and lenses for high power IR laser [9].

4.5.3 Absorption coefficient

Using the Equation (2.7) presented in Chapter 2, absorption coefficient (α) is calculated. Variation of the absorbance coefficient with photon energy ($h\nu$) of the ZnSe thin films in different time duration (30, 40, 50, and 60 min,) and for different molar concentration of Se

source are shown in Figs. 4.15 and 4.16, respectively. It is observed that the absorption coefficient increases of the ZnSe thin films with increasing photon energy and the increase is exponential at the region of photon energy ~3.75 eV. Chen et al. [10] reported that the value of the absorption coefficient is depends upon radiation energy as well as the composition of films. The absorption of the ZnSe thin films deposited in different time duration and for different molar concentration of Se source increase exponentially at ~3.9 eV, but do not show any other distinct absorption edges. This absorption energy region may correspond to the less amount of Se in the films.

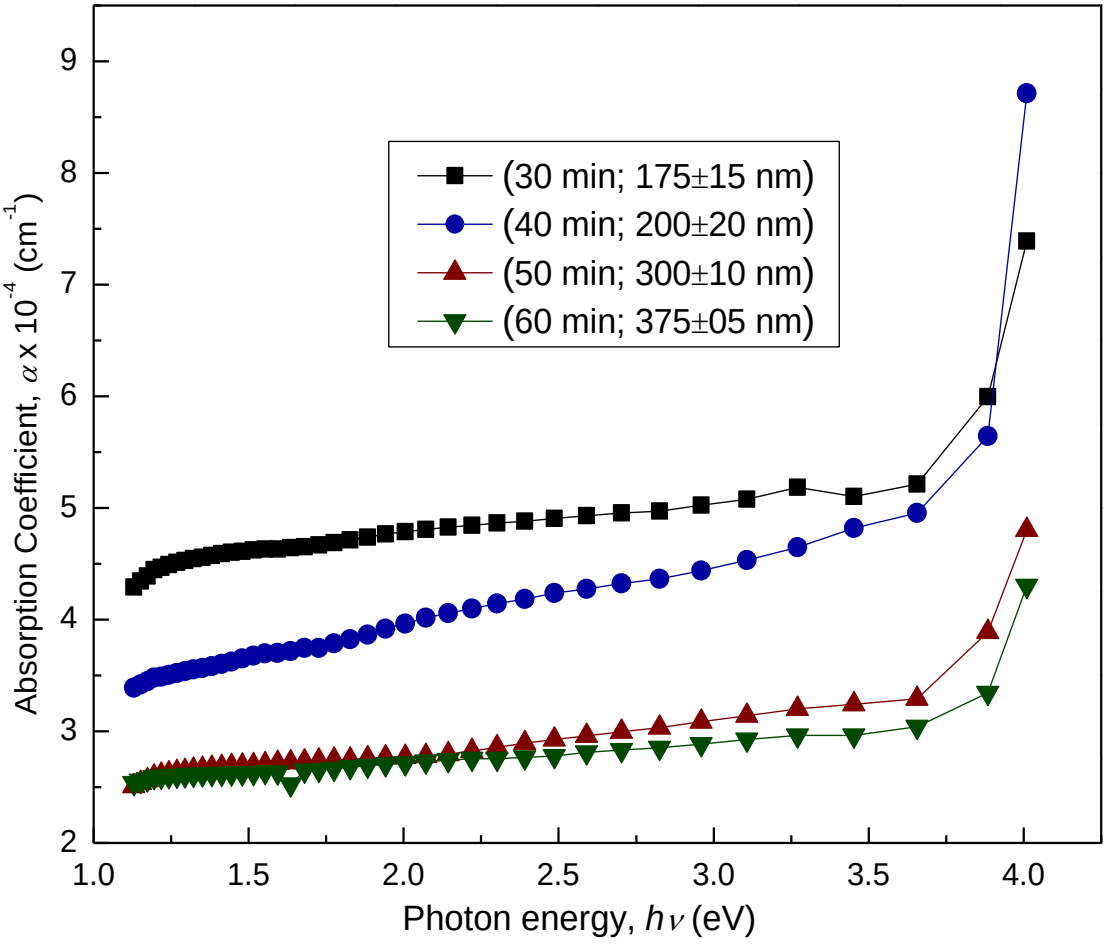

Fig. 4.15: Absorption coefficient vs. photon energy for the ZnSe thin films deposited at different time duration.

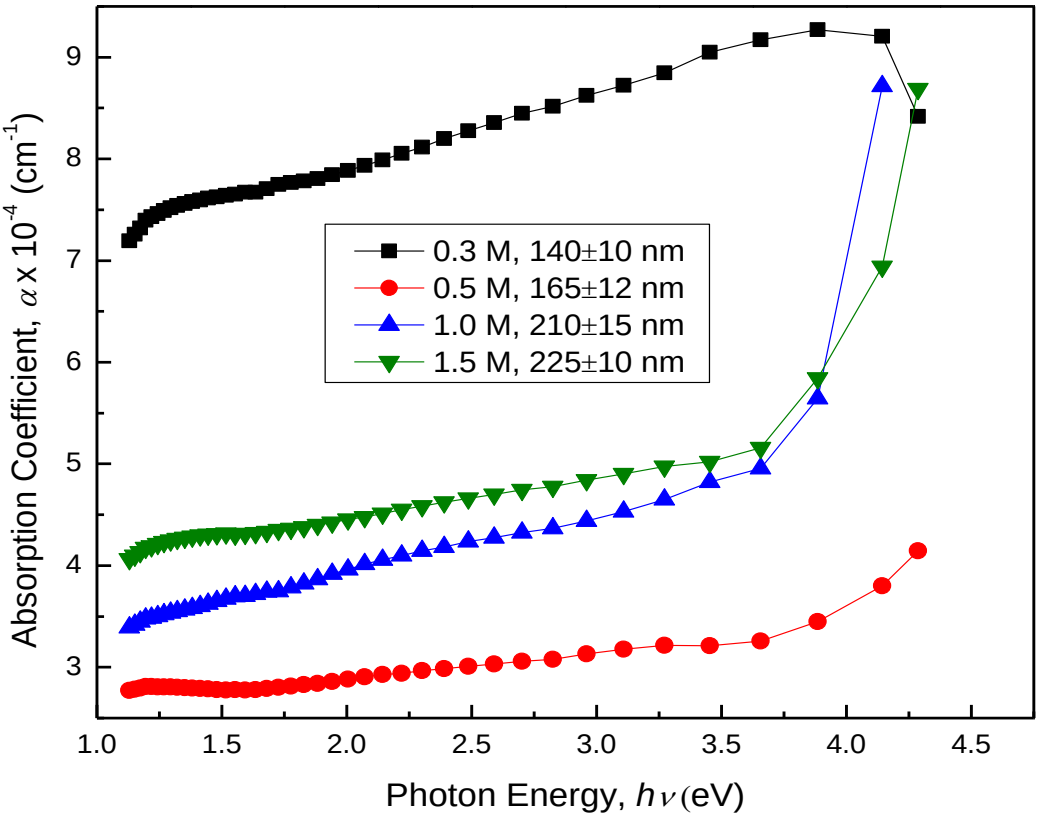

Fig. 4.16: Absorption coefficient vs. photon energy for the ZnSe thin films deposited at different concentration of Se source.

4.5.4 Comparative Study of the Absorbance of the As-deposited and Annealed ZnSe Thin Films

The comparative study of absorbance of the as-deposited and annealed ZnSe thin films deposited at 90 ^{o}C with 1:1 molar concentration of Zn and Se source in chemical bath for 60 min is presented in Fig. 4.17. It is observed that after annealing the decrease in absorbance of the ZnSe thin film becomes more exponential than that of the as-deposited film with increasing of wavelength.

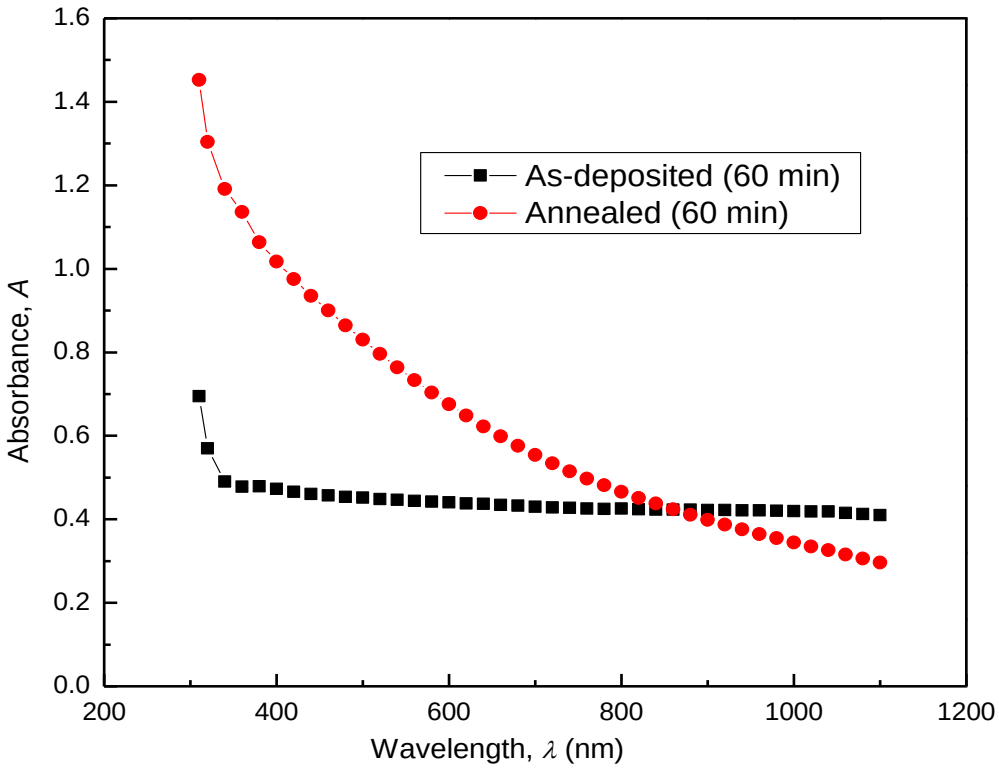

Fig. 4.17: Absorbance vs. wavelength graph for the as-deposited and annealed ZnSe thin films deposited for 60 min.

4.5.5 Optical band gap

Using Tauc relation Eqn. 2.7, as mentioned in chapter 2, optical band gaps of ZnSe thin films deposited at different time durations are calculated by plotting $(\alpha hv)^2$ vs. hv graph shown in Figure 4.18. It is observed that the optical band gaps of the ZnSe thin films are almost same in spite different thickness of the deposited films at same molar concentration (1 M) of Zn and Se sources. The value of E_g is calculated by extrapolating the straight line portion of the $(\alpha h\nu)^2$ vs. $h\nu$ graph. The linear dependence showed by $(\alpha hv)^2$ with hv indicates that this transition is direct [10]. Fig. 4.19 shows $(\alpha hv)^2$ vs. hv graph of the ZnSe thin films for different molar concentration of Se source and deposited for 40 min. It is observed that the optical band gaps are increasing with increasing the concentration of Se source. This is due to the quantum size effects induced by nanoscale crystallite size of the ZnSe thin films [11]. The films deposited at different time durations and different molar concentration of Se source show wide band gap energies of 3.75–3.80 eV and 2.77–3.80 eV, respectively and the reasons for this wide band gap energy are attributed to increased non-uniformity and the

presence of excess hydroxide phases in the films [3] which have been confirmed by EDX analysis.

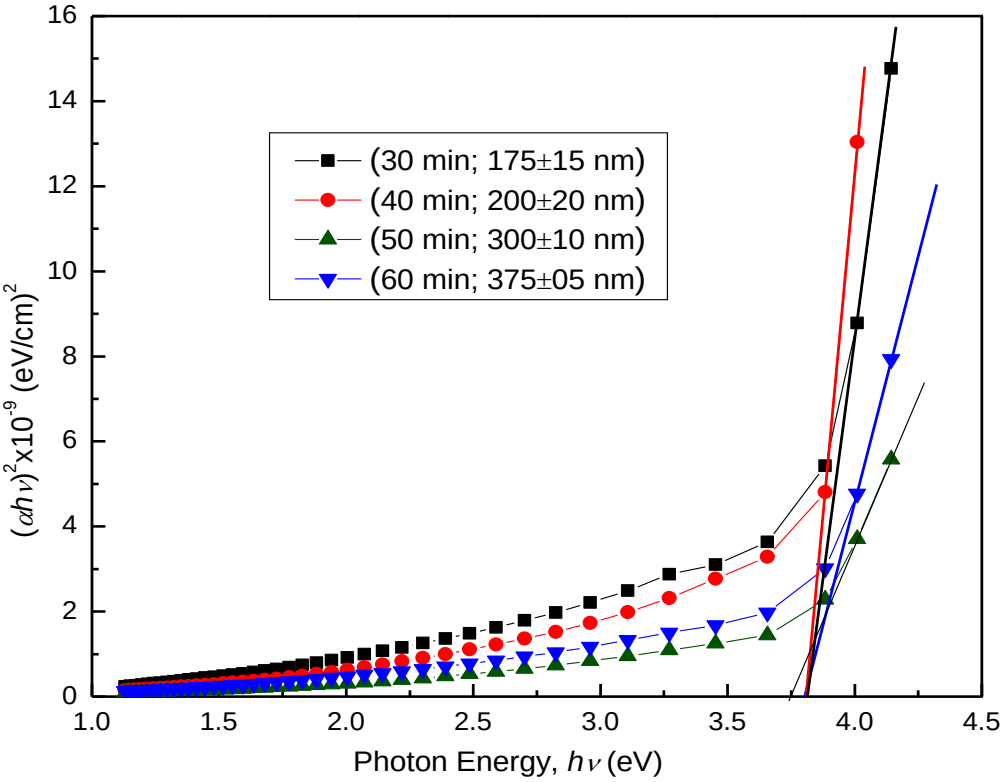

Fig. 4.18: $(\alpha h\nu)^2$ vs. $h\nu$ curves for the ZnSe thin films deposited for different time duration.

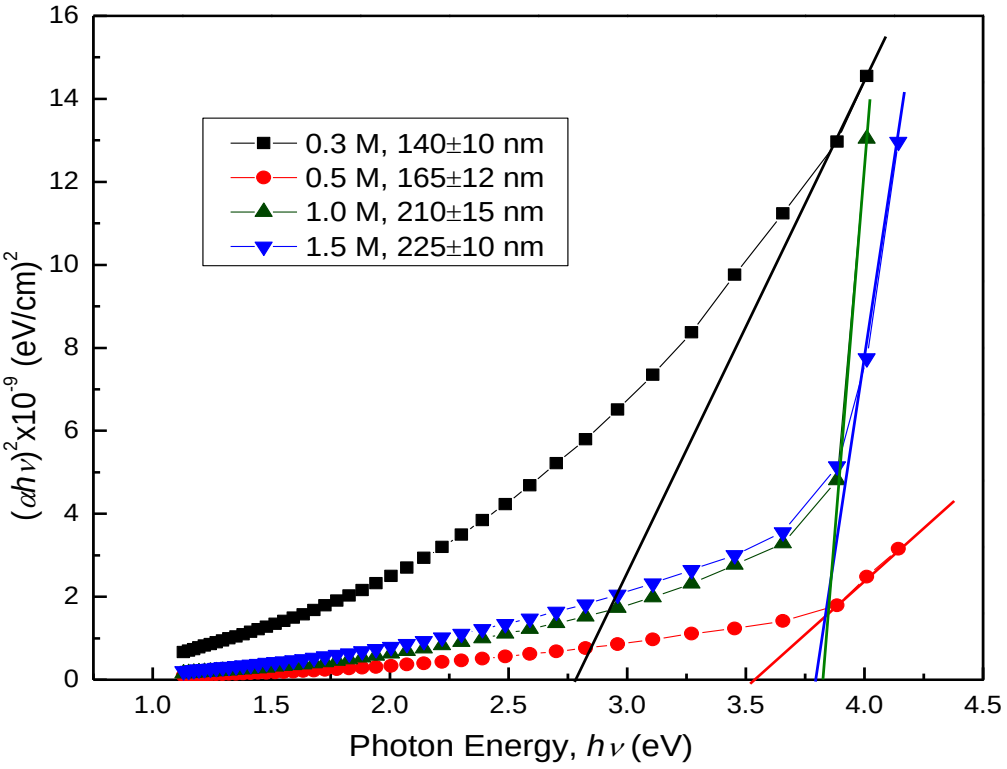

Figure 4.19: $(\alpha h\nu)^2$ vs. $h\nu$ curves for the ZnSe thin films deposited for different molar concentration of Se source.

A comparative study for the band gaps of the ZnSe thin films deposited for 40 min at 1:1 molar concentration of Zn and Se source is shown in Fig. 4.20. The film was annealed at 300 ^{o}C for 1 hr. In Figure 4.20, it is observed that the band gap of the ZnSe thin film increase after heat treatment. These changes of the energy band gap have been attributed to the morphological dependent properties of the films [142] or due to decrease of the particle size after annealing.

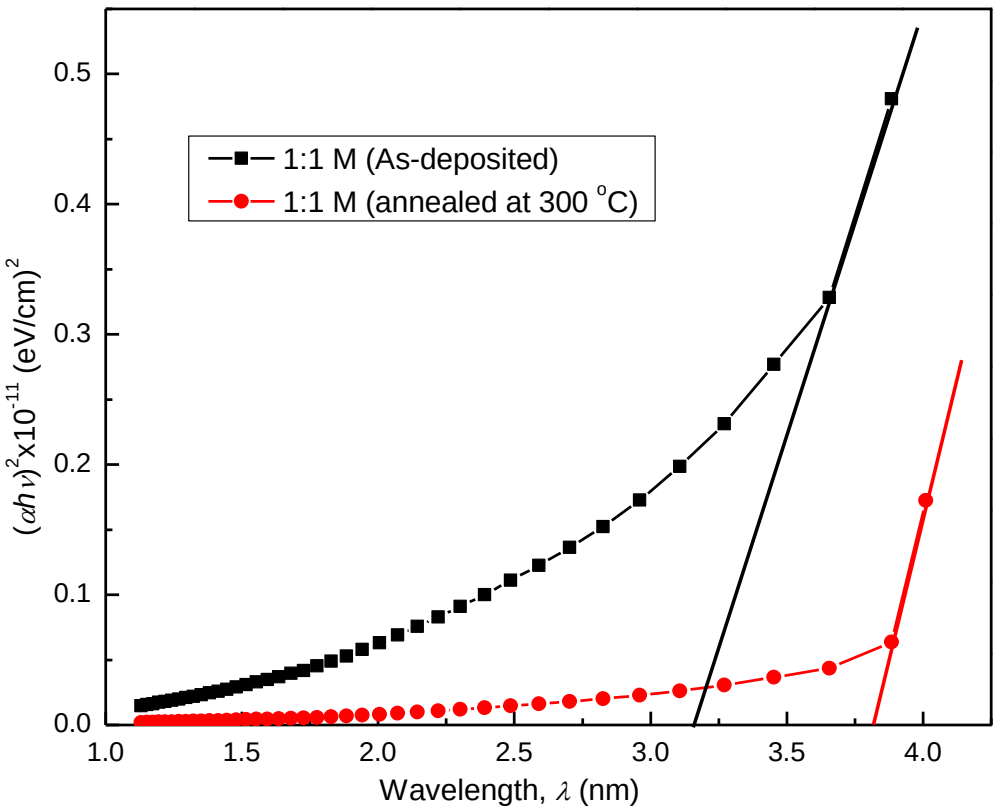

Fig. 4.20: Plot of $(\alpha h\nu)^2$ vs. $h\nu$ for the as–deposited and annealed ZnSe thin films deposited at molar concentration of Zn: Se = 1:1.

4.5.6 Refractive Index

The refractive index (n) has been calculated from the reflectance and extinction co-efficient which is calculated from the absorbance data using Equation. Fig. 4.21 shows the variation of refractive index with wavelength of the ZnSe thin films deposited for different time durations. From the Figure, it is observed that n is constant for the visible region of the spectrum and that increases with decreasing in wavelength. Therefore, the speed of light incident on the films is decreasing from UV to visible region. As the wavelength increases, the transmittance and extinction coefficient increase and refractive index decreases. It may be

due to that as the wavelength increases (lowering of the photon energy), the photon energy is not sufficient for the ZnSe to release photo electron. As a result maximum number of photons are transmitted through the band gap of ZnSe thin films and a fewer number of photons are interacted with the ZnSe molecule. Due to this reason the refractive index decreases and the extinction coefficient increases with wavelength [11].

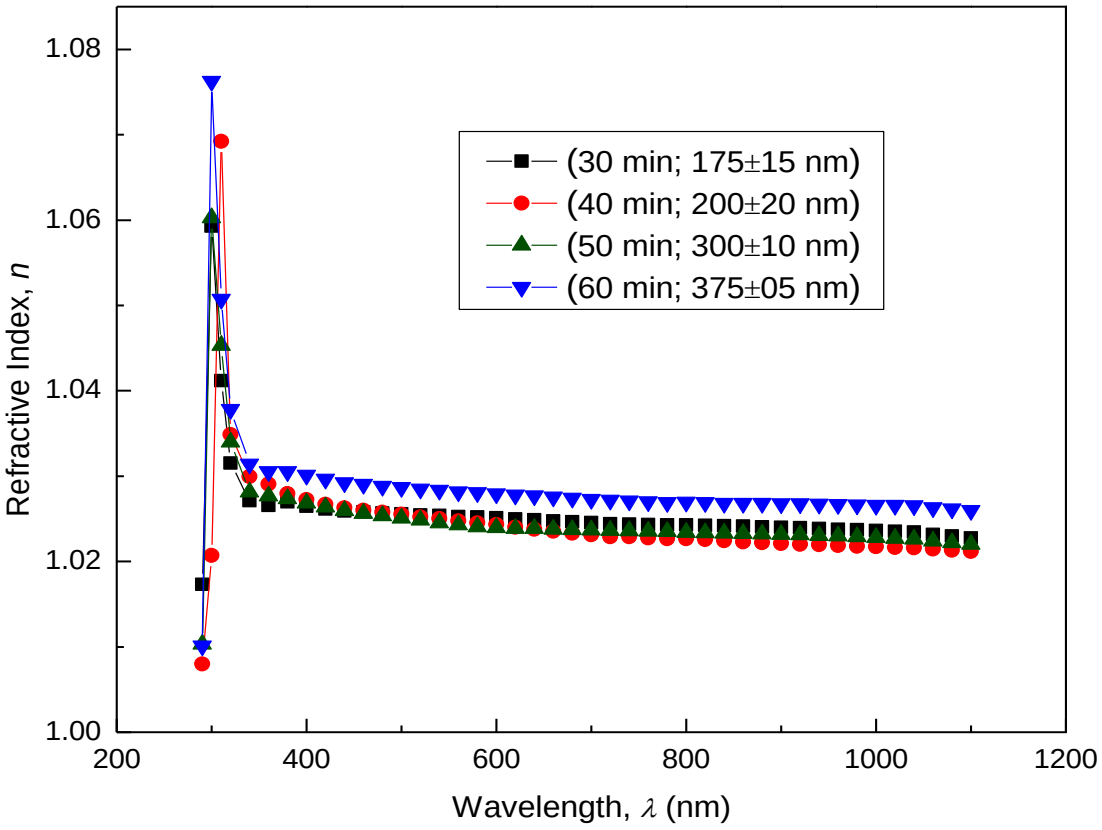

Fig. 4.21: Variation of the refractive index with wavelength of the ZnSe thin films deposited for different time durations

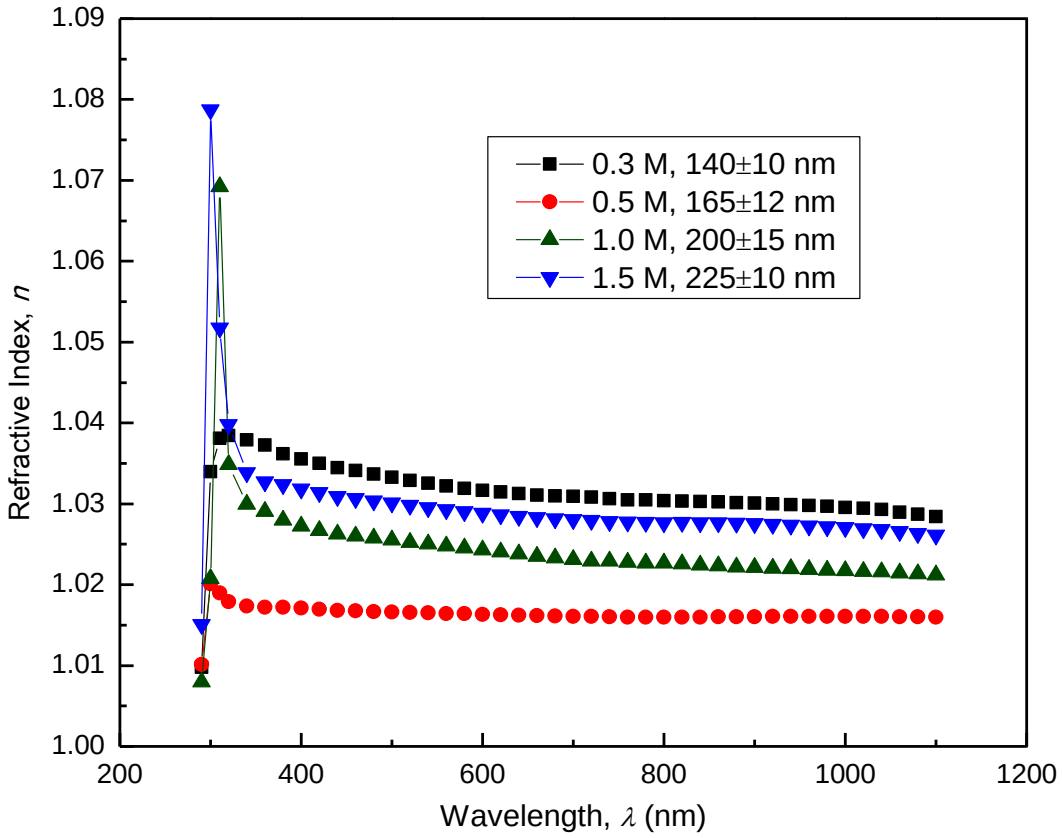

Fig. 4.22: Variation of the refractive index with wavelength of the ZnSe thin films deposited at different concentration of Se source.

4.5.7 Extinction Co-efficient

Using Equation (2.18), the extinction co-efficient, k is calculated for the ZnSe thin films. Figure 4.23 shows the variation of extinction co-efficient with wavelength of the ZnSe thin films deposited at different time duration. The fall in k may be due to the absorption of light at the grain boundaries. It increases in the higher wavelength region. The high value of k is a qualitative indication of the surface roughness of the thin films. The dependence of extinction coefficient k of the studied films on the wavelength λ is presented in Figs. 4.23 and 4.24. It is obvious that k for each composition has the tendency to increase of λ towards higher values which corresponds to strong electronic absorption between the valence and conduction band and tends to high at longer wavelengths where the transmittance is high.

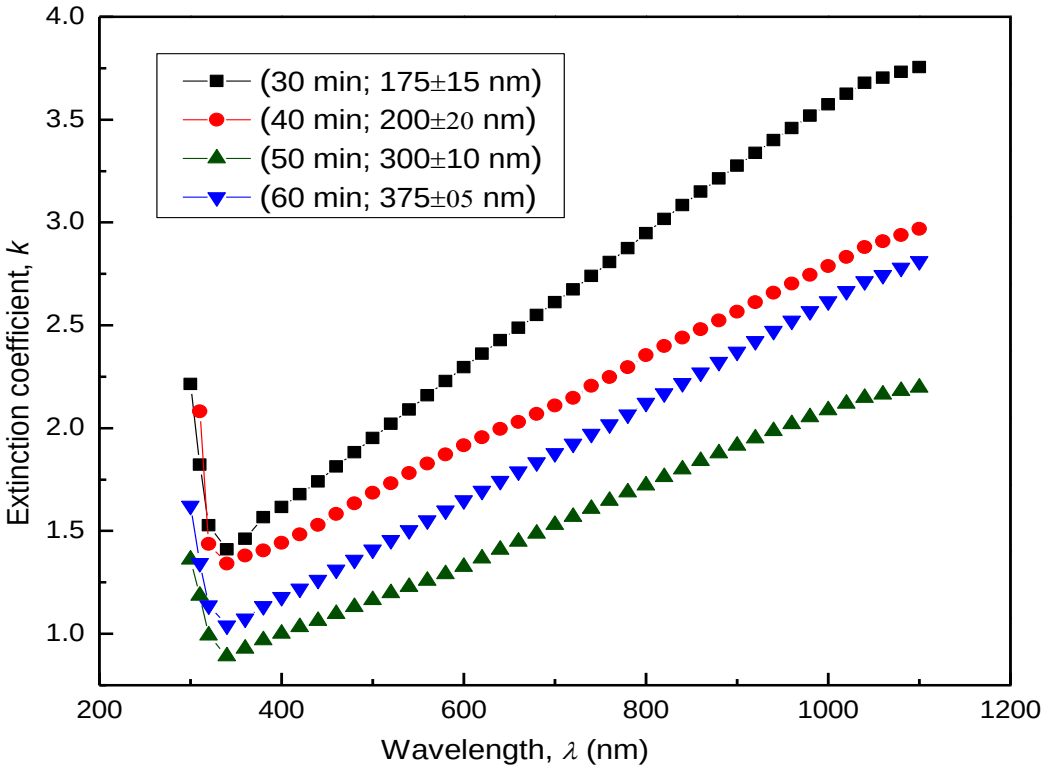

Fig. 4.23: Variation of extinction co-efficient with wavelength of the ZnSe thin films deposited for different time duration.

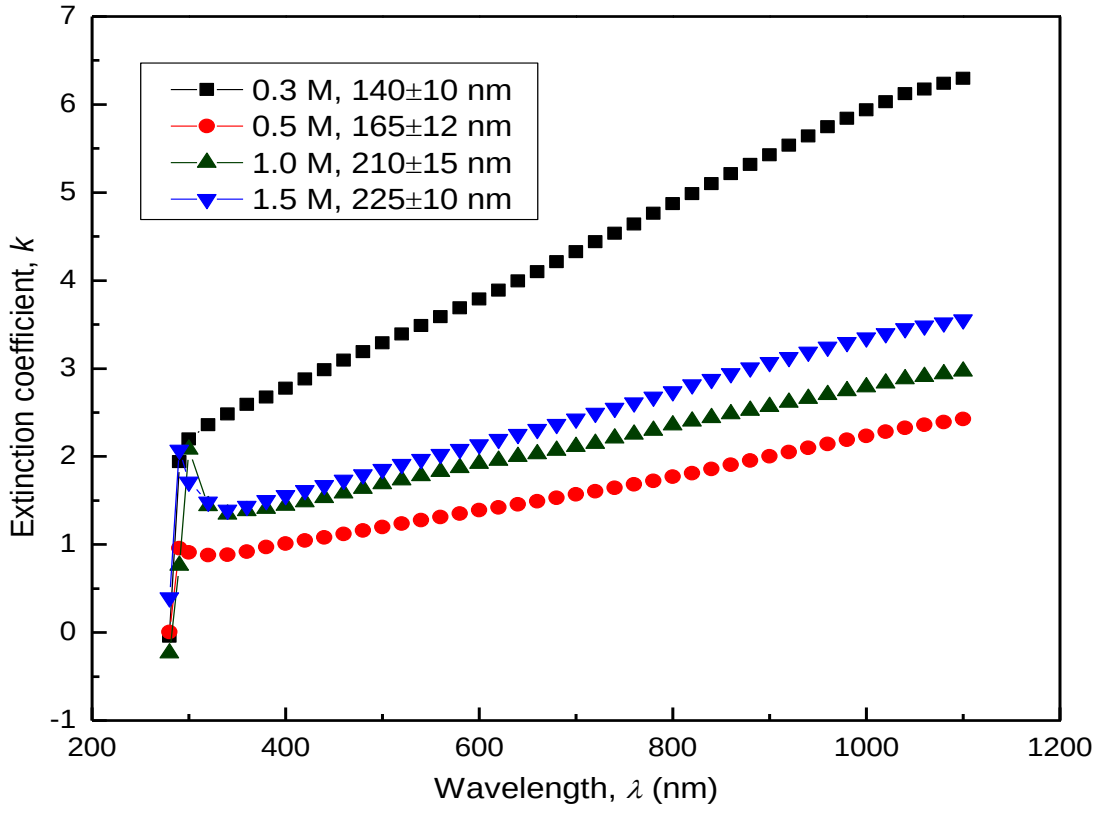

Figure 4.24: Variation of extinction co-efficient with wavelength of the ZnSe thin films deposited at different concentration of Se source.

4.5.8 Optical Conductivity

The optical conductivity is determined using the usual relation (2.18) Fig. 4.25 displays the variation of conductivity of the ZnSe thin films deposited onto glass substrate as a function of photon energy. In this case optical conductivity of the ZnSe thin films is increased in higher photon energy. The almost same behavior is exhibited in all time varying thin films and is as shown in Fig. 4.25. This is may be due to the increase of band gap that increases with the thickness.

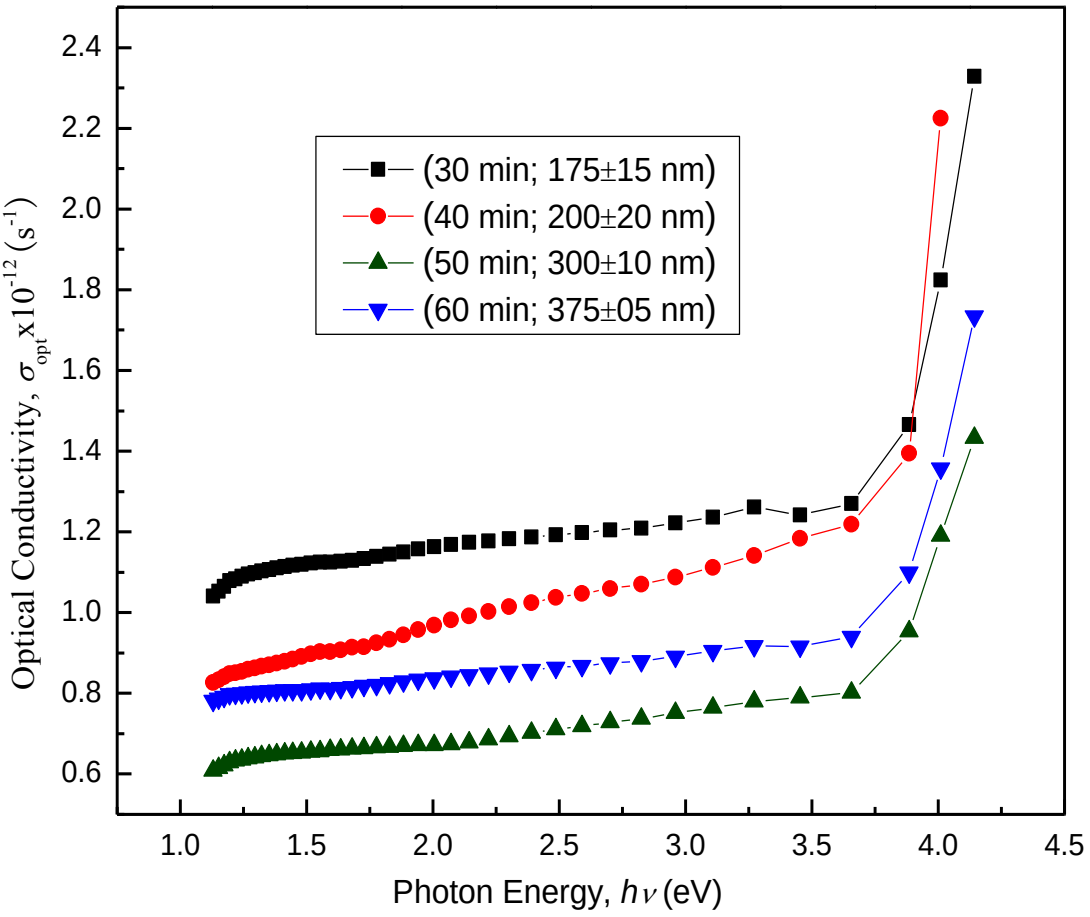

Figure 4.25: Variation of optical conductivity with photon energy of the ZnSe thin films deposited at different time intervals.

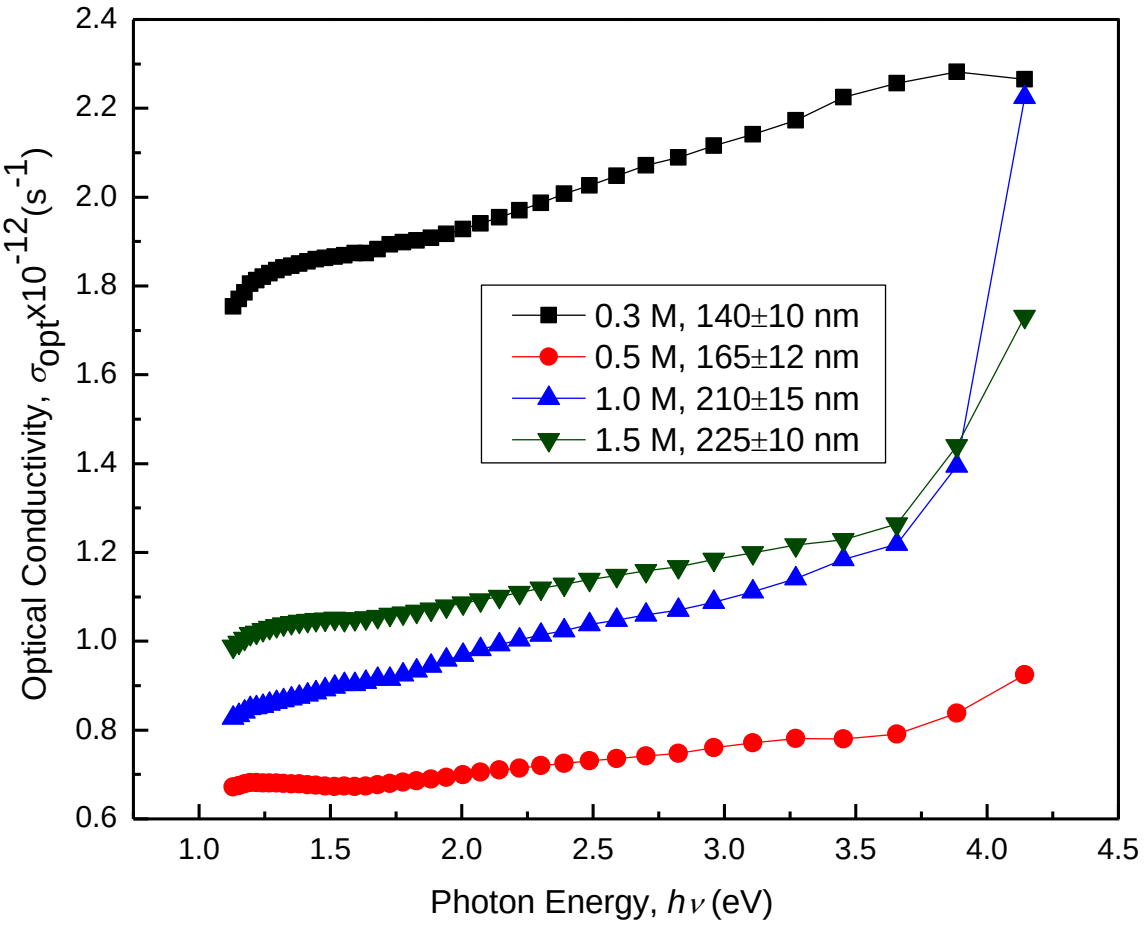

Figure 4.26: Variation of optical conductivity with photon energy of the ZnSe thin films deposited at different concentration of Se source.

Table 4.3: Optical information of the ZnSe thin films deposited different concentration of Se source.

Sample	Optical properties				
Parameter	E_g(eV)	T(%)	A	n	ζ_{opt} (×10^{12}s^{-1})
ZnSe (0.3 M, 140±10)	2.77	35	0.20	1.04	3.5
ZnSe (0.5 M, 165±12)	3.50	40	0.55	1.02	3.6
ZnSe (1.0 M, 200±15)	3.77	50	0.70	1.07	3.7
ZnSe (1.5 M, 225±10)	3.80	65	0.83	1.08	3.8

Table 4.4: Optical information of the ZnSe thin films deposited different time duration.

Sample	Optical properties				
Parameter	E_g (eV)	T(%)	A	n	ζ_{opt} ($\times 10^{12} s^{-1}$)
ZnSe (30 min; 175±15 nm)	3.75	40	0.55	1.030	1.1
ZnSe (40 min; 200±20 nm)	3.80	45	0.25	1.027	0.9
ZnSe (50 min; 300±10 nm)	3.80	42	0.40	1.028	0.7
ZnSe (60 min; 375±05 nm)	3.80	35	0.50	1.032	0.8

4.6 Electrical Analysis

4.6.1 Current – Voltage Characteristics

I-V graph of as-deposited time varying ZnSe thin films prepared by CBD is shown in Figure 4.27. During *I-V* measurement, the supply voltage was 0-20 Volts. From the Figs. 4.27 and 4.28, it is observed that the *I-V* graph shows the ohmic nature of ZnSe thin films [13]. From Figs. 4.27 and 4.28, it is observed that the *I-V* slop of the time varying ZnSe film are almost similar, but shown variation for the films deposited at different concentration of Se-source.

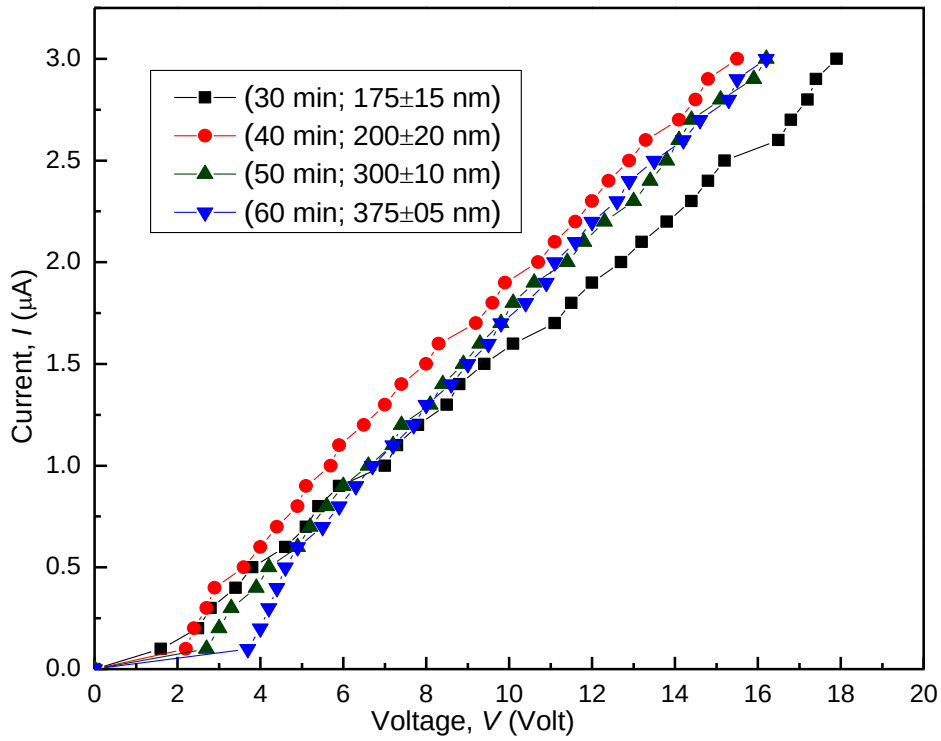

Fig. 3.27**:** *I-V* characteristics graph of as-deposited ZnSe thin films deposited for different time duration.

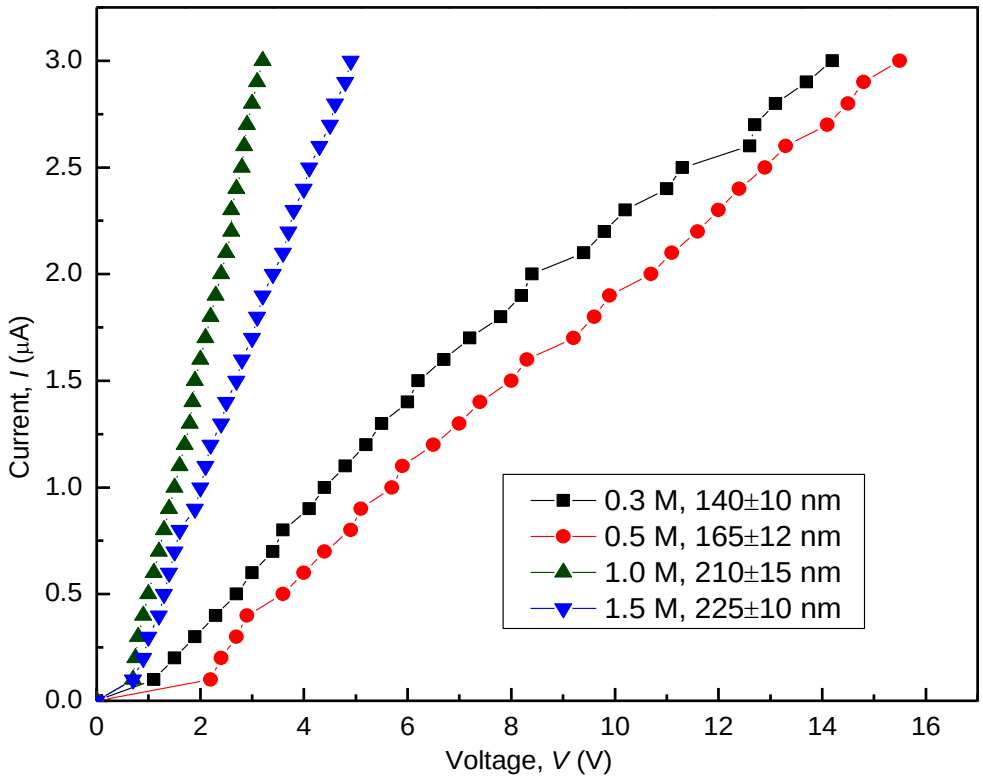

Fig. 4.28**:** *I-V* characteristic graph of as-deposited concentration varying ZnSe thin films.

4.6.2 Variation of Resistivity with Temperature

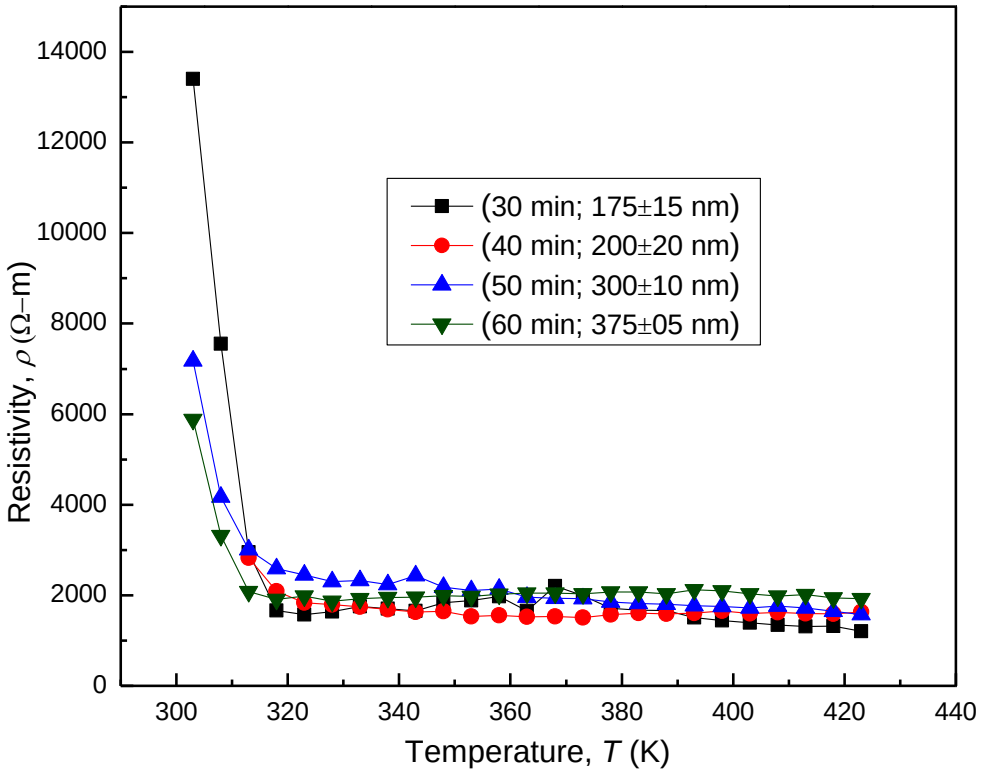

Fig. 4.29**:** Variation of electrical resistivity with temperature for time varying ZnSe thin films.

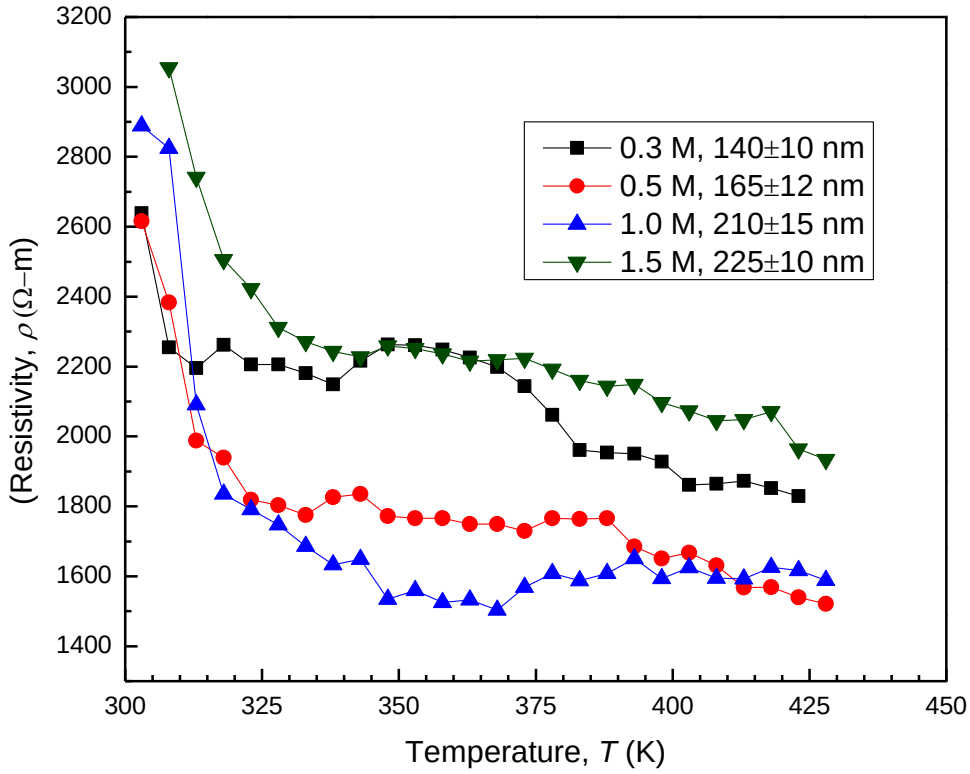

Fig. 4.30**:** Variation of electrical resistivity with temperature for concentration varying ZnSe thin films.

The variation of electrical resistivity with temperature for the ZnSe thin films annealed at temperature 300 ^{o}C for 1 hour are shown in Figs. 4.29 and 4.30. From the Figs. 4.29 and 4.30, it is observed that the resistivity decreases with the increase of temperature. This type of variation indicates the semiconducting behavior of the films.

4.6.3 Variation of Conductivity with Temperature

The variation of electrical conductivity with temperature for the ZnSe thin films annealed at temperature 300 ^{o}C for 1 hour are shown in Fig. 4.31. From the Fig 4.32, it is observed that the conductivity increases with the increase of temperature. This type of variation indicates the semiconducting behavior of the films.

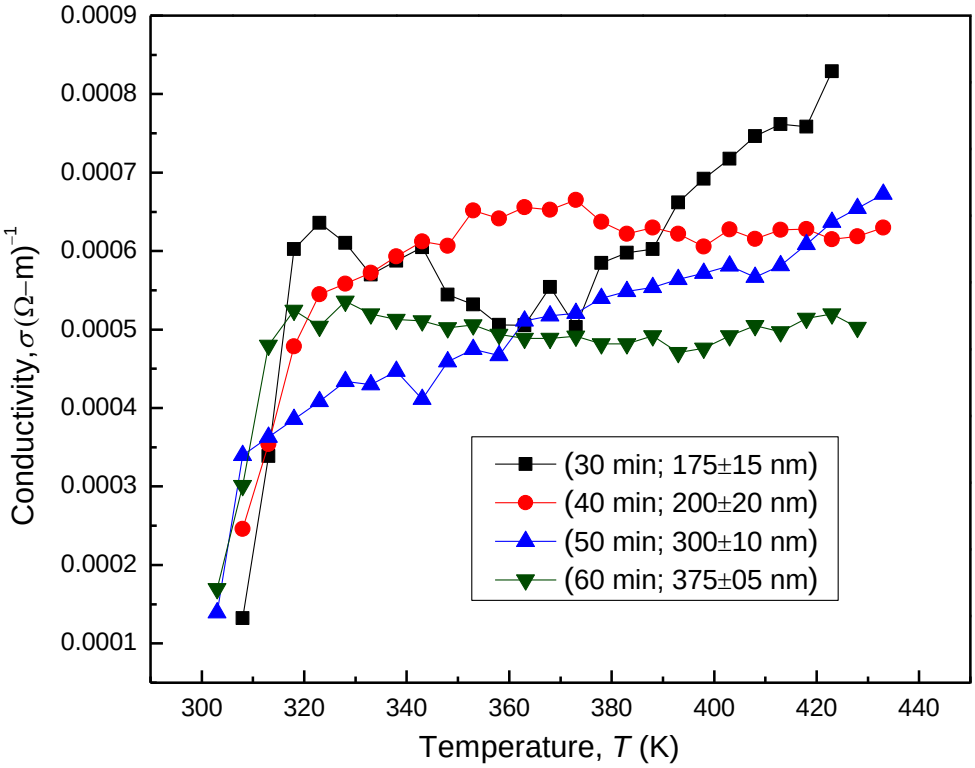

Fig. 4.31**:** Variation of electrical conductivity with temperature for time varying ZnSe thin films.

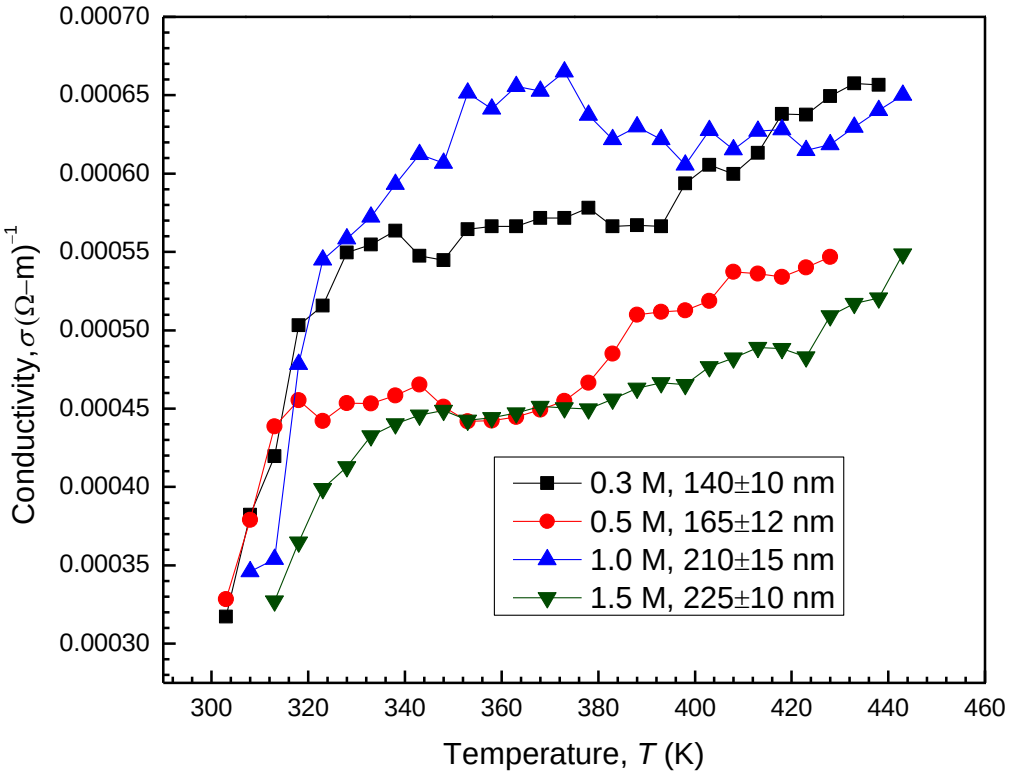

Fig. 4.32**:** Variation of electrical conductivity with temperature for concentration varying ZnSe thin films.

4.6.4 Variation of Activation Energy

The lnζ vs 1000/T graph for the annealed ZnSe thin films are represented in Fig. 4.33 and 4.34. The straight lines for the films of different concentrations and different time duration were drawn by using least mean square fitting method (not seen here). From the slope, the activation energy of the films of different concentration and time duration has been calculated. From the graph of lnζ vs $\frac{1}{T}$, ΔE has been calculated

$$\Delta E = \left(\frac{ln\sigma}{\frac{1}{T}}\right) \times 2\, k_B\ (eV)$$

Table 4.5 Activation energy of the ZnSe thin films deposited at different molar concentration of Se and different time duration.

Sample ID	Activatition Energy (eV)
ZnSe (0.3 M, 140±10 nm)	0.093863
ZnSe (0.5 M, 165±12 nm)	0.089155
ZnSe (1.0 M, 210±15 nm)	0.081616
ZnSe (1.5 M, 225±10 nm)	0.071185
ZnSe (30 min; 175±15 nm)	0.17876
ZnSe (40 min; 200±20 nm)	0.08915
ZnSe (50 min; 300±10 nm)	0.07553
ZnSe (60 min; 375±05 nm)	0.06729

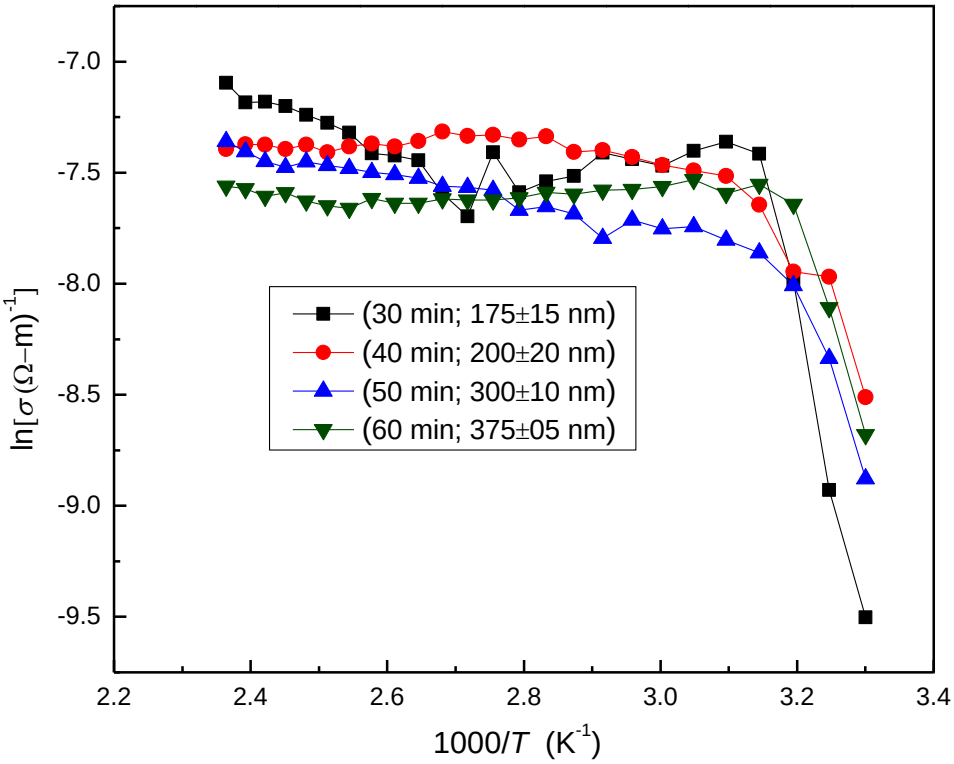

Fig. 4.33: Plots of ln(ζ) vs 1000/T graph for time varying ZnSe thin films annealed at 300 °C for 1 hr.

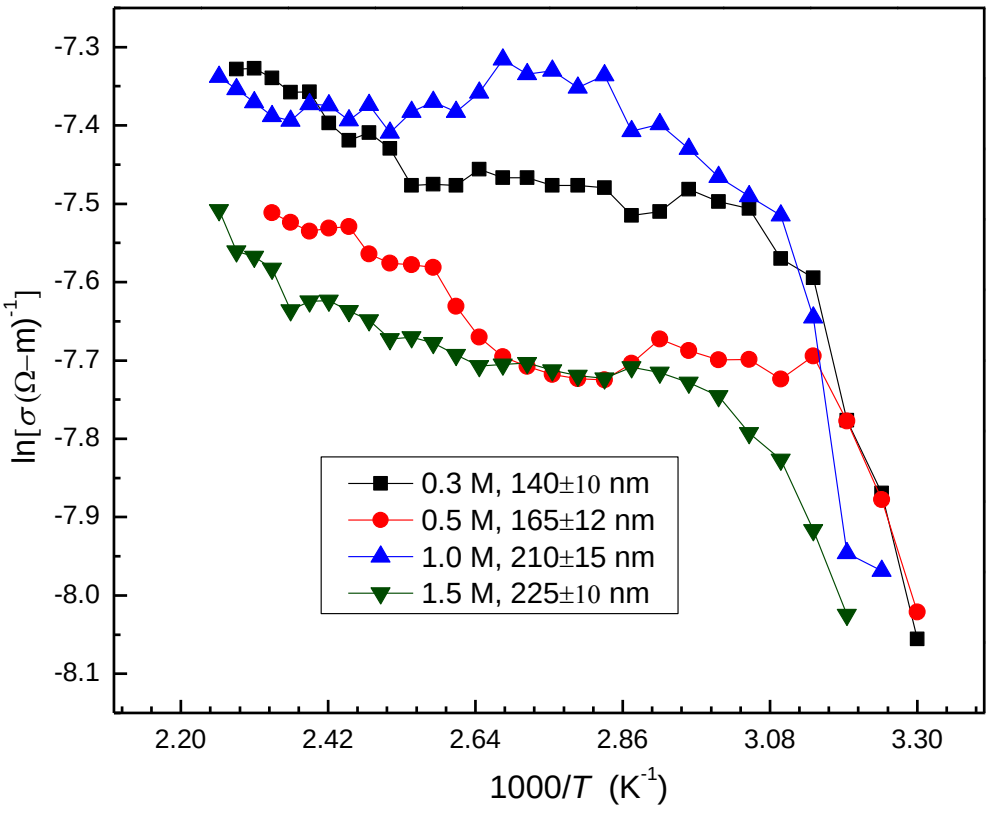

Fig. 4.34: Plots of ln(ζ) vs. 1000/T graph for concentration varying ZnSe thin films annealed at 300 °C for 1 hr.

Reference

[1] Wei, A., Zhao, X., Liu, J., Zhao, Y., 'Investigation on the structure and optical properties of chemically deposited ZnSe nanocrystalline thin films', Physica B. vol. 410, p. 120–125, (2013).

[2] Ezema, F. I., Ekwealor, A. B. C. Osuji, R. U., 'Effect of thermal annealing on the band gap and optical properties of chemical bath deposited ZnSe thin films', Turk. J. Phys. vol. 30, p. 157–163, (2006).

[3] Agawane, G. L., Shin, S. W., Suryawanshi, M. P., Gurav, K. V., Moholkar, A. V., Lee, J. Y., Patil, P. S. Yun, J. H., Kim, J. H., 'Novel reduced toxic route synthesis and characterization of chemical bath deposited ZnSe thin films', Ceramics Int. vol. 40, p. 367-374, (2014).

[4] Kathalingam. A., Mahalingam, T., Sanjeeviraja, C., 'Optical and structural study of electrodeposited zinc selenide thin films', Meter. Chem. Phy., vol. 106, p. 215-221, (2007).

[5] Dhansekaran, V., Mahalingam, T., Rhee, J. K., Chu, J. P., 'Structural and optical properties of electrosynthesized ZnSe thin films', optik, vol.124 (3), p. 255-260, (2012).

[6] Lohar, G. M., Shinde, S. K., Rath, M. C., Fulari. V. J., 'Structural, optical, photoluminescence, electrochemical, and photoelectrochemical properties of Fe doped ZnSe hexagonal nanorods', Mater. Sci. Semi. Process. vol. 26, p. 548–554, (2014).

[7] Kassim, A., Min, H. S., Tee, T. W., Kelvin, Nagalingam, S., 'Composition, morphology and optical characterization of chemical bath deposition ZnSe thin films', European J. App. Sci. vol. 3, p. 75–80, (2011).

[8] Nweze, C. I., and Ekpunobi, A. J., 'Effect of applied voltage on optical properties of zinc selenide thin films deposited on conducting glasses', African Review Phy., vol. 10, p. 15, (2015).

[9] Mahalingam, T., Kathalingam, A., Lee, S., Moon, S., and Kim, Y. D., 'Studies of Electro synthesized Zinc Selenide Thin Films', J. New Mater. Electrochemi. Sys., vol. 10, p. 15-19 (2007).

[10] Chen, L., Zhang, D., Zhai, G., Zhang, J.,' Comparative study of ZnSe thin films deposited from modified chemical bath solutions with ammonia-containing and ammonia-free precursors,' Mater. Chem. Phy. vol.120, p. 456–460, (2010).

[11] Kumar, P., Kumar, A., et al., 'Study of wavelength dependence of optical constants for ZnSe vacuum evaporated thin films', Int. J. Latest Research in Sci. and Tech., vol.1, Issue 4, p. 342-344 , (2012).

[12] Deshmukh, L. P., Pingale, P. C., Kamble, S. S., Lendave, S. A., Mane, S. T., Pirgonde, B. R., Sharonb, M., Sharon, M., 'Role of reducing environment in the chemical growth of zinc selenide thin films', Mater. Letter, vol. 92, p. 308–312, (2013).

[13] Thirumavalavan1, S., Mani, K., and Sagadevan, S., 'Investigations on the photoconductivity studies of ZnSe, ZnS and PbS thin films', Acadamic J., vol. 10(10), p. 362-366, (2015).

CHAPTER 5

CONCLUSIONS

5.1 Conclusions

The purpose of this chapter is to summarize the results obtained in this research work. We have investigated ZnSe thin films deposited by CBD onto the glass substrate in different concentration of Se and for different time duration. The thickness of the films deposited at different concentration of Se and different time duration are 140–225 nmand 175–375 nm, respectively. The structural, optical and electrical properties of the ZnSe thin films are investigated. The results of the present work are summarized and the following noteworthy conclusions are drawn:

In FESEM micrographs, it is observed that amalgamation occurs in the as-deposited ZnSe thin film onto the glass substrate showing the grain size decreases with increasing concentration of Se source. For time varying deposited films, it is observed that the grain size increases with increasing time duration. After annealing the films became porous in nature and looked more fibrous.The SEM micrograph showed that the ZeSe thin films prepared at different time duration are not compact but have good coverage on the glass substrate. These films revealed that grains were very small in size with well defined grain boundaries. EDX analysis reveals that all thedeposited films are stoichiometric.

X-ray diffraction studies show that though the as–deposited ZnSe thin films do not show crystaline nature but, annealed ZnSe thin films are polycrystalline in nature with preferential orientation along the (111), (220), and (311) planes. The films also have ZnO and Se phase. The average crystallite size is found to be 23.21±3.61 nm. The strain and dislocation density are found to be 1.62×10^{-3} lines^{-2} m^{-4} and 2.18×10^{15} m^{-2}, respectively. The number of crystals per unit area is 2.633×10^{16}m^{-2}. All the diffraction peaks can be assigned to face centered cubic with lattice constants ($a = b = c = 5.670$ Å), which are in good agreement with the previous work.

Various optical parameters such as absorbance, transmittance, refractive index, extinction coefficient and dielectric constant of the films have been studied for the as-deposited ZeSe thin films and are recorded in the wavelength range from 250 to 1100 nm. The films prepared for 60 min exhibit higher absorption as compared to other deposition times. The maximum transmittance is 65% for the ZnSe thin film deposited at 0.5 M concentration of Se. The direct optical band gap of the films deposited at different time duration and different molar concentration of Se source show wide band gap energies of 3.50–3.55 eV and 2.70–3.55 eV, respectively. The band gap of the ZnSe thin film deposited for 40 min of 1.0 M concentration

have been increased from 3.5 to 3.75 eV by annealing effect. It is observed that the refractive index decreases, as the wavelength increased. However, the extinction coefficient increases with the increase of wavelength. As the wavelength increases, the transmittance and extinction coefficient increases and refractive index decreases. It may be due to that as the wavelength increases (lowering of the photon energy), the photon energy is not sufficient for the ZnSe to release photo–electron. The optical conductivity of the ZnSe thin films is increased in higher photon energy due to the increase of band gap that increases with the thickness.

The electrical properties of the as–deposited and annealed ZnSe thin films have been observed. The resistivity decreases with the increase of temperature and the conductivity increases with the increase of temperature which reveals the semiconducting nature of the films. The maximum resistivity of the ZnSe Films deposited for 30 min is 7.6×10^{3} Ω–m. The activation energy of the ZnSe thin film deposited at 0.3M concentration for 40 min is 0.11 eV, which supports the values of previous research.

From the investigations of optical and electrical properties of the ZnSe thin films, it can be interred that the films may be useful as a buffer layer of solar cell, suitable for optical sensors and other optoelectronic devices.

5.2 Suggestions for Future Work

More investigations can be done to explain different characteristics elaborately, which will help to reveal the suitable applications of ZnSe thin films. For further understanding of this material the following studies may be carried out:

1. To study the optimization of film growth conditions.
2. To study the TEM and AFM for better understanding of surface nature.
3. To study the photoluminescence and photosensitivity of those materials of the films.
4. To study homojunction and heterojunction properties of the films.
5. To study the magnetic properties of the films.
6. To study the Hall effect and temperature dependence of hall mobility and carrier concentration.